AN INVESTIGATION OF THE RADIATING CHARACTERISTICS OF AN ELECTROMAGNETIC HORN

ROBERT E. LEE
EARL DEROHAN BARONDES

AN INVESTIGATION OF THE RADIATING CHARACTERISTICS OF AN ELECTROMAGNETIC HORN

by

Robert E. Lee
Lieutenant Junior Grade, U.S.Navy
B.S., U.S. Naval Academy, 1946

Earl de Rohan Barondes
Lieutenant Junior Grade, U.S.Navy
B.S., U.S. Naval Academy, 1947

Submitted in partial fulfillment of the
requirements for the degree of

NAVAL ENGINEER

from the

MASSACHUSETTS INSTITUTE OF TECHNOLOGY

(1952)

ABSTRACT

Title of Thesis: An Investigation of the Radiating Characteristics of an Electromagnetic Horn

Names of Authors: Earl de Rohan Barondes, LTJG, USN

Robert Earl Lee, LTJG, USN

Submitted to the Department of Naval Architecture and Marine Engineering on 16 May, 1952 in partial fulfillment of the requirements for the degree of Naval Engineer.

The radiating and impedance characteristics of a laterally radiating X band electromagnetic horn were investigated. The horn has a flare angle of 90 degrees in the H plane and at a radius of 37.8 cm. it is bent through 90degrees to form an aperture in the shape of a quadrantal arc. The aperture has a chord length of 16.7 λ at λ = 3.2 cm.

Experimental results verified computed field patterns and indicated that a constant phase was obtained across the aperture. Illumination was considered to be the distribution of the $H_{1,0}$ mode across the aperture.

The pattern of the uncompensated horn is elliptically polarized. In the H plane the E plane polarization has a beam width of 4.3 degrees and first side lobe level is 21 db. down at λ = 3.2 cm. The H plane polarization gives two main lobes 12 db. down from the E plane polarization.

Impedance measurements indicate reflection coefficients, due to reflection at the throat and at the aperture of the horn. Reflection at the 90 degree bend appears to be negligible. Representative values are Γ_t = 0.0726, Γ_a = 0.159. Should reflection at the throat be eliminated by a curved transition a VSWR = 1.38 over a band of 200 mcs. is obtainable.

To eliminate the cross polarization due to H plane polarization various schemes were tried. E plane flare was added. This combined with a paralled plate filter at the aperture reduced the cross polarization 20 db. VSWR less than 1.50 over a 675 mcs. band, with elimination of the throat reflection, were obtained.

Other schemes tried included adding a parallel plane filter with no flare and using E plane flare and a parallel wire filter. Cross polarization was reduced in all cases.

It is concluded that this type horn provides a constant phase illumination across a wide aperture resulting in a narrow beam with reasonably low side lobes. The cross components of polarization inherent in the design may be eliminated by mode filters. The impedance characteristics may be improved by designing for mutual cancellation of reflections in the frequency band desired.

ABSTRACT

Title of Thesis: An Investigation of the Radiating Characteristics of an Electromagnetic Horn

Names of Author: Earl de Hoban Beronden, LT(S), USN

Robert Earl Lee, LT(S), USN

Submitted to the Department of Naval Architecture and Marine Engineering on 16 May, 1952 in partial fulfillment of the requirements for the degree of Naval Engineer.

The radiating and impedance characteristics of a laterally radiating X band electromagnetic horn were investigated. The horn has a flare angle of 90 degrees in the H plane and at a radius of 37.8 cm. it is bent through 90degrees to form an aperture in the shape of a quadrantal arc. The aperture has a chord length of 16.7 λ at λ = 3.2 cm.

Experimental results verified computed field patterns and indicated that a constant phase was obtained across the aperture. Illumination was considered to be the distribution of the H_1^0 mode across the aperture.

The pattern of the uncompensated horn is elliptically polarized. In the H plane the E plane polarization has a beam width of 4.3 degrees and first side lobe level is 21 db. down at λ = 3.2 cm. The H plane polarization gives two main lobes 12 db. down from the E plane polarization.

Impedance measurements indicate reflection coefficients, due to reflection at the throat and at the aperture of the horn. Reflection at the 90 degree bend appears to be negligible. Representative values are Γ_t = 0.0726, Γ_a = 0.159. Should reflection at the throat be eliminated by a curved transition a VSWR = 1.38 over a band of 200 mcs. is obtainable.

To eliminate the cross polarization due to H plane polarization various schemes were tried. E plane flare was added. This combined with a parallel plate filter at the aperture reduced the cross polarization 20 db. VSWR less than 1.50 over a 6.5 mcs. band, with elimination of the throat reflection, were obtained.

Other schemes tried included adding a parallel plane filter with no flare and using E plane flare and a parallel wire filter. Cross polarization was reduced in all cases.

It is concluded that this type horn provides a constant phase illumination across a wide aperture resulting in a narrow beam with reasonably low side lobes. The cross components of polarization inherent in the design may be eliminated by mode filters. The impedance characteristics may be improved by designing for mutual cancellation of reflections in the frequency band desired.

Cambridge, Massachusetts
16 May 1952

Professor J. S. Newell
Secretary of the Faculty
Massachusetts Institute of Technology
Cambridge, Massachusetts

Dear Sir:

In accordance with the requirements for the Degree of Naval Engineer, we submit herewith a thesis entitled "An Investigation of the Radiating Characteristics of an Electromagnetic Horn."

Respectfully,

Robert E. Lee
Lieutenant Junior Grade
U.S. Navy

Earl de Rohan Barondes
Lieutenant Junior Grade
U.S. Navy

Cambridge, Massachusetts
15 May 1944.

Professor J. C. Jewett,
Secretary of the Faculty,
Massachusetts Institute of Technology,
Cambridge, Massachusetts.

Dear Sir:

In accordance with the requirements for the degree of Naval Engineer, we submit herewith a thesis entitled "An Investigation of the Resistance, Stability, and Seakeeping Qualities of Destroyers."

Respectfully,

Arthur E. Lee
Lieutenant (Junior Grade)
U.S. Navy

Lewis de Haven Lawrence
Lieutenant (Junior Grade)
U.S. Navy

ACKNOWLEDGEMENTS

The authors of this thesis are principally indebted to Dr. L. J. Chu for the initial inspiration and advice given during the thesis investigation. In addition the authors are indebted to the engineers and technical personnel of the Air Force Cambridge Research Center for their aid in the experimental phase of the thesis. To the personnel of the Coppersmith's Shop of the Boston Naval Shipyard for the excellent job of fabricating the horn and flare section, and to the personnel of Project Meteor who permitted us to use their impedance measuring equipment.

The authors of this thesis are particularly indebted to Dr. L. A. Cox for the initial inspiration and advice given during the thesis investigation. In addition, the authors are indebted to the engineers and technical personnel of the Air Force Materials Laboratory Center for their aid in the experimental phase of the thesis. To the personnel of the Experimental Shop of the Boston University Supported for the unselfish job of fabricating the jigs and figure section, and to the personnel of Project Files who assisted us to use their facilities unsparingly anytime.

CONTENTS

SYMBOLS

a The radius of the mean circular bend on the laterally radiating horn, type "A."

A The percentage area covered by a parallel wire screen. $\left(100\,\frac{v-d}{v}\right)$

$A(n,\phi_o)$ A coefficient in the Fourier-Bessel series method of field computations. It is defined by Formula (A-52).

b The short dimension of the inner surface of a rectangular waveguide.

b_1 The inner bend radius of the inner surface of the type "A" horn.

$B(n,\phi)$ A coefficient in the Fourier-Bessel series method of field computations. It is defined by Formula (A-55).

B_i The maximum magnitude of the H_{io}th harmonic at the aperture.

c The outer bend radius of the inner surface of the type "A" horn.

$C(n,\phi_o)$ A coefficient in the Fourier-Bessel series method of field computations. It is defined by formula (A-58).

d The diameter of a wire in the parallel wire filter.

d_1 The distance along the mean arc of the bend of the type "A" horn.

$D(n,\phi)$ A coefficient in the Fourier-Bessel series method of field computations. It is defined by Formula (A-59).

e The shorter dimension of the inner surface of the waveguide

E Electric field strength

E_x The x component of the electric field strength.

E_y The y component of electric field strength

f The longer dimension of the inner surface of a rectangular waveguide.

$\mathcal{L}$ The Lagrange literation of the linear surface of a n-dimensional manifold.

$\mathcal{L}^{\lambda}$ The λ component of literal-like tensor.

$\mathcal{M}^{\mu}$ The μ component of literal-like tensor.

$\mathbb{N}$ Electric field strength

$\mathcal{O}$ The surface literation of the inner sphere of the condenser

$\mathcal{P}(r,\theta)$ A coefficient in the Legendre-Bessel series method of field computations. It is defined by formula (I-24).

$\mathcal{P}^{\rho}$ The distance along the outer arc of the bowl of the type $\mathcal{P}$ meter.

$\mathcal{Q}$ The literation of $\mathcal{Q}$ when it is the partial sine filter.

$\mathcal{Q}(r,\theta_0^{\prime})$ A coefficient in the Legendre-Bessel series method of field computations. It is defined by formula (I-28).

$\mathcal{R}$ The outer bowl radius of the inner surface of the type "A" meter.

$\mathcal{R}^{\rho}$ The maximum magnitude of the $\mathcal{R}^{\rho}$th harmonic of the spectrum.

$\mathcal{S}(r,\theta_0^{\prime})$ a coefficient in the Legendre-Bessel series method of field computations. It is defined by formula (I-13).

$\mathcal{S}^{\rho}$ The inner bowl radius of the inner surface of the type "A" meter.

$\mathcal{S}^{\rho}$ The inner dimension of the inner surface of a rectangular waveguide.

$\mathcal{T}$ The permeability when applied to a material like bismuth, where $\mu<1$.

$\mathcal{T}^{\rho}$ The permeability when applied to a material like bismuth, where $\mu<1$.

$\mathcal{U}$ The radius of the most distant point on the Lagrangian radiating

$G(\theta)$	The E plane field pattern of an E plane flared sectoral horn determined by theory or by experimental investigation
H	A Hankel function.
j	$\sqrt{-1}$
k	The free space wave propagation constant.
k_1	A design constant used in the design of the type "A" horn.
M	A substitute variable defined by Equation (42) to facilitate algebraic manipulation.
M_1	Area excluded from the E plane array factor integration.
n	Any integral numerical value.
N1	Area included in the E plane array factor integration.
N_x	A diffraction integral defined by Equation (A-4).
N_y	A diffraction integral defined by Equation (A-5).
P,p	A point of field measurement.
r'	The distance from the origin of the coordinates to a point on the radiating aperture.
r_1	The radial distance from the origin of the coordinates to the inner radius of the aperture.
r_2	The radial distance from the origin of the coordinates to the outer radius of the aperture.
Δr	The radial aperture distance
R	The distance from the origin of the coordinates to a point of field measurement.
s	Refers to the aperture surface.
t	The dimension of the parallel plane filter sections in the direction of wave propagation.

$\mathbb{C}(\mathbb{N})$ The 2 plane field pattern of an N plane flared monopole

determined by numerical integration

Γ A Gamma function.

$\sqrt{-1}$

$\mathbb{R}$ The Real-axis Projective Hyperplane.

$\mathbb{R}^3$ A Hedgehog manifold in Euclidean 3 space.

$\mathbb{M}$ A manifold evaluator defined by Algorithm (qu) to Quantitate

algebraic manifolds.

$\mathbb{R}^1$ Area enclosed from the 1 Sphere using Jordan Integration.

$\mathbb{R}$ Any Integral algebraic value.

$\mathbb{R}^3$ Area enclosed in the 3 plane using Jordan Integration.

$\mathbb{R}^{\mathbb{R}}$ A differentiable topological deficit by Definition (4-5).

$\mathbb{R}^2$ A differential Topological deficit by Definition (1-1).

$\mathbb{R}^3$ 3 paths for Field measurement.

$\mathbb{R}^1$ The distance from the origin of the coordinates to a point on

the realizable locations.

$\mathbb{R}^3$ The radial distance from the origin of the coordinates to the

inner radius of the sphere.

$\mathbb{R}^3$ The radial distance from the origin of the coordinates to the

outer radius of the sphere.

$\mathbb{R}^3$ The radial spherical distance.

$\mathbb{R}$ The distance from the origin of the coordinates to a point of

field measurement.

$\mathbb{R}$ Refers to the hyperbole surface.

$\mathbb{R}$ The dimension of the partial ruled filter matrix in the

direction of wave propagation.

T	The power transmitted through a filter grating in per cent.
v	The center to center spacing of parallel wires or parallel planes.
x	The coordinate direction in the E plane and normal to the H plane.
X'	The coordinate direction in the E plane and on the plane which contains the aperture surface.
$\Delta x'$	The aperture distance in the x' direction
x_o	The aperture distance in the x direction.
y	The coordinate direction in the H plane, normal to the E plane and defined by Figure II.
y_o	Half the distance along the cord of the arc of the aperture. (Figure IV).
y'	The coordinate direction in the H plane, on the plane which contains the aperture surface, and defined by Figure IV.
z	The coordinate direction normal to both x and y, and forms a right handed orthogonal coordinate system of sequence, (x,y,z).
α	The attenuation constant.
β	The angle of the major axis of elliptical polarization from the ϕ direction.
Γ	The reflection coefficient.
Δ	An incremental quantity.
δ	A differential quantity
e	The base of natural logarithms.
θ	The polar angle from the z axis.
λ	Free space wavelength.
μ	The permeability of free space.

π	3.1416.
ρ	The length of a sectoral horn.
$\sum$	Summation.
ϕ	The longitudinal angle which has the x axis as the origin.
ϕ'	The longitudinal angle for points in the xy or aperture plane.
ϕ_o	The total flare angle of either type "A" or type "B" horns.
ω	2π (frequency)

I INTRODUCTION

Concurrent with the practical employment of microwave frequencies, extensive theoretical and experimental work has been accomplished in the field of using electromagnetic horns as antennas.[4] The theoretical computations indicate that narrow beam sectoral horns may be constructed by increasing the flare angle and the radius. In the theoretical part of this work the aperture diffraction method of computing radiation fields is currently the most practical procedure.[1][2][3] If it were possible to determine the current distribution on the interior and exterior surfaces of the horn, the fields could be computed directly; but since this is not known, the aperture diffraction field method must be employed. However, when the computed radiation patterns of sectoral horns are compared with the radiation patterns obtained experimentally, there is only general agreement. There are three reasons for the disagreement in detail in the field patterns:

1. The theory neglects the current on the outside walls of the horn.
2. The theory neglects the higher mode fields at the aperture.
3. Phase error effects have been neglected in the field computations. The aperture was considered to be a constant phase radiating surface in a plane.

Phase error effects cause the main lobe of a horn of constant flare angle to undergo changes in width and structure as the horn length is increased.[4][5] On the basis of experiments, optimum dimensions for E plane and H plane electromagnetic horns have been determined.

3. [illegible]

[illegible] with the general equations of antenna theory, otherwise theoretical and experimental work has been correlated in the field of radio electromagnetic lenses in antennas.[4] The theoretical computations indicate that certain types of metallic lenses may be constructed by increasing the Fluid angle and the radius. In the theoretical part of this work the equation differential method of computing radiation fields is carried out to the most practical procedure.[3][5][6] If it were possible to determine the entire distribution on the interior and exterior surfaces of the lens, the fields could be computed directly but since this is not known, the aperture diffraction field method must be employed. However, when the complex reflecting patterns of metallic lens are compared with the reflection patterns obtained experimentally, there is only general agreement. There are three reasons for the disagreement in detail in the field patterns

1. The theory neglects the current on the outside walls of the lens.
2. The theory neglects the higher mode fields at the aperture.
3. There are effects have been neglected in the field computations. The aperture was considered to be a rectangular plane reflecting surface in a plane.

These error effects cause the main lobe of a lens of rectangular Fluid angle to reduce in width and structure as the wave length is increased.[4][5] On the basis of experiments, optimum dimensions for a given and a finite transmitting area have been determined.

See Figure VIII.[6]

In order to obtain a narrow beam horn antenna with moderate side lobes, it is necessary to resort to excessively long radius sectoral horns of small flare angles or to employ dielectric lenses or metal plate lenses. However, dielectric lenses complicate the impedance matching problems and cause power loss,[7] and metal plate lenses are frequency sensitive devices.[8] Thus, in order to obtain a narrow beam electromagnetic horn with low side lobes it is necessary to compromise one of the three advantages of horn antennas; small theoretical size, minor matching problems with low power loss, and wide band operation.

It is the object of this thesis to build an antenna with a constant phase radiating surface, experimentally and theoretically determine its radiating characteristics, experimentally determine its impedance characteristics, investigate methods of pattern improvement, and present a design procedure for other investigators to follow. The horn will be designed to be as insensitive to frequency changes as is possible and to suppress higher mode fields before they arrive at the aperture.

This could be accomplished by employing an antenna of design type "A," Figure I or design type "B" Figure V. These antennas employ the optical principle that electromagnetic waves emanating from a point source have a constant phase front which is determined by equal geodesic distances (or mean path distances) measured in a radial direction from the point source.

It is apparent that the radiating surface is no longer rectangular in shape as in the case of the rectangular guide sectoral

horn, but is now a circular arc. This introduces difficulties in solving the aperture diffraction integrals and handling the cross components (H plane components) of polarization. In the process of solving the phase difficulty and minimizing surface current effects and higher mode field effects, the problem of cross polarization has been created.

II PROCEDURE

Development of Theoretical Field Pattern Expressions

The aperture of the laterally radiating electromagnetic horn is formed along the arc of a circle. An assumption was made that the field will vary sinusoidally over the arc of the aperture and that the fields are polarized in the radial direction. It was now possible to solve the aperture diffraction integrals to obtain the fields in space. The array factor describing the aperture geometry and illumination could be easily integrated for angles of flare of the form $\frac{\pi}{n}$, n an integer. A change of variable was made which had the effect of considering the straight line equivalent of the aperture. The results for the horn design in Figure V are:*

$$E_x \alpha + 0.00728 \frac{\text{Sin } (ky_o \text{ Sin } \theta)}{\text{Sin}^3 \theta} - 0.038 \frac{\text{Cos } (ky_o \text{ Sin } \theta)}{\text{Sin}^2 \theta} \qquad (1)$$

An assumption of a linear equivalent source in the H plane was made to obtain an approximate field pattern for the E plane polarized, H plane field pattern for any value of r_{av} or ϕ_o. If the linear equivalent source in the H plane is assumed to have an E plane polarized field of

$$E_{sx} = B_1 \text{ Cos } \frac{\pi y}{2y_o} \text{ Cos } \frac{\phi_o y}{2y_o} \qquad (2)$$

which would be the approximate fields resulting when the fields in the aperture were projected into the H plane, (See Figure IV for the definition of geometrical terms.), the resulting H plane field pattern was

---

* See Appendix, Section B.

Interaction of Plane Wave Light Scattering Harmonics

The equation of the Laguerre resolving electromagnetic wave in terms along the axis of a cylinder, as investigated and that the field exit and simultaneously over the set of the equations and that the fields are polarized in the radial direction. It will now possible to solve the Laplace differential equation to obtain the fields in terms. The study factor respectively the electric potential and illumination might be easily integrated for angles of class of the form $\frac{\pi}{n}$, n an integer. A change of variable was made which was the effect of considering the straight line equivalent of the spectrum. The results for the form display in Figure 7 were*

$$E_{\theta}^{m} = \frac{\sin(n\beta)\cos\phi}{\sin\beta} - \frac{\cos(n\beta)\sin\phi}{\sin^{2}\theta} \qquad (1)$$

An examination of a Taylor equivalent series in the 0 plane was made to obtain an approximate field pattern for the 2 plane polarized, 4 plane field pattern for any value of ϕ_{m} or ϕ_{o}. If the linear equivalent nature in the 2 plane is assumed to have an 2 plane polarized field of

$$E_{\theta}^{m} = E_{o}^{2} \cos\frac{\pi\phi}{\phi_{o}} \sin\frac{\pi\theta}{\theta_{o}} \qquad (2)$$

which would be the approximate field resulting when the fields in the spectrum were projected into the 2 plane. Since Figure 2 for the variations of resonant tones, the resulting 2 plane field patterns are

---

* See Appendix, Section C.

determined to be:

$$E_x = \frac{jk\,\varepsilon^{-jkR}}{4\pi R}(1+\cos\theta)\,B\,x_o y_o \left\{ \sin\frac{\left[\frac{(\pi+\phi_o)}{2y_o} - k\sin\theta\right]y_o}{\left[\frac{(\pi+\phi_o)}{2y_o} - k\sin\theta\right]y_o} + \right.$$

$$+ \sin\frac{\left[\frac{(\pi+\phi_o)}{2y_o} + k\sin\theta\right]y_o}{\left[\frac{(\pi+\phi_o)}{2y_o} + k\sin\theta\right]y_o} + \sin\frac{\left[\frac{(\pi-\phi_o)}{2y_o} - k\sin\theta\right]y_o}{\left[\frac{(\pi-\phi_o)}{2y_o} - k\sin\theta\right]y_o} +$$

$$\left. + \sin\frac{\left[\frac{(\pi-\phi_o)}{2y_o} + k\sin\theta\right]y_o}{\left[\frac{(\pi-\phi_o)}{2y_o} + k\sin\theta\right]y_o} \right\} \qquad (3)$$

However, the diffraction integrals may be integrated directly if the geometry of Figure II is employed and the simplifying assumption is made that $(r_1 - r_2)$ is a great deal less than the average radius of the aperture. The assumptions of the fields at the aperture are:

$$E_{ax} = B_1 \cos\frac{\pi\phi'}{\phi_o}\cos\phi' \qquad (4)$$

$$E_{ay} = B_1 \cos\frac{\pi\phi'}{\phi_o}\sin\phi' \qquad (5)$$

resulting in the field patterns in space being given by*

$$E_{p\theta} = \frac{jkB_1\phi_o r_1 \Delta r\,\varepsilon^{-jkR}}{16\pi R}(1+\cos\theta)\left\{\left[\cos\phi\left[A(0,\phi_o)\,J_o(kr_1\sin\theta) + \right.\right.\right.$$

$$\left. + \sum_{n=1}^{\infty} J_n(kr_1\sin\theta)\,A(n,\phi_o)\,B(n,\phi)\right] - j\left[\sin\phi\;\; C(0,\phi_o)\right.$$

$$\left.\left.\left. J_o(kr_1\sin\theta) + \sum_{n=1}^{\infty} J_n(kr_1\sin\theta)\,C(n,\phi_o)\,D(n,\phi)\right]\right\}\right] \qquad (6)$$

---

*See Appendix, Section B.

determined to be:

$$\left\{ \frac{\left[\frac{\partial^2}{\partial r^2} + \nu \frac{\partial}{\partial r} \right] J_\nu}{\left[\frac{\partial^2}{\partial r^2} - \frac{(\nu-1)}{r^2} \right] J_\nu} \right\}_{r=a} = \frac{\left[\frac{\partial^2}{\partial r^2} + \nu \frac{\partial}{\partial r} \right] J_\nu}{\left[\frac{\partial^2}{\partial r^2} - \frac{(\nu-1)}{r^2} \right] J_\nu} \cdot \frac{\left[\frac{\partial^2}{\partial r^2} - \nu \frac{\partial}{\partial r} \right] J_\nu}{\left[\frac{\partial^2}{\partial r^2} - \frac{(\nu-1)}{r^2} \right] J_\nu} \cdot \frac{\left[\frac{\partial^2}{\partial r^2} + \nu \frac{\partial}{\partial r} \right] J_\nu}{\left[\frac{\partial^2}{\partial r^2} - \frac{(\nu-1)}{r^2} \right] J_\nu} \cdot \frac{\left[\frac{\partial^2}{\partial r^2} - \nu \frac{\partial}{\partial r} \right] J_\nu}{\left[\frac{\partial^2}{\partial r^2} - \frac{(\nu-1)}{r^2} \right] J_\nu}$$

$$= \left\{ \frac{\left[\frac{\partial^2}{\partial r^2} + \nu \frac{\partial}{\partial r} \right] J_\nu}{\left[\frac{\partial^2}{\partial r^2} - \frac{(\nu-1)}{r^2} \right] J_\nu} \right\}^4 \tag{2}$$

However, the diffraction integrals may be integrated directly if the geometry of Figure 22 is employed and the cylindric symmetries it owns that $(v^2 - x^2)$ is a root; that then the general value of the expression is

$$E^{pq} = E^{pq} \cos \frac{\pi}{2} \sin \tag{a}$$

$$I^{pq} = I^{pq} \cos \frac{\pi}{2} (1) \tag{1}$$

resulting in the final solution in terms only of

$$E^{pq} = \frac{}{} (1 + \cos \left[\cos \left[\right] \right] + \tag{b}$$

$$+ \sum \; \cos \left[\right] \left[\right] \tag{3}$$

$$E_{p\phi} = \frac{-jkR_1\phi_o r_1 \Delta r\, e^{-jkR}}{16\pi R}(1+\cos\theta)\Big[\sin\phi\Big\{A(0,\phi_o)\ J_o\ (kr_1\sin\theta) +$$

$$+\sum_{n=1}^{\infty} J_n(kr_1\sin\theta)\ A(n,\phi_o)\ B(n,\phi)\Big\} + j\cos\phi\Big\{C(0,\phi_o)$$

$$J_o(kr_1\sin\theta) + \sum_{n=1}^{\infty} J_n(kr_1\sin\theta)\ C(n,\phi_o)\ D(n,\phi)\Big\}\Big] \qquad (7)$$

Formula (3) was derived on the basis that the E plane polarized H plane field pattern is primarily a function of the chord of the arc of the aperture. It was possible to reason that the field pattern is dependent on a product of a function of the flare angle and a function of the radius. Formulas (7) and (8) illustrate that the pattern is a summation of an infinite series of such products. This permits an infinite number of combinations of ϕ_o and r_1 to be employed to obtain a given beamwidth.

The Design and Fabrication of the Horn

To obtain an aperture of given dimensions two parameters were available, the radius of the sectoral section and the flare angle. Ninety degrees was arbitrarily chosen as the initial angle of flare since this presented an aperture exhibiting measurable H plane polarization and gave a relatively wide aperture for a fixed sectoral radius. Also, reducing the flare angle would be relatively easy should this be desired. A sectoral radius was chosen to give a chord length of 16.7 λ (for λ = 3.2 cm.) in order to investigate the possibilities of obtaining a constant phase across a wide aperture. The ninety degree bend at the end of the sectoral section was designed from empirical data contained in ADRDE Research Report No. 129.[33] The laterally radiating

horn type "B" (Figure V) was fabricated by the Coppersmith Shop of the Boston Naval Shipyard under close supervision by the thesis members.

Field Pattern Measurement Procedure

Field pattern measurements were taken for five conditions of horn operation.

1. The uncompensated horn as described by Figure V.
2. The horn with a parallel plane filter located 0.318 cm. from the aperture.
3. The horn with a flare consisting of 0.318 cm. brass rod 9.6 cm. long separated by 0.635 cm. on centers in the H plane and bent to form a flare of 40° in the E plane.* (80° total sector angle)
4. The horn with 40° E plane flare and a parallel plane filter located 0.079 cm. from the aperture.**
5. The horn with 40° E plane flare and a parallel wire filter located 0.079 cm. from the aperture.**

The field patterns were measured on an audio automatic antenna pattern recorder similar to that described in Reference (34). The pen positioning system is given in block diagram form in Figure VI and the overall test setup is given in Figure VII. The X band radar transmitter could transmit either H plane polarized or E plane polarized electromagnetic energy. H plane and E plane patterns were taken by shifting either the polarization of the transmitter or the physical position of the horn antenna. The four principal patterns were taken for horn conditions 1, 2, 3, 4, but only the H plane polarized, H plane

---

* See Photograph, Figure .
** See Figure X.

** See Figure X.

field pattern was taken for Condition 5. The frequency of the transmitter was varied in Condition 1 in order to determine the sensitivity of the pattern to frequency changes.

Evaluation of the E Plane Polarized E Plane Field Pattern When E Plane Flare Is Added to the Horn

It was important to be able to make an engineering estimate of the change in the field pattern when E plane flare was added to the horn. The E plane polarized E plane field pattern of an E plane sectoral horn determined either theoretically[26][36] or experimentally[35] was designated G(θ). The aperture was then considered to be a continuous array of infinitesimal E plane sectoral horns. The array factor for this continuous array would be $E_{p\theta}(\theta\ )$ in Equation (6) evaluated for $\phi = 0^{\circ}$. The resulting E plane pattern then became:

$$E_{\theta,2} = G(\theta)\ E_{p\theta}\ (\theta,0) \qquad (8)$$

The resulting field pattern may be plotted by adding decibel values. A comparison plot of the computed horn field pattern obtained in this manner with the measured horn field pattern was plotted on Figure XXXI.

Impedance Measurement Procedure

Voltage standing wave ratio measurements were made for the various horn designs using a standard slotted section of wave guide, an amplitude modulated signal, a square law crystal detector, and an ECA 16EA amplifier to measure the output. A 2K39 klystron furnished power. The probe depth was adjusted for minimum penetration and tuned for each frequency.

Measurements were made of the VSWR in the guide. Positions of the minima were determined for the horn terminated in space, with a

short circuit at the aperture, and with a short circuit at the throat. All frequency measurements were in a band from 8600-9400 mcps.

III RESULTS

The Principal Field Patterns of the Laterally Radiating Electromagnetic with No Flare or Filters Added

The results of the field pattern tests of the horn are given by the solid curves of Figures XII, XIII, XIV, and XV. The E plane polarized H plane field pattern reveals that a 4.33° half power beam with -20 db. side lobes was achieved, but also that there is some phase distortion near the right side lobe and minor asymetries in the pattern. The H plane polarized E plane pattern, which theoretically should be zero for all values of θ, shows negligible values of field strength. The E plane polarized, E plane field pattern gives a 24° half power beam width. The "side lobes" are -7.8 db. and a generally ragged field pattern for values of θ away from the "main lobe" is obtained. In the H plane polarized H plane field pattern the two major lobes are slightly asymetrical and the rest of the pattern is highly asymetrical in that the third side lobe is missing on one side. This "cross component" of polarization has a peak value of between -10 db. and -12 db. in accordance with minor deflections of the aperture of the horn.

The Results of Varying Frequency on the E Plane Polarized H Plane Field Pattern

Figure XVI indicates a slight increase in half power beamwidth with frequency and a reduction in the peak power density of the first side lobes together with considerable distortion of the field pattern beyond the first side lobe. However, the general symmetry of the main and side lobes is maintained.

The Results of Comparing the Experimentally Determined Values with the Computed Values of the Field Patterns in the H Plane

The Polarized Plane Patterns of the Invention (E) Using Perpendicularly Oriented Plane or Circular Dipoles

The results of the Plane pattern tests of the Sets are given by the solid curves of Figures III, IIII, IV, and V. The E plane pattern of the Plane Dipole systems extends from a [illegible] half power beam width of 81. Side lobes are evident, but also first nulls in these plane directions near the right side lines and minor departures in the pattern. The H plane polarized E plane pattern, which theoretically should be zero for all values of θ, shows negligible values of Plane electric. The E plane polarized, H plane Dipole pattern plots a 64° half power beam width. The "side lobes" are -17.5 db. and a generally negligible Plane polarization for values of θ near Zero (the "main lobe" is displaced. In the H plane polarized E plane/field pattern the two major lobes are slightly asymetrical and the nulls of the pattern is slightly displaced in that the total side lobe is reduced on one side. This "phase compensation" of polarization for a pair values of θ, and π - θ, is in accordance with minor deficiencies of the simplicity of the theory.

The Results of Similar Measures on the E Plane Polarized H Plane Plane Patterns

Figure VII illustrates a slight departure in half power beamwidth with frequency and a reduction in the peak power density of the first side lobes appears with consideration displacement of the first pattern toward the first side lobe. However, the general character of the side and side lobes is maintained.

The Results of Measures the Perpendicular Polarized Patterns with the Longitud Values of the Plane Dipoles in the E Plane

The computed values determined by the linear equivalent source method and the Fourier-Bessel series method are plotted on Figures XVII and XVIII. Formula (1) gives close corellation with measured H plane field patterns but it is not included in the results section. There is excellent agreement between the experimentally determined and theoretically determined values of the half power points of the main lobe in the case of the E plane polarized field pattern. In the case of the H plane polarized field pattern the peak power points and the half power points of the two main lobes are in agreement with the computed values. In the case of the E plane polarized fields, the Fourier-Bessel series gives a good indication of the angle at which the first side lobe will appear. The linear equivalent source method gives a better approximation of the magnitude of the side lobes.

A Comparison of the Principal Field Patterns of the Laterally Radiating Electromagnetic Horn with and without a Parallel Plane Filter

The parallel plane filter performed its function of eliminating the H plane polarization from the radiation field. A loss of peak power density of 1.3 db. together with a distortion of the side lobe pattern was experienced for the H plane pattern. The E plane pattern was also distorted in the side lobes, but there was no change in half power beam width and only a slight change in the relative peak power density of the "side lobes."

The Results of Adding a 40° E Plane Flare to the Horn

Figures XIX, XX, XXI, and XXII show the results of adding a 40° E plane flare to the horn. Minor alterations to the negligible H plane polarized E plane field pattern results. The symmetry of the E plane polarized H plane pattern was improved somewhat and minor

alterations occurred in the main lobes. In the E plane polarized H plane field pattern a slight increase in half power beam width occurred when the flare was added and the peak power density of the first side lobes dropped to -22.2 db. A significant change occurred in the E plane polarized E plane field pattern. The half power beamwidth increased from 24° to 31°; the overall beam pattern is narrower; and the side lobes are nonexistent. "Side lobes" at angles less than -30° and at angles more than +30° have been thoroughly suppressed.

The Effect of Adding a Parallel Plane Filter to the Horn with 40° E Plane Flare

Figures XXIII, XXIV, XXV, and XXVI demonstrate the results of adding a parallel plane filter at the aperture of the horn with a 40° E plane flare. A minor change in the negligible H plane polarized E plane field pattern resulted. The parallel plane filter reduced the "cross component" field pattern 19 db. causing minor variations in the E plane polarized E plane field pattern. For the E plane polarized H plane field pattern the first side lobes occur at -27.8 db.; the second side lobes have a peak value of -24.5 db. and are asymmetrical. A slight increase of half power beam width from 4.5° to 4.7° also occurred.

The Effect of Adding a Parallel Wire Filter to the Horn with E Plane Flare

Approximately a -10 db. attenuation was achieved in reducing the "cross component" of polarization by using the parallel wire filter. See Figure XXVII.

A Comparison of the Computed and Measured Field Patterns in the E Plane

Figure XXX is a correlation of computed and measured values of the E plane polarized, E plane field pattern and includes a graph of the

computed values of phase shift encountered when the origin of the flared section is employed as the origin of the coordinates. The slope of the phase shift curve indicates that the center of radiation of this particular horn is 32.6 cm. from the origin of the coordinates and on the x axis.

Figure XXXI is a correlation of computed and measured values for the E plane pattern of the horn with 40° E plane flare.

A Plot of Ellipticity of the Uncompensated Electromagnetic Horn

Figure XXVIII is a plot of the theoretical ellipticity of the H plane field pattern. Also included is a plot of the measured magnitudes with theoretical phase values for positive values of θ. $(\frac{\pi}{2} = \emptyset)$. Figure XXIX is a plot of the theoretical ellipticity and measured magnitudes with theoretical phase values for negative values of θ. $(\frac{\pi}{2} = \emptyset)$. The magnitudes of the power densities in these elliptically polarized waves is given adjacent to the plotted points. These graphs include only the fields in the main lobe located on the H plane. The derivation of the use of the Smith Chart for this purpose is given in Reference (13).*

Impedance Measurements

The results of VSWR tests made for the five horn conditions are shown on Smith charts. See Figures XXXII through XXXVII.

---

* See Appendix, Section B for detailed interpretation.

---

* See especially Section 5 for detailed discussion.

IV DISCUSSION OF RESULTS

Evaluation of the Accuracy of Fabrication of the Laterally Radiating Horn

The asymmetries in the side lobe patterns in the H plane fields indicate that highly refined mechanical symmetry did not exist. Although minor phase distortions were present in all of the H plane patterns, correlation may be achieved between an ideally constructed horn and the horn employed. Therefore, the fabrication accuracy of the horn is considered adequate for the purpose of this thesis. Improvement in performance might be achieved by electroforming the horn or constructing the horn of aluminum alloy with an improved horn bend shown in Figure XI in order to improve structural rigidity.

A further measure of the accuracy of fabrication may be made by considering the H plane polarized, E plane field pattern in Figure XIII. The theoretical horn would give a zero field pattern for all values of θ, and in the physical horn all field strengths are negligible. Therefore, a high degree of symmetry was present in the horn and the horn was properly oriented with respect to the incident wave polarization for the field pattern tests.

Evaluation of the Methods of Computing Field Patterns

The change of variable method employed to obtain the H plane field pattern for the E plane polarized wave is highly accurate for obtaining field patterns of a sectoral horn that has a 90° H plane flare at the throat. The expression is easy to evaluate. However, it is limited to $\frac{\pi}{n}$ sectors. In general design work Formula (3) is recommended as a first approximation to the field pattern. Formula (3) has the advantage that any value of flare angle or radius may be employed to give

IV. Discussion of Results

Evaluation of the Accuracy of Synthesis of the Magnetic Deflection Yoke

The asymmetries in the six lobe patterns in the 3 plane field indicate that highly refined mechanical symmetry did not exist. Although stator plane d exercises were provided in all of the 3 planes, correlation may be attained between mechanically constructed yoke and the ones analyzed. Therefore, the fabrication accuracy of the yoke is considered adequate for the purpose of this thesis. Improvements in performance might be achieved by electronically the yoke or mechanically the bore of electron gun with an improved cross sectional figure if in order to improve structural rigidity.

A further examination of the accuracy of fabrication may be made by considering the 3 plane polarized, 3 plane field patterns in Figure III. The theoretical zero would give a zero field pattern for all values of θ, and in the ideal zero all field sensings are negligible. Therefore, a high degree of symmetry was present in the bore and the yoke was primarily evaluated with respect to the deflection wave polarization for the field pattern tests.

Evaluation of the Methods of Theoretical Field Patterns

The change of variable method employed to obtain the 3 plane field patterns for the 3 plane polarized wave is highly accurate for obtaining field patterns of a magnetic bore that has a 90^0 plane flux at the throat. The computation is easy to evaluate. However, it is limited to $\frac{\pi}{n}$ radians. In general design work formula (1) is recommended as a first approximation to the field patterns. Formula (2) has the advantage that any value of flare angle or radius may be employed to give

the designer a first estimate of physical size. Figure XVII indicates the linear equivalent source method gives accurate values for the half power beam angles and good results on the magnitudes and angles of the first side lobes.

The derivation of the Fourier-Bessel series method involved slightly more refined approximations. It gives the field pattern for all values of R, ϕ, and θ, and it should prove to be the most useful method of computing the fields. As a result the calculated ellipticity of a given design of laterally radiating horn may be plotted by Smith chart methods.[12] The Fourier-Bessel series gives accurate results for the half power beam width and the angle of the first side lobe together with approximate values for the magnitude of the first side lobe and angle of the second side lobe.

Formulas (6) and (7) appear to be formidable infinite series of Bessel functions, but a study of the coefficients given in formulas (A-52), (A-55), A-58) and (A-59) reveals that the values of $A(n,\phi_o)$ and $C(n,\phi_o)$ decrease very rapidly with increasing values of n if ϕ_o is a moderately large value. For this antenna the computations did not involve Bessel functions of order greater than 6. In addition, no single field computation involved more than 4 orders of Bessel functions. The references[10][11] had sufficient values of the arguments of the Bessel functions and $\frac{\sin \beta}{\beta}$ tabulated that all sectors of the H plane field patterns that were of interest could be plotted. The H plane polarized, E plane field pattern becomes zero both through symmetry considerations and through the coefficients of the Bessel functions being all zero.

In the E plane polarized, E plane field pattern a sector of

only 40° could be plotted since the Harvard University series of tabulated values of Bessel functions did not list arguments greater than 20. When a more complete set of Bessel function values is published, it will be possible to plot the E plane field patterns through a wider range of θ values. About five hours of concentrated effort is required to evaluate one field pattern.

The Effectiveness of the Parallel Plane Filter

That the parallel plane filter employed was overdesigned is evidenced by the absence of any H plane polarized radiation in Figure XV. It was designed this way in order to determine the affect on horn impedance when the cross components of polarization were completely eliminated. Because the elimination of the cross components was accompanied by only minor decreases in peak power and minor variations in the field patterns of the E plane polarized components, the parallel plane filter is considered to be an excellent method of reducing or eliminating elliptical polarization.

The Results of Varying Wavelength in the Field Pattern Tests

The laterally radiating horn is not a frequency sensitive radiator. See Figure XVI. This was demonstrated by the results of varying the frequency from 9380 mcps. to 8860 mcps. The expected phenomena occurred. The half power beam width increased slightly due to a reduction in aperture length measured in wavelengths. The angle at which the first side lobe occurs increased and the magnitude of the first side lobe decreased. There was no large alteration of the shape of either the major lobe or the first side lobes. Correlation of the results in the side lobes beyond the first side lobe depends upon a knowledge of the variation of the horn geometry from the ideal and a knowledge of the magnitudes of the higher mode fields.

A Comparison of the Laterally Radiating Horn Field Patterns with and without a Parallel Plane Filter

A check on the symmetry of the assembly of horn and filter from the field patterns reveals that symmetry is good.*

That the peak power of the main lobe is down 1.5 db. indicates that the filter at this frequency is reflecting or dissipating some of the energy. That higher mode fields are being generated in the filter is evidenced by the fact that the half power beam width is increased in the E plane and the side lobes are more prominent and at a higher level. See Figure XII. This particular point could be a field for further investigation, but the ragged side lobe pattern with high peak values indicates that not much could be gained from an attempt to improve the E plane pattern through the use of this filter alone.

Computed Design Curves

Although the design formulas were developed in this thesis, there was not enough time available to compute a full set of laterally radiating horn design curves because experimental verification of the theoretical field patterns was essential. Further investigation of the H plane half power beam widths, the H plane side lobe level, the E plane half power beam widths, the peak level of cross polarization, and the ellipticity of the fields in Fraunhofer space would be desirable. Plots of these quantities could be made as functions of $\frac{r_1}{\lambda}$ and ϕ_0. If the ellipticity is of interest, plots of this quantity could be made on the Smith chart.(12) Some of the points could be verified experimentally.

---

* The H plane polarization was practically eliminated from the radiation fields.

Dynamics of the Internal Solitons with a Passive Plane Failure

A study of the dynamics of the internal solitons with a passive plane failure [2] [3] [4] [5] [6] [7] [8] [9] [10] [11] [12] [13] [14] [15] [16] [17] [18] [19] [20] [21] [22] [23] [24] [25] [26] [27] [28] [29] [30] [31] [32] [33] [34] [35] [36] [37] [38] [39] [40] [41] [42] [43] [44] [45] [46] [47] [48] [49] [50] [51] [52] [53] [54] [55] [56] [57] [58] [59] [60] [61] [62] [63] [64] [65] [66] [67] [68] [69] [70] [71] [72] [73] [74] [75] [76] [77] [78] [79] [80] [81] [82] [83] [84] [85] [86] [87] [88] [89] [90] [91] [92] [93] [94] [95] [96] [97] [98] [99] [100] [101] [102] [103] [104] [105] [106] [107] [108] [109] [110] [111] [112] [113] [114] [115] [116] [117] [118] [119] [120] [121] [122] [123] [124] [125] [126] [127] [128] [129] [130] [131] [132] [133] [134] [135] [136] [137] [138] [139] [140] [141] [142] [143] [144] [145] [146] [147] [148] [149] [150] [151] [152] [153] [154] [155] [156] [157] [158] [159] [160] [161] [162] [163] [164] [165] [166] [167] [168] [169] [170] [171] [172] [173] [174] [175] [176] [177] [178] [179] [180] [181] [182] [183] [184] [185] [186] [187] [188] [189] [190] [191] [192] [193] [194] [195] [196] [197] [198] [199] [200] [201] [202] [203] [204] [205] [206] [207] [208] [209] [210] [211] [212] [213] [214] [215] [216] [217] [218] [219] [220] [221] [222] [223] [224] [225] [226] [227] [228] [229] [230] [231] [232] [233] [234] [235] [236] [237] [238] [239] [240] [241] [242] [243] [244] [245] [246] [247] [248] [249] [250] [251] [252] [253] [254] [255] [256] [257] [258] [259] [260] [261] [262] [263] [264] [265] [266] [267] [268] [269] [270] [271] [272] [273] [274] [275] [276] [277] [278] [279] [280] [281] [282] [283] [284] [285] [286] [287] [288] [289] [290] [291] [292] [293] [294] [295] [296] [297] [298] [299] [300] [301] [302] [303] [304] [305] [306] [307] [308] [309] [310] [311] [312] [313] [314] [315] [316] [317] [318] [319] [320] [321] [322] [323] [324] [325] [326] [327] [328] [329] [330] [331] [332] [333] [334] [335] [336] [337] [338] [339] [340] [341] [342] [343] [344] [345] [346] [347] [348] [349] [350] [351] [352] [353] [354] [355] [356] [357] [358] [359] [360] [361] [362] [363] [364] [365] [366] [367] [368] [369] [370] [371] [372] [373] [374] [375] [376] [377] [378] [379] [380] [381] [382] [383] [384] [385] [386] [387] [388] [389] [390] [391] [392] [393] [394] [395] [396] [397] [398] [399] [400] [401] [402] [403] [404] [405] [406] [407] [408] [409] [410] [411] [412] [413] [414] [415] [416] [417] [418] [419] [420] [421] [422] [423] [424] [425] [426] [427] [428] [429] [430] [431] [432] [433] [434] [435] [436] [437] [438] [439] [440] [441] [442] [443] [444] [445] [446] [447] [448] [449] [450] [451] [452] [453] [454] [455] [456] [457] [458] [459] [460] [461] [462] [463] [464] [465] [466] [467] [468] [469] [470] [471] [472] [473] [474] [475] [476] [477] [478] [479] [480] [481] [482] [483] [484] [485] [486] [487] [488] [489] [490] [491] [492] [493] [494] [495] [496] [497] [498] [499] [500] [501] [502] [503] [504] [505] [506] [507] [508] [509] [510] [511] [512] [513] [514] [515] [516] [517] [518] [519] [520] [521] [522] [523] [524] [525] [526] [527] [528] [529] [530] [531] [532] [533] [534] [535] [536] [537] [538] [539] [540] [541] [542] [543] [544] [545] [546] [547] [548] [549] [550] [551] [552] [553] [554] [555] [556] [557] [558] [559] [560] [561] [562] [563] [564] [565] [566] [567] [568] [569] [570] [571] [572] [573] [574] [575] [576] [577] [578] [579] [580] [581] [582] [583] [584] [585] [586] [587] [588] [589] [590] [591] [592] [593] [594] [595] [596] [597] [598] [599] [600] [601] [602] [603] [604] [605] [606] [607] [608] [609] [610] [611] [612] [613] [614] [615] [616] [617] [618] [619] [620] [621] [622] [623] [624] [625] [626] [627] [628] [629] [630] [631] [632] [633] [634] [635] [636] [637] [638] [639] [640] [641] [642] [643] [644] [645] [646] [647] [648] [649] [650] [651] [652] [653] [654] [655] [656] [657] [658] [659] [660] [661] [662] [663] [664] [665] [666] [667] [668] [669] [670] [671] [672] [673] [674] [675] [676] [677] [678] [679] [680] [681] [682] [683] [684] [685] [686] [687] [688] [689] [690] [691] [692] [693] [694] [695] [696] [697] [698] [699] [700] [701] [702] [703] [704] [705] [706] [707] [708] [709] [710] [711] [712] [713] [714] [715] [716] [717] [718] [719] [720] [721] [722] [723] [724] [725] [726] [727] [728] [729] [730] [731] [732] [733] [734] [735] [736] [737] [738] [739] [740] [741] [742] [743] [744] [745] [746] [747] [748] [749] [750] [751] [752] [753] [754] [755] [756] [757] [758] [759] [760] [761] [762] [763] [764] [765] [766] [767] [768] [769] [770] [771] [772] [773] [774] [775] [776] [777] [778] [779] [780] [781] [782] [783] [784] [785] [786] [787] [788] [789] [790] [791] [792] [793] [794] [795] [796] [797] [798] [799] [800] [801] [802] [803] [804] [805] [806] [807] [808] [809] [810] [811] [812] [813] [814] [815] [816] [817] [818] [819] [820] [821] [822] [823] [824] [825] [826] [827] [828] [829] [830] [831] [832] [833] [834] [835] [836] [837] [838] [839] [840] [841] [842] [843] [844] [845] [846] [847] [848] [849] [850] [851] [852] [853] [854] [855] [856] [857] [858] [859] [860] [861] [862] [863] [864] [865] [866] [867] [868] [869] [870] [871] [872] [873] [874] [875] [876] [877] [878] [879] [880] [881] [882] [883] [884] [885] [886] [887] [888] [889] [890] [891] [892] [893] [894] [895] [896] [897] [898] [899] [900] [901] [902] [903] [904] [905] [906] [907] [908] [909] [910] [911] [912] [913] [914] [915] [916] [917] [918] [919] [920] [921] [922] [923] [924] [925] [926] [927] [928] [929] [930] [931] [932] [933] [934] [935] [936] [937] [938] [939] [940] [941] [942] [943] [944] [945] [946] [947] [948] [949] [950] [951] [952] [953] [954] [955] [956] [957] [958] [959] [960] [961] [962] [963] [964] [965] [966] [967] [968] [969] [970] [971] [972] [973] [974] [975] [976] [977] [978] [979] [980] [981] [982] [983] [984] [985] [986] [987] [988] [989] [990] [991] [992] [993] [994] [995] [996] [997] [998] [999] [1000]

---

[*] The 3 plane polarizations are perpendicular alternated from the radiation fields.

A Comparison of the Field Patterns of the Horn with and without a 40° Parallel Wire E Plane Flare.

A check on the H plane polarized, E plane field pattern with and without E plane flare indicates that symmetry is good.

It was considered that the addition of parallel wires in the E plane would cause currents to flow along the wires in the E plane and thus force more energy into the E plane polarized fields. This was not measurable in the field patterns. Since the center to center spacing of the flare wires was 0.198λ and the diameter of the flare wires was about 0.099λ only about 1 per cent of the normally incident radiation should pass through the flared section for E plane polarized energy and H plane polarized energy should pass through only slightly attenuated.(27) However, since incidence of the energy on the sides of the flare is parallel rather than normal, little energy of H plane polarization should pass through the flare wires and it will act as a pure flare section. If the wires were spaced farther apart, there would be larger loss of E plane polarized energy through the wires, and the wires would no longer provide the results usually obtained by flaring with solid metallic strips.

In general, the addition of 1/8 inch brass rods spaced 0.635 cm. on centers in the H plane and flared in the E plane at an angle of 40° resulted in the affect of adding pure flare to the horn. Actual improvements in symmetry resulted in the H plane field patterns.

When E plane flare was added a moderate increase in gain was realized and there was an increase in H plane half power beam width. In the E plane the "side lobes" were severely attenuated so that only

one lobe of any consequence was left. That the half power beam width of the E plane field pattern was increased by adding 40° E plane flare indicated that phase distortion at the flare aperture is a problem. A series of experiments could be conducted similar to those of D. R. Rhodes[26] in which flare was added and the field patterns measured for various lengths of flare in order to determine the optimum flare angle and radius of flare. This could be done for the laterally radiating horn.

A Comparison of the Field Patterns of the Horn with 40° E Plane Flare and a Parallel Plane Filter at the Aperture and the Field Patterns of the Horn with 40° E Plane Flare and No Filter at the Aperture

From the field patterns it can be generalized that symmetry was good. The parallel plane filter was effective in eliminating E plane polarization.

Small variations in the E plane polarized, E plane field pattern might result from higher mode generation in the filter. The E plane field pattern is sufficiently well formed that it could meet 31° half power beam pattern specifications with extremely low side lobe levels, whether the filter is employed or not. It may be concluded that the parallel plane filter does not materially affect the E plane field pattern.

Of particular interest is the fact that the 21 db. side lobe level of the flared horn was reduced 7 db. through the addition of the parallel plane filter at the aperture. Even though there were minor increases in the second side lobe levels, manipulation of the variables in the filter design might reduce both the first and second side lobes

to a symmetrical -27 db. side lobe pattern. In the experimental process of manipulating these variables, it would be necessary to make impedance studies on the horn as well as field pattern studies. A theoretical analysis of the higher mode generation at the filter may be possible. W. D. Hayes concluded that the appearance of higher order modes in a grating of large spacing was undesirable when the grating was employed as a beam forming reflector.(27) It was discovered that under the conditions of this experiment the appearance of higher order modes at the widely spaced grating may be employed to improve the E plane polarized, H plane field pattern.

The result of the investigation of the presence of higher order modes might be that the development of favorable higher modes may be dependent upon frequency in which case the first side lobes would vary with frequency.

The Specifications Fulfilled by the Horn with 40° E Plane Parallel Wire Flare and a Parallel Plane Filter

Considering the field patterns for the horn with 40° E plane flare and a parallel plane filter in Figures XXIII, XXIV, XXV, and XXVI the following specifications have been met:

1. A half power beam width of 4.5° in the H plane.
2. A half power beam width of 31° in the E plane.
3. A side lobe pattern in the E plane which has one side lobe at -19.2 and the other side lobe at -24 db.
4. First side lobes in the H plane at -28 db.
5. Maximum second side lobe in the H plane at -24.6 db.
6. Negligible ellipticity.

The Effectiveness of the Parallel Wire Filter in Attenuating the H Plane Polarized Fields

The parallel wire filter caused only minor changes in the E plane field pattern, but it was sufficiently effective to reduce the H plane component 9 to 10 db. From assumptions made in developing the attenuation curves from parallel plane waveguide theory, the attenuation measured was a great deal more than the computed values. The parallel plane theory omits the scattering effect of the wires which is important. An empirical formula was developed by W. D. Hayes[27] from experimental evidence. This formula gives accurate results. Equation (9) yielded an attenuation of 9.86 db. when the parallel wire filter parameters were substituted.

The following equation may be employed to obtain the attenuation of the H plane polarized component when a parallel wire filter is used.

$$\text{Log } T = 0.0917 A + 12.6 \frac{d}{\lambda} - 7.06 \qquad (9)$$

A Comparison of the Computed and Measured Values of the H Plane Field Pattern of the Horn with E Plane Flare

An error of 15 per cent exists between the measured and computed values of the half power beam width in Figure XXXI. This figure also demonstrated that a rough estimate of the beam pattern can be made by employing the pattern computation method given by Equation (8).

Admittance Characteristics

The Uncompensated Horn (Condition 1)

Admittances in the frequency range from 9266 to 8616 mcps. (7.5 per cent band) were transferred to the horn throat and plotted on a Smith chart. See Figure XXXII.

Investigation of the plot indicates that there is a frequency insensitive component of Γ. It is concluded that this component, denoted Γ_t, is due to reflection at the throat. This mismatch appears to be inductive, which is to be expected for the H plane flare. Γ_t = 0.0726. This compares with Γ_t = 0.03 measured by J. R. Riser[37] for a horn with 30 degree H plane flare. Γ_t was then subtracted from the admittances which were then transferred to the horn aperture. See Figure XXXVII.

The mechanical length of the horn is approximately 44 cm. If the change of frequency required to cause a rotation on the Smith chart is considered the virtual length of the horn is determined as

$$R = \frac{(\Delta\phi) \cdot \pi_1 \pi_2}{\pi_1 - \pi_2}$$

where

$\Delta\phi$ = rotation around the Smith chart.

π_1, π_2 = the wavelengths of the two frequencies, assumed to be in free space.

The mean of these computations indicates a virtual horn length of 51.9 cm. At a virtual length of 51.2 cm. the minimum spread of Γ_a (at the aperture) was noted for a variation in frequency. Γ_a indicates that the aperture admittance has a capacitive susceptance which is to be expected. Γ_a = 0.178. If the aperture is considered to be the same as TEM propagation through two plane parallel plates spaced 1.02 cm. theoretical computations indicate Γ_a = 0.322.[38]

Additional Characteristics

The Gravitational Field Equations (7)

Any component of reflection due to a mismatch at the 90° bend is not discernible from the data obtained.

The Horn with Parallel Plane Filter, No E Plane Flare (Condition 2)

Admittances in the frequency range from 9349 to 8729 mcps. were transferred to the horn throat and plotted on a Smith chart. See Figure XXXIII.

Γ_t of the same order of magnitude as that for Condition 1 is observed. The admittance plot follows the same contour except at the lower frequencies. The filter is in effect a cut-off wave guide for the H plane components of E. That it is effective in shorting out these components was apparent from the field pattern.

The Horn with 40° E Plane Flare Added, No Filter (Condition 3)

Admittances in the frequency range 9343 to 8608 mcps. (8.5 per cent band) were transferred to the horn throat and plotted on a Smith chart. See Figure XXXIV.

Γ_t similar to Condition 1 was observed.

The admittance plot indicates that there is a condition of resonance in the horn. The rates of rotation of λ for different frequencies indicates a virtual horn length of 51 cm. Γ_a has been reduced at the higher frequencies and increased at the low end of the band. For the length of E plane flare employed, 9.3 cm. (~3λ), it would be expected that the aperture is well matched to space.[39] The resonant element is probably to be found in the wire rods (spaced 0.635 cm. on centers) used to obtain the E plane flare. It had been hoped that these rods would provide not only flare, but also would serve to eliminate the H plane polarization in the field pattern. Since this was not accomplished, E plane flare could be obtained using

is too dissimilar from the data obtained.

The Data with Positive Plane Plate Impedance

Substitution in the foregoing equation from Page to Page, were transferred to the Data Sheet and plotted on a Polar Chart. See Figure XXXIII.

[illegible] of the same order of magnitude as that for Curve 1 be observed. The admittance plot follows the same characteristic in lower frequencies. The filter is in effect a band-pass plate to-plate capacity of 1. That it is effective in avoiding the dispersion was apparent from the field patterns.

The Data with [illegible] Plane Plate Impedance

Substitution in the foregoing equation [illegible] (0.1 per each band) were transferred to the Data Sheet and plotted on a Polar chart. See Figure XXXIV.

[illegible] similar to Condition 1 was observed.

The admittance plot indicates that there is a condition of resonance in the mode. The value of admittance [illegible] quantities indicates a virtual zero length of it was [illegible] tuned at the higher frequencies was increased at the top and of the band. For the length of 2 plate fibers neglected, Eq. (-A). It would be expected that the impedance is real addition to plate. The resultant element is probably at is found in the Polar Plot (plotted 0.631 cm. as centered that to obtain the 2 Plate-Plate. It had been hoped that these would provide two unit Data, but plate would serve to eliminate the 1 plate polarization at the third polarity.

Since this was not successful, these Data would be obtained using

solid sheet. H plane polarization is best eliminated by employing one of the mode filters. The horn dimensions could be adjusted to give the best impedance characteristics as is done with a compound horn.(40)

The Horn with 40° E Plane Flare, Parallel Plane Filter (Condition 4), and with 40° E Plane Flare, Parallel Wire Filter (Condition 5)

The admittance characteristics for these conditions follow those of Condition 3. The filters appear to have no adverse effects on the admittance characteristics.

V CONCLUSIONS

1. The Laterally radiating electromagnetic horn has a radiating aperture in a plane surface and the surface is formed along an arc of a circle. This plane surface is also a plane of constant phase.
2. The E plane polarized, H plane fields can be computed by means of a linear equivalent source or a Fourier-Bessel series.
3. The Fourier-Bessel series method can be employed to compute the fields in Fraunhofer space for all modes at the aperture.
4. The addition of E plane flare to the laterally radiating electromagnetic horn will result in increased gain, but the E plane half power beam width may increase.
5. The addition of a parallel plane filter will eliminate undesirable H plane polarization.
6. The addition of the parallel plane filter can reduce the first side lobe level in the H plane field pattern.
7. The parallel wire filter is also effective in attenuating H plane polarization. This attenuation may be approximated by an empirical formula.
8. When the frequency is decreased the E plane polarized H plane field pattern increases in half power beam width slowly, increases in angle at which the first side lobe occurs, and reduces in the magnitude of the first side lobe. The general contour of the beam pattern is unchanged.

SUMMARY

9. The main lobe of the uncompensated laterally radiating electromagnetic horn is linearly polarized in the E plane, and right elliptically polarized to the right of the E plane, and left elliptically polarized to the left of the E plane.

10. The mismatch of the uncompensated horn at the throat appears to have components due to lumped admittances at the horn throat and aperture. The throat component can probably be eliminated by rounding the transition at the beginning of H plane flare.

11. The mismatch at the aperture may be reduced by employing E plane flare which is also desirable in terms of the field pattern. The use of wire rods to obtain this flare apparently causes a resonance in the admittance characteristics. Since these rods are not successful in eliminating H plane polarization a sheet E plane flare should be used. For best admittance characteristics the horn should be designed as a compound horn with cancelling reflections over the band desired.

12. The use of mode filters at the aperture to eliminate H plane polarization does not have any characteristics which affect adversely the admittance characteristics. When designing the horn their effect over the frequency band should be determined and considered as a means of minimizing .

VI RECOMMENDATIONS

The following recommendations are presented:

1. A complete set of design graphs could be made of main lobe half power beam widths, first side lobe magnitudes and angles at which they occur, the amplitude of the "cross polarization" lobes in the H plane, the E plane half power beam pattern, and ellipticity patterns for the uncompensated laterally radiating horn. The Fourier-Bessel series method of computation could be employed.
2. An experimental investigation of the affect of various E plane flare angles and lengths of flare on the E plane field patterns could be conducted.
3. A thorough investigation of the affect of varying the filter parameters on the field patterns and the impedance characteristics of the horn should be made. It should be determined whether the higher order modes formed in the filter are sensitive to changes in frequency.
4. An investigation over a larger band of frequencies, perhaps 20 per cent, could be conducted to determine what positions of beginning of E and H plane flares, bend, and mode filter gives the best impedance characteristics.

XI RECOMMENDATIONS

The following recommendations are presented.

1. A complete set of design graphs (such as those in this report) for other types of lenses should be prepared. First the type employed in radio (or other) waves, the dielectric of the "cross polarization" lenses in use (Figure), the H-plane half-wave lens parallel, and circularly polarizing (or two wavelength) lenses should be considered. The Fourier-Bessel series method of computation would be employed.

2. An experimental investigation of the effect of various E plane flare angles and lengths of flare on the H plane field patterns should be conducted.

3. A thorough investigation of the effect of varying the filter parameters on the field patterns and the impedance characteristics of the lens should be made. It should be determined whether the slower wave-modes found in the flare are sensitive to changes in frequency.

4. An investigation over a larger band of frequencies, perhaps 20 per cent, should be conducted to determine what position of height of H and E plane flare, and mode filter gives the most desirable characteristics.

APPENDIX

APPENDIX, SECTION A

ILLUSTRATIONS

Figure	Title
I	Laterally Radiating Electromagnetic Horn, Design Type A.
II	General Coordinate System.
III	Coordinates for H Plane Sectoral Horn.
IV	Linear Equivalent Source Geometry.
V	Laterally Radiating Electromagnetic Horn, Design Type B.
VI	Block Diagram of the Pen Positioning System.
VII	Block Diagram of the Field Pattern Measurement Apparatus.
VIII	Experimentally Determined Optimum Dimensions for Rectangular Horn Antennas.
IX	The Geometry Employed in the Solution for the E Plane Array Factor.
X	Description of Filters.
XI	Recommended Bend Cross Section Design.
XII	E Plane Polarized, H Plane Field Pattern of the Laterally Radiating Horn with and without Parallel Plane Filter.
XIII	H Plane Polarized, E Plane Field Pattern of the Laterally Radiating Horn with and without Parallel Plane Filter.
XIV	E Plane Polarized, E Plane Field Pattern of the Laterally Radiating Horn with and without Parallel Plane Filter.
XV	H Plane Polarized, H Plane Field Pattern of the Laterally Radiating Horn with and without Parallel Plane Filter.
XVI	E Plane Polarized, H Plane Field Pattern of the Laterally Radiating Horn for $\lambda = 3.2$ cm. and $\lambda = 3.382$ cm.

Illustrations

Figure	Title
I	Laterally Radiating Electromagnetic Horn, Design Type E.
II	Cameron Coordinate System.
III	Coordinates for 4 Plane Natural Horn.
IV	Linear Equivalent Source Geometry.
V	Laterally Radiating Electromagnetic Horn, Design Type E.
VI	Block Diagram of the Pre-Processing System.
VII	Block Diagram of the Field Pattern Measurement Apparatus.
VIII	Experimentally Generated Typical Directional Gain Radiation Pure Antenna.
IX	The Geometry Employed in the Solution for the 3 Plane Array Factor.
X	Description of Figures.
XI	Conventional Horn Cross Section Design.
XII	E Plane Polarized, E Plane Field Pattern of the Laterally Radiating Horn with and without Parallel Plane Filter.
XIII	H Plane Polarized, H Plane Field Pattern of the Laterally Radiating Horn with and without Parallel Plane Filter.
XIV	H Plane Polarized, H Plane Field Pattern of the Laterally Radiating Horn with and without Parallel Plane Filter.
XV	H Plane Polarized, H Plane Field Patterns of the Laterally Radiating Horn with and without Parallel Plane Filter.
XVI	H Plane Polarized, H Plane Field Patterns of the Laterally Radiating Horn for λ = 3.2 cm. and λ = 3.38 cm.

Figure	Title
XVII	Computed and Measured Values of the E Plane Polarized, H Plane Field Pattern of the Laterally Radiating Horn.
XVIII	Computed and Measured Values of the H Plane Polarized, H Plane Field Pattern of the Laterally Radiating Horn.
XIX	E Plane Polarized, H Plane Field Pattern of the Laterally Radiating Horn with and without 40° E Plane Flare.
XX	H Plane Polarized, H Plane Field Pattern of the Laterally Radiating Horn with and without 40° E Plane Flare.
XXI	E Plane Polarized, E Plane Field Pattern for the Laterally Radiating Horn with and without 40° E Plane Flare.
XXII	H Plane Polarized, E Plane Field Pattern for the Laterally Radiating Horn with and without 40° E Plane Flare.
XXIII	E Plane Polarized, H Plane Field Pattern for the Laterally Radiating Horn (with 40° E Plane Flare) with and without the Parallel Plane Filter.
XXIV	E Plane Polarized, E Plane Field Pattern for the Laterally Radiating Horn (with 40° E Plane Flare) with and without the Parallel Plane Filter.
XXV	H Plane Polarized, E Plane Field Pattern for the Laterally Radiating Horn (with 40° E Plane Flare) with and without the Parallel Plane Filter.
XXVI	H Plane Polarized, H Plane Field Pattern x for the Laterally Radiating Horn (with 40° E Plane Flare) with and without the Parallel Plane Filter.

Theorem	Title
XVII	Conjoined and Denumerably Infinite Set of Plane Projectors.
	A Plane Fixed Pattern or Its Inherently Reflecting Dual.
XVIII	Conjoined and Enumerably Infinite Set of Plane Projectors.
	A Plane Fixed Pattern or Its Inherently Reflecting Dual.
XIX	A Plane Projector, A Plane Fixed Pattern or Its Inherently Reflecting Dual with without $4\mathcal{D}_2^0$ A Plane Plane.
XX	A Plane Projector, A Plane Fixed Pattern or Its Inherently Reflecting Dual with without $4\mathcal{D}_2^0$ A Plane Plane.
XXI	A Plane Projector, A Plane Fixed Pattern for the Inherently Reflecting Dual with without $4\mathcal{D}_2^0$ A Plane Plane.
XXII	A Plane Projector, A Plane Fixed Pattern for the Inherently Reflecting Dual with without $4\mathcal{D}_2^0$ A Plane Plane.
XXIII	A Plane Projector, A Plane Fixed Pattern for the Inherently Reflecting Dual with without $4\mathcal{D}_2^0$ A Plane Fixed with and without the Parallel Plane Filter.
XXIV	A Plane Projector, A Plane Fixed Pattern for the Inherently Reflecting Dual with $4\mathcal{D}_2^0$ A Plane Fixed with and without the Parallel Plane Filter.
XXV	A Plane Projector, A Plane Fixed Pattern for the Inherently Reflecting Dual with $4\mathcal{D}_2^0$ A Plane Fixed with and without the Parallel Plane Filter.
XXVI	A Plane Projector, A Plane Fixed Pattern A for the Inherently Reflecting Dual (with $4\mathcal{D}_2^0$ A Plane Fixed with and without the Parallel Plane Filter.

Figure	Title
XXVII	H Plane Polarized, H Plane Field Pattern of the Laterally Radiating Horn (with 40° E Plane Flare) with and without a Parallel Wire Filter.
XXVIII	Plot of the Ellipticity of the Laterally Radiating Electromagnetic Horn for Positive θ and Right Elliptical Polarization.
XXIX	Plot of the Ellipticity of the Laterally Radiating Electromagnetic Horn for Negative θ and Left Elliptical Polarization.
XXX	Comparison of Measured and Computed Values of E_{θ} in the E Plane
XXXI	A Comparison of Measured and Computed Values of E_{θ} in the E Plane for the Laterally Radiating Electromagnetic Horn with 40° E Plane Flare.
XXXII	Admittances of the Uncompensated Horn, (Condition 1), for Different Frequency.
XXXIII	Admittances of the Horn with Plane Parallel Plate Filter, No E Plane Flare, (Condition 2), for Different Frequency, Transferred to the Throat.
XXXIV	Admittances of the Horn with E Plane Flare, No Filter, (Condition 4), for Different Frequency, Transferred to the Throat.
XXXV	Admittances of the Horn with E Plane Flare, Plane Parallel Filter, (Condition 4), for Different Frequency, Transferred to the Throat.
XXXVI	Admittances of the Horn with E Plane Flare, Parallel Wire Filter, (Condition 5), for Different Frequency, Transferred to the Throat.

Figure	Title
XXXVII	Admittance Components at the Horn Aperture for the Uncompensated Horn, (Condition 1), for Different Frequency, Transferred to the Aperture from the Throat.
XXXVIII	Photograph of the Laterally Radiating Horn on the Turntable.
XXXIX	Photograph of the Laterally Radiating Horn (with 40° E Plane Flare) on the Turntable.

FIG. I

LATERALLY RADIATING ELECTROMAGNETIC HORN

DESIGN-TYPE A

E. & R. Bassenbe R. E. Lee

14 APRIL 1952

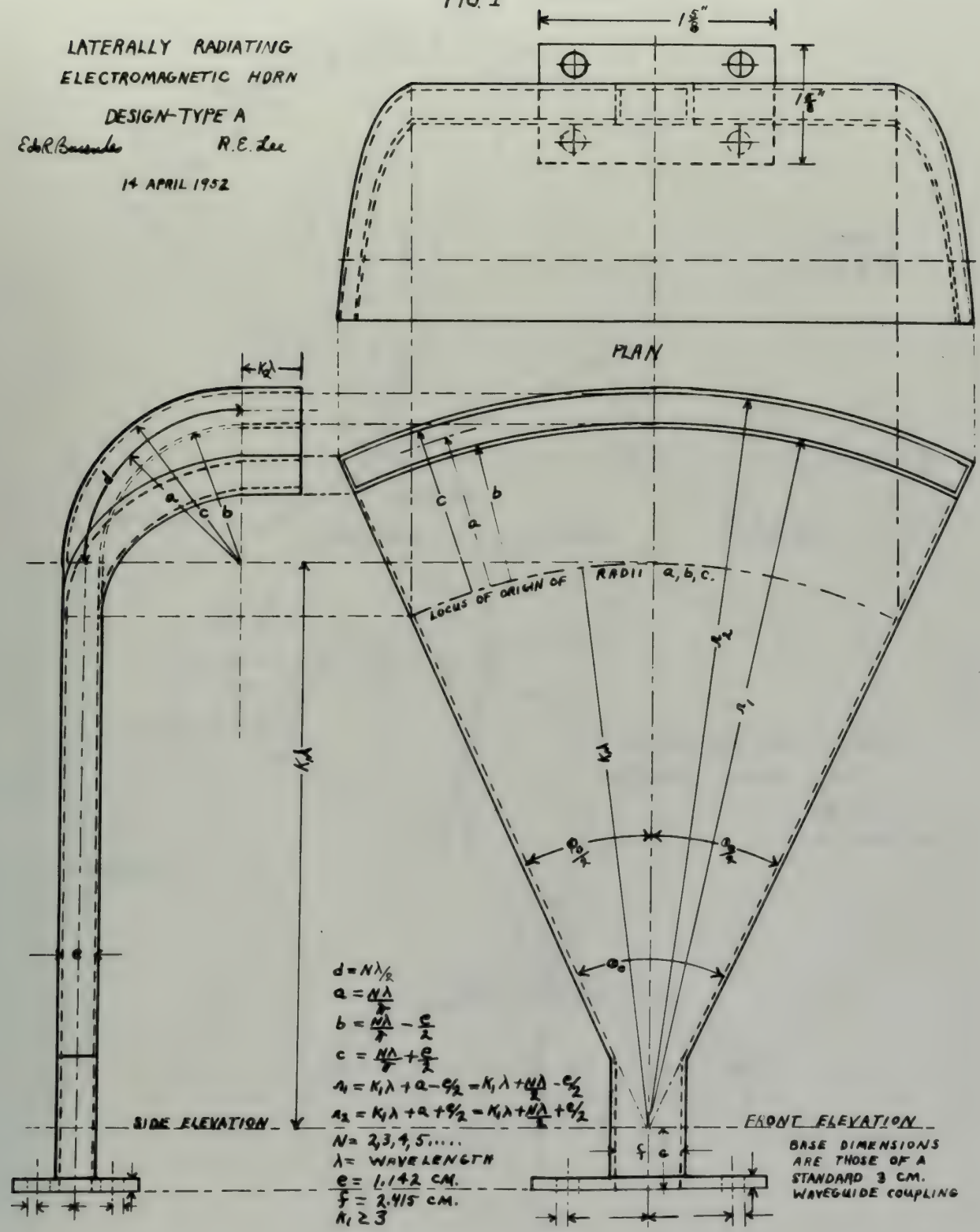

$d = N\lambda/2$

$a = \frac{N\lambda}{2}$

$b = \frac{N\lambda}{2} - \frac{e}{2}$

$c = \frac{N\lambda}{2} + \frac{e}{2}$

$r_1 = K_1\lambda + a - e/2 = K_1\lambda + \frac{N\lambda}{2} - e/2$

$r_2 = K_1\lambda + a + e/2 = K_1\lambda + \frac{N\lambda}{2} + e/2$

$N = 2, 3, 4, 5 \ldots$

λ = WAVELENGTH

$e = 1.142$ CM.

$f = 2.415$ CM.

$K_1 \geq 3$

FIG. II

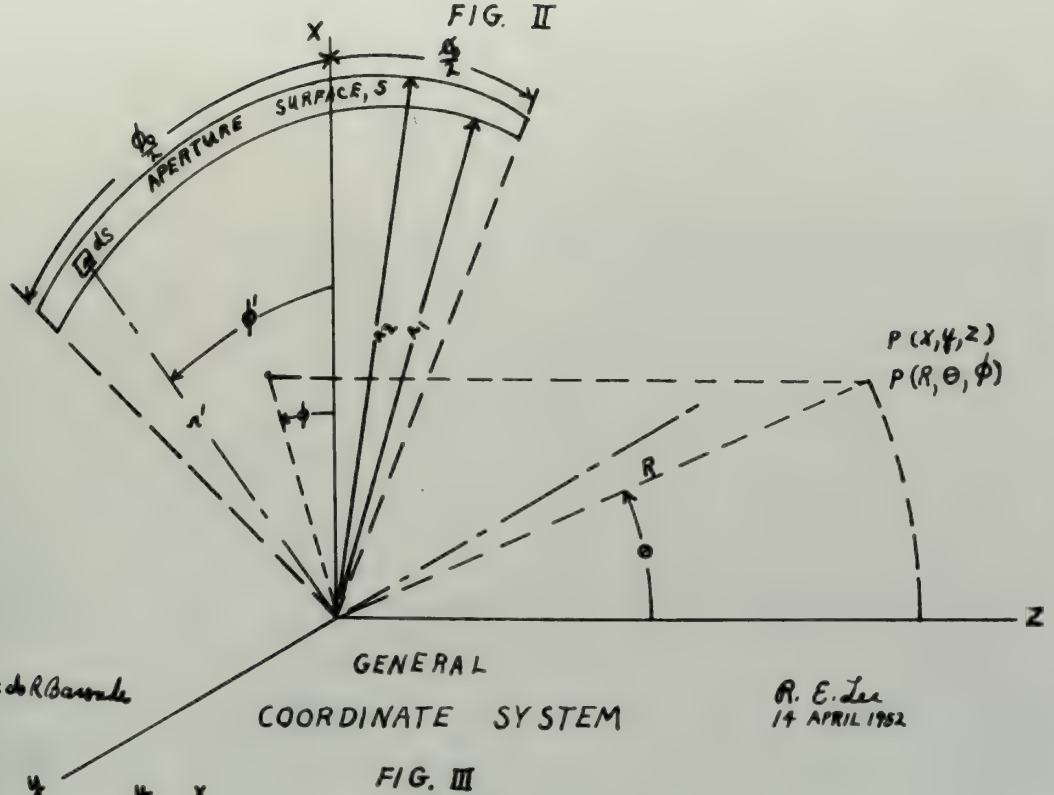

GENERAL
COORDINATE SYSTEM

E. de R. Barnes

R. E. Lee
14 APRIL 1952

FIG. III

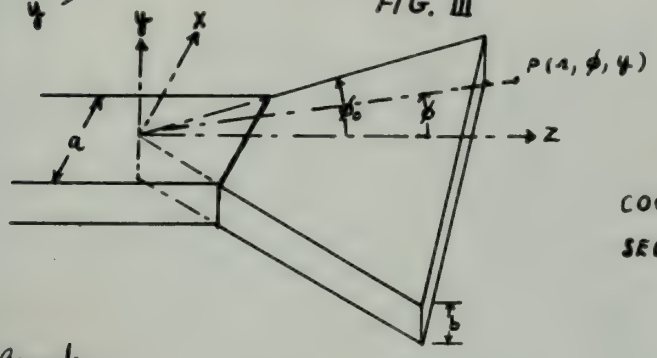

COORDINATES FOR H PLANE
SECTORAL HORN ONLY

R. E. Lee
14 APRIL 1952

E. de R. Barnes

FIG IV

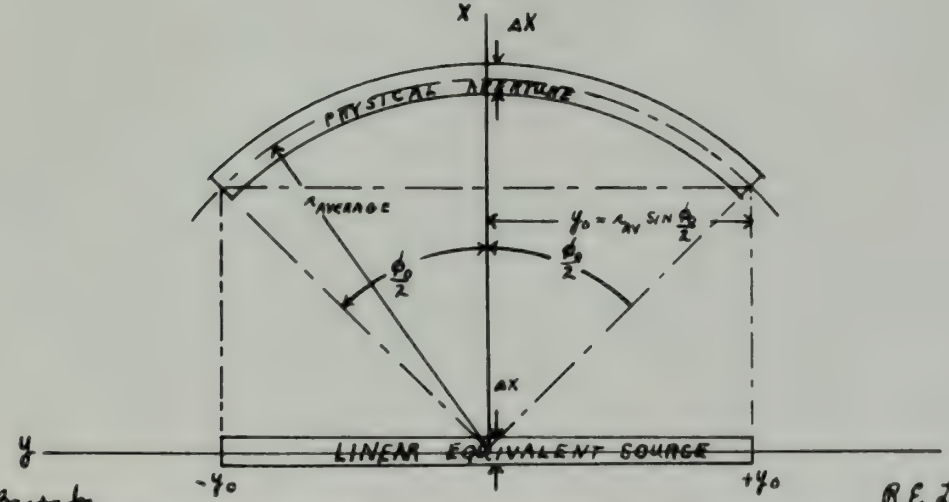

E. de R. Barnes

LINEAR EQUIVALENT SOURCE GEOMETRY

R. E. Lee
14 APRIL 1952

FIG. V

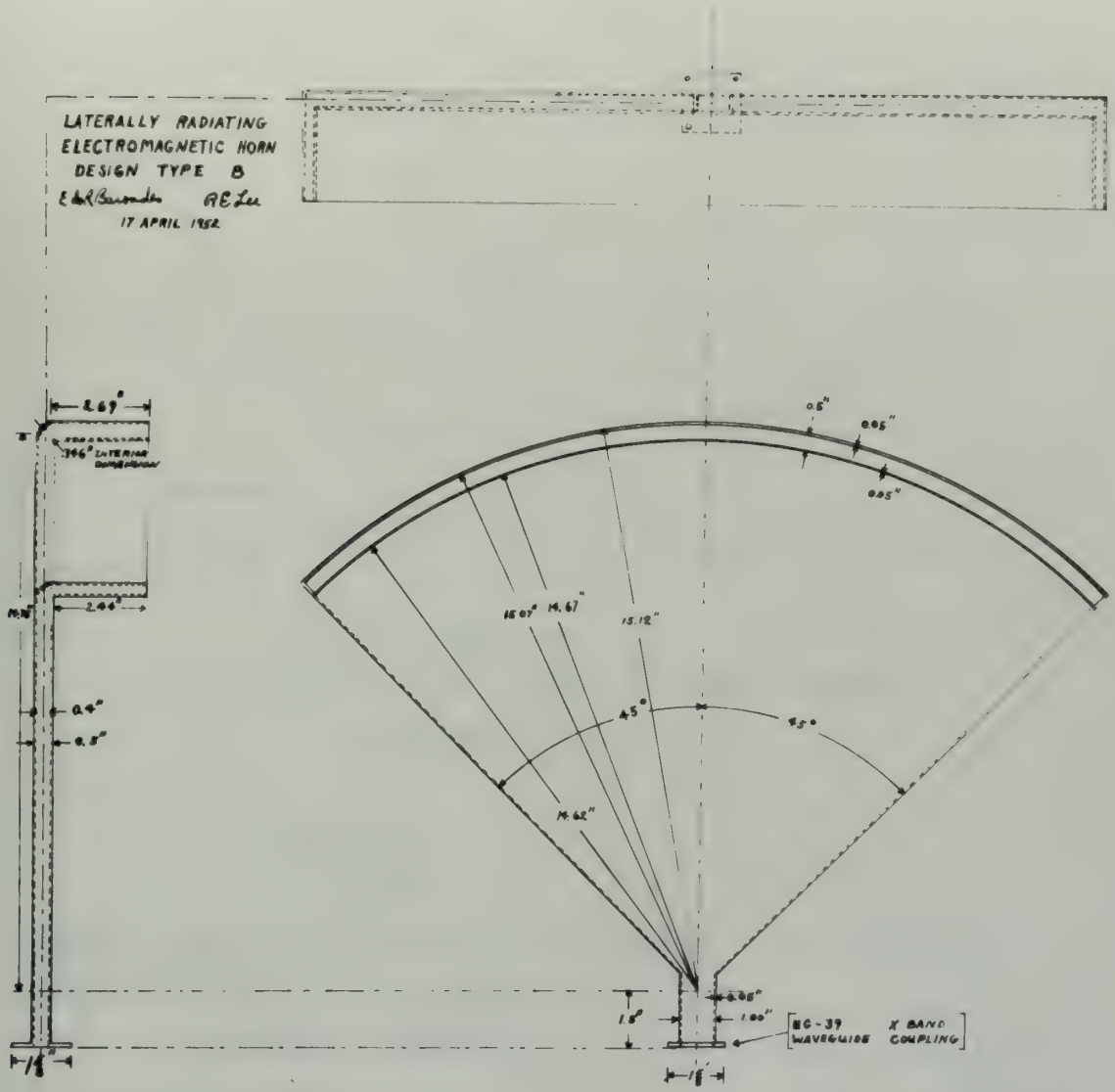
LATERALLY RADIATING
ELECTROMAGNETIC HORN
DESIGN TYPE B
E. & R. Barnaby R.E. Lee
17 APRIL 1952
2.69"
.396" INTERIOR DIMENSION
2.00"
0.4"
0.5"
0.5"
0.05"
0.05"
15.07"
14.67"
15.12"
45°
45°
14.62"
0.05"
1.8"
1.00"
RG-39 X BAND WAVEGUIDE COUPLING

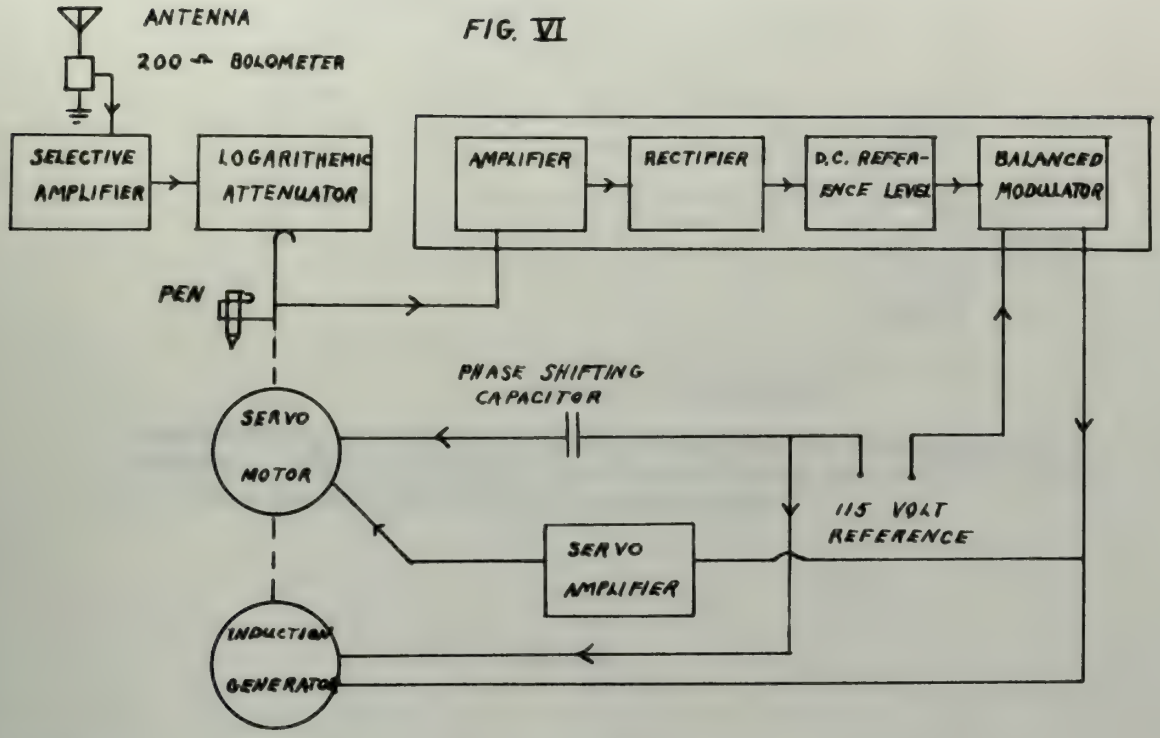

Ed R Barnes 15 APRIL 1952 R E Lee

BLOCK DIAGRAM OF THE PEN POSITIONING SYSTEM

FIG. VII

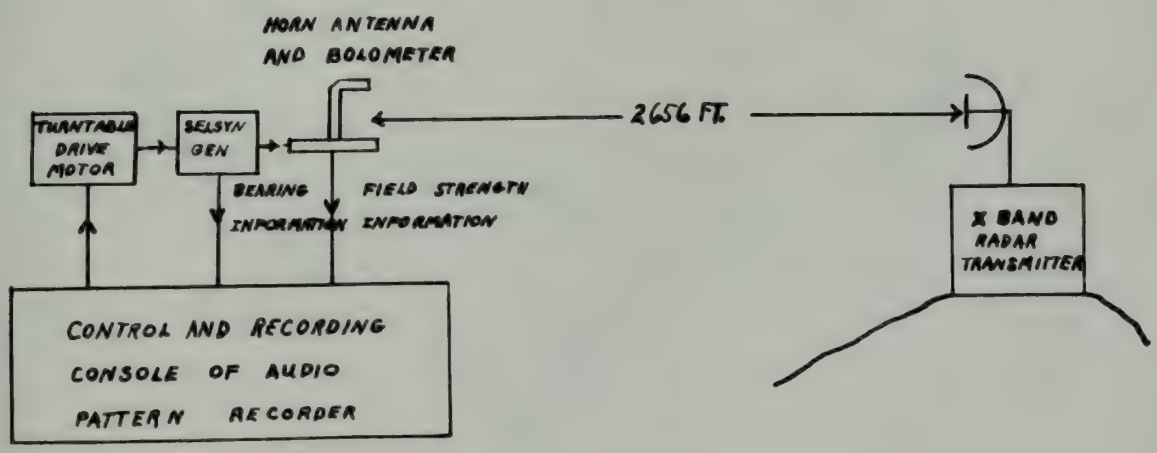

BLOCK DIAGRAM OF THE FIELD PATTERN MEASUREMENT APPARATUS

Ed R Barnes 15 APRIL 1952 R E Lee

FIG. VIII

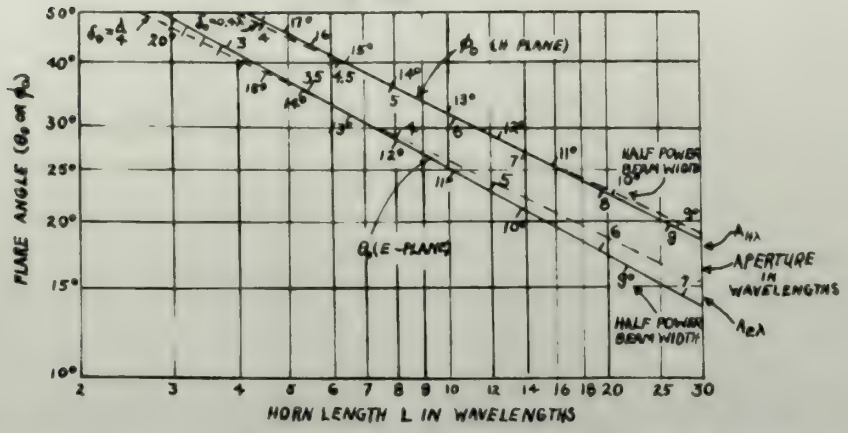

Experimentally determined optimum dimensions for rectangular horn antennas. Solid curves give relation of flare angle θ_0 in E plane and flare angle ϕ_0 in H plane to horn length.(7)

FIG. IX

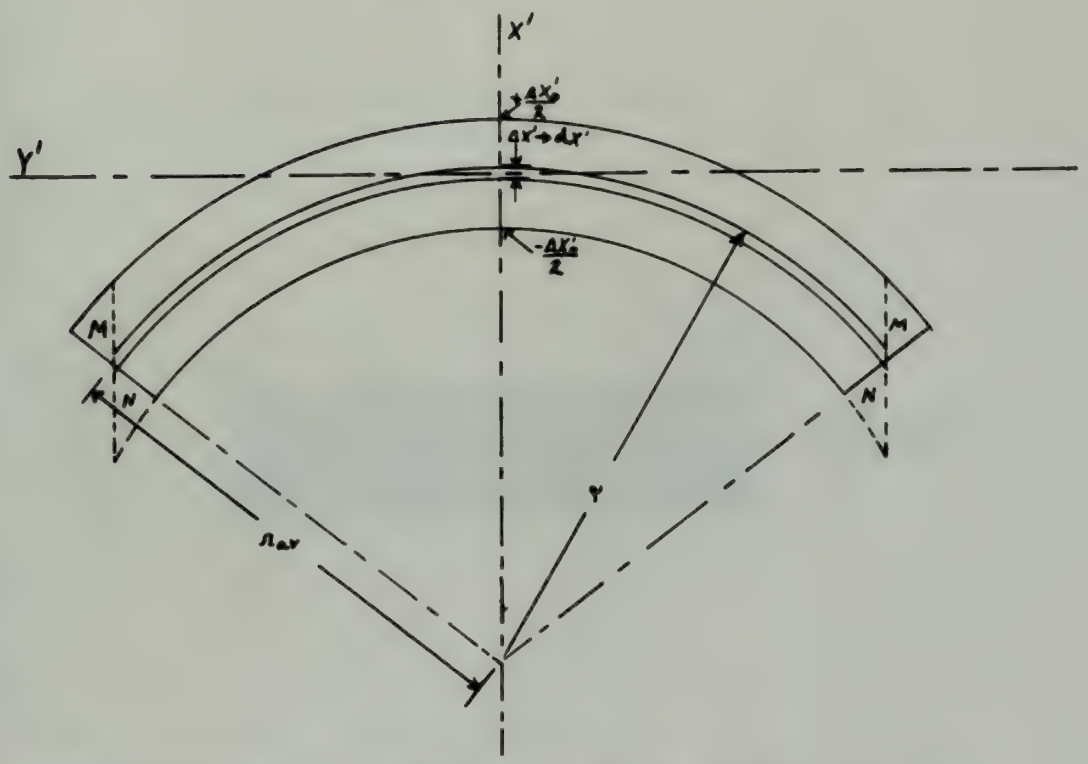

THE GEOMETRY EMPLOYED IN THE SOLUTION FOR THE E PLANE ARRAY FACTOR

E M R Saunders R E Lee

17 APRIL 1952

FIG. X

DESCRIPTION OF FILTERS

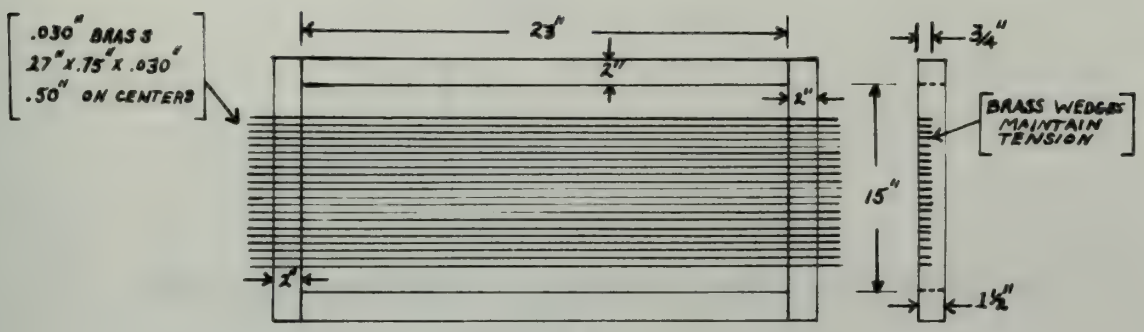

PARALLEL PLANE FILTER

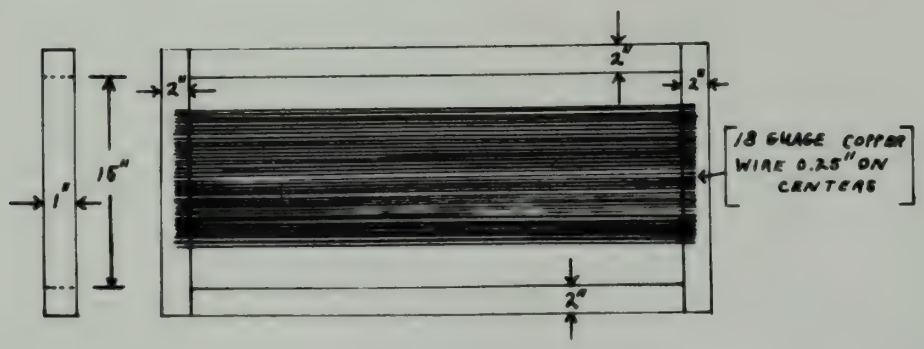

PARALLEL WIRE FILTER

E de R. Baisondeo

R E Lee

21 APRIL 1952

FIG. XI

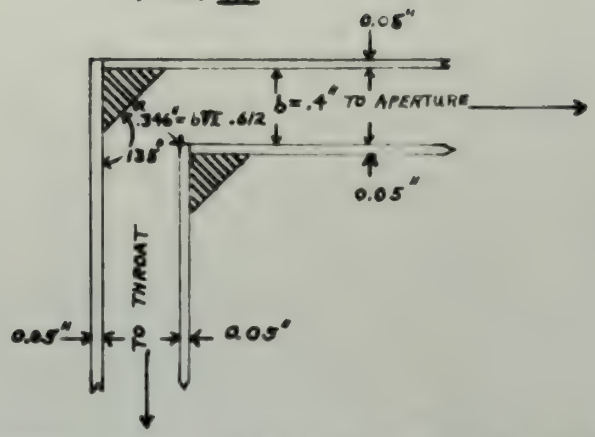

RECOMMENDED BEND CROSS SECTION DESIGN

E & R Barnes

R E Lee

24 APRIL 1952

FIG. XII

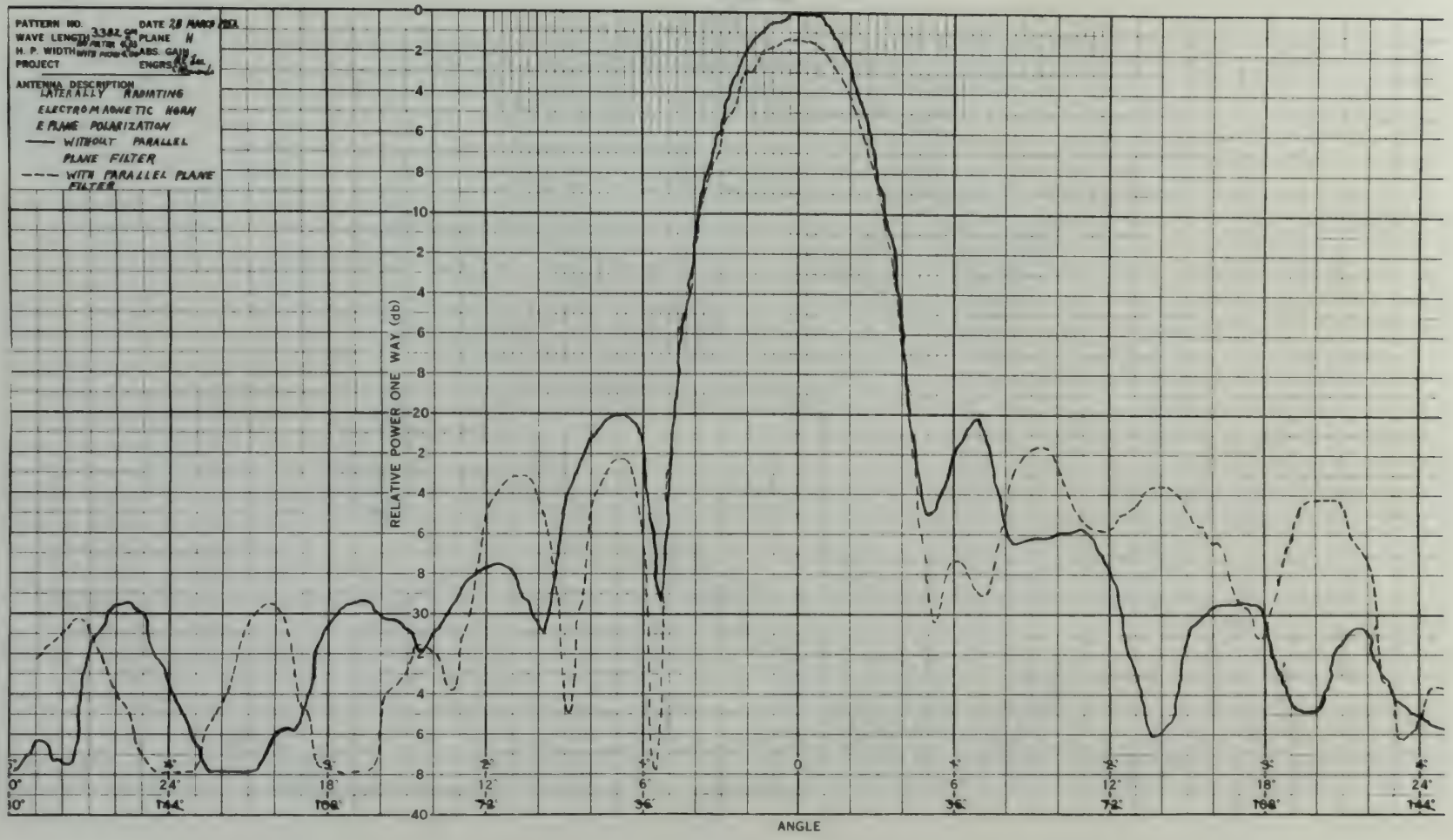
PATTERN NO.
DATE 28 MARCH 1951
WAVE LENGTH 3.382 cm
PLANE H
H. P. WIDTH
ABS. GAIN
PROJECT
ENGRS.
ANTENNA DESCRIPTION
LATERALLY RADIATING
ELECTROMAGNETIC HORN
E PLANE POLARIZATION
WITHOUT PARALLEL PLANE FILTER
WITH PARALLEL PLANE FILTER
RELATIVE POWER ONE WAY (db)
0
2
4
6
8
10
20
30
40
4°
3°
2°
1°
0
24'
18'
12'
6'
144'
108'
72'
36'
ANGLE

FIG. XIII

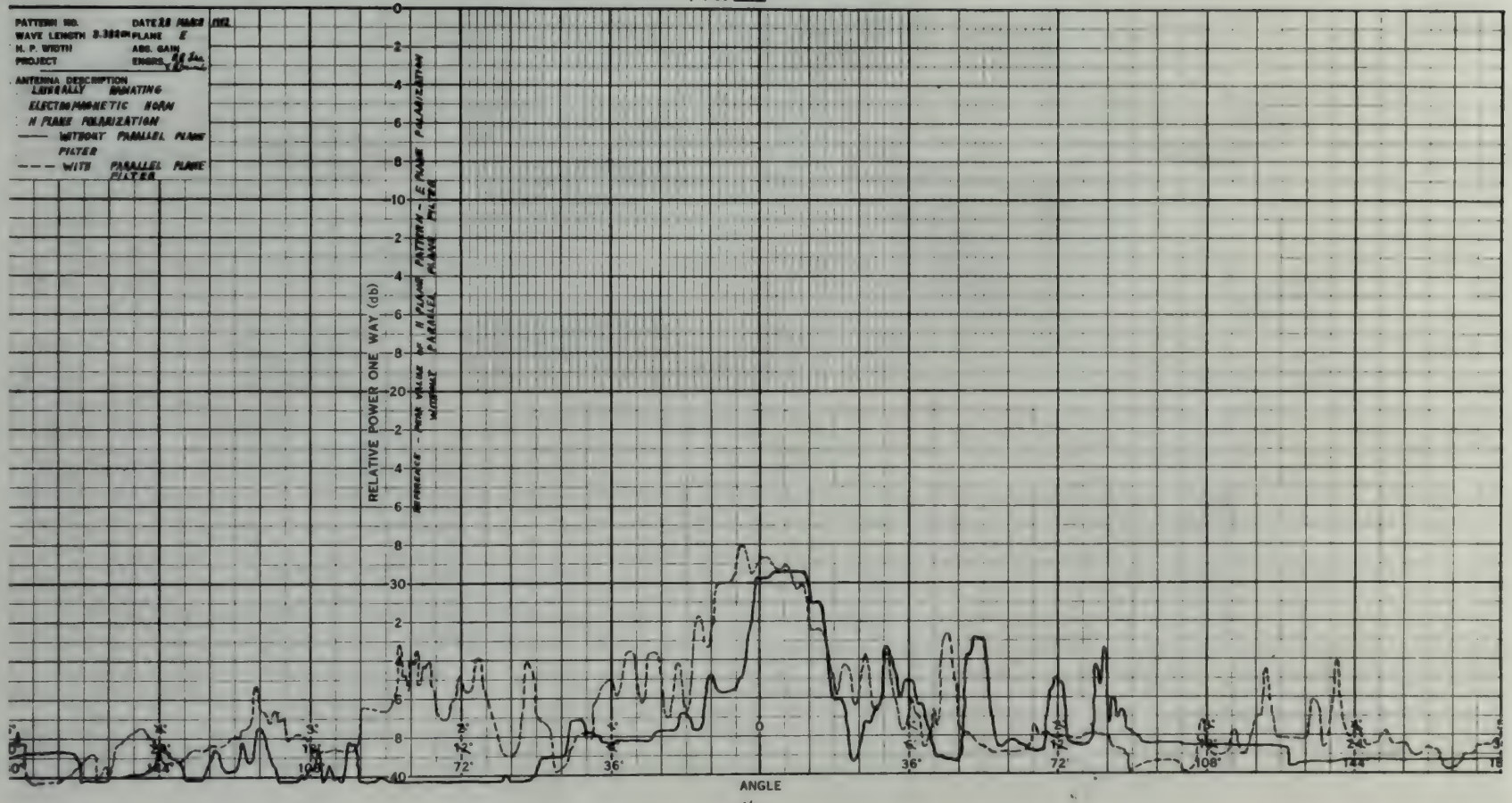
PATTERN NO.
DATE 28 MARCH 1952
WAVE LENGTH 3.332cm PLANE E
H. P. WIDTH
ABS. GAIN
PROJECT
ENGRS.
ANTENNA DESCRIPTION
LATERALLY RADIATING
ELECTROMAGNETIC HORN
H PLANE POLARIZATION
—— WITHOUT PARALLEL PLANE FILTER
--- WITH PARALLEL PLANE FILTER
REFERENCE - PEAK VALUE OF H PLANE PATTERN - E PLANE POLARIZATION WITHOUT PARALLEL PLANE FILTER
RELATIVE POWER ONE WAY (db)
0
2
4
6
8
10
20
30
40
ANGLE
72°
36°
108°
144°

FIG. XIV

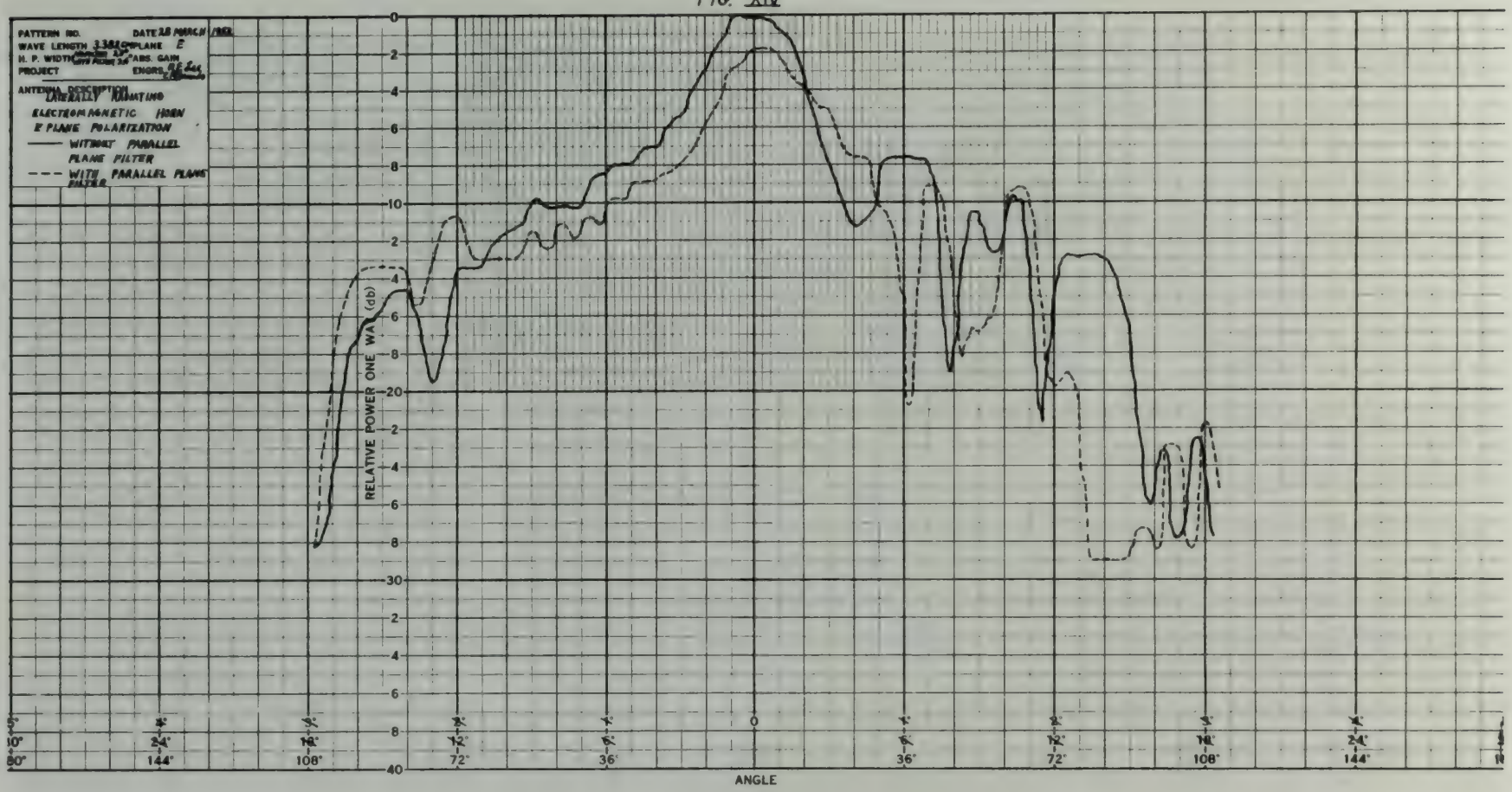
PATTERN NO.
DATE 28 MARCH
WAVE LENGTH 3.384 cm PLANE E
H. P. WIDTH
ABS. GAIN
PROJECT
ENGRS.
ANTENNA DESCRIPTION
ELECTROMAGNETIC HORN
E PLANE POLARIZATION
WITHOUT PARALLEL PLANE FILTER
WITH PARALLEL PLANE FILTER
RELATIVE POWER ONE WAY (db)
0
2
4
6
8
10
20
30
40
5°
10°
24°
144°
80°
18°
108°
12°
72°
6°
36°
0
ANGLE

FIG. XV

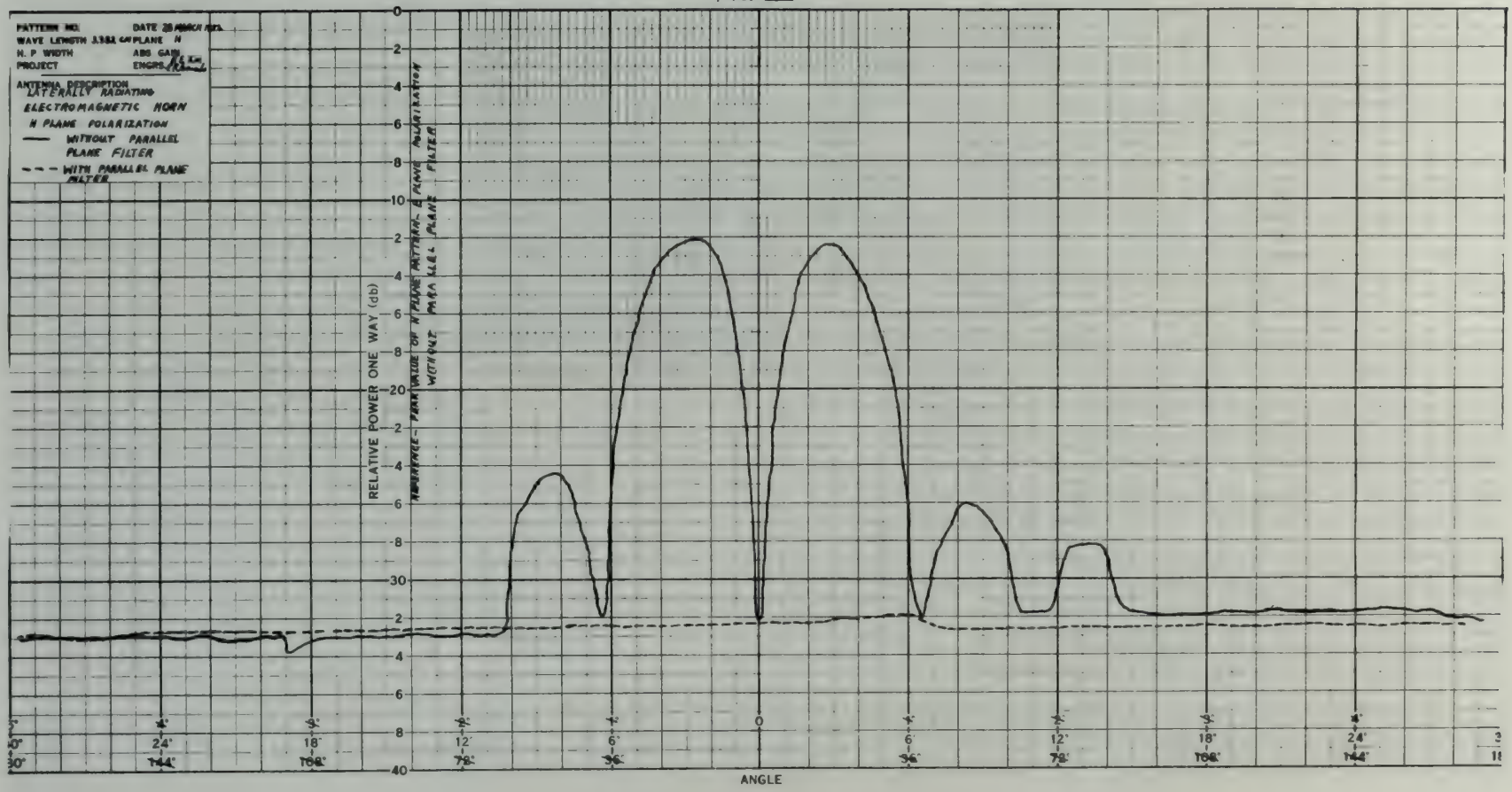
PATTERN NO.
DATE 28 MARCH 1951
WAVE LENGTH 3.382 cm
PLANE H
H. P WIDTH
ABS GAIN
PROJECT
ENGRS.
ANTENNA DESCRIPTION
LATERALLY RADIATING
ELECTROMAGNETIC HORN
H PLANE POLARIZATION
WITHOUT PARALLEL PLANE FILTER
WITH PARALLEL PLANE FILTER
REFERENCE - PARK VALUE OF H PLANE PATTERN - E PLANE POLARIZATION WITHOUT PARALLEL PLANE FILTER
RELATIVE POWER ONE WAY (db)
0
2
4
6
8
10
20
30
40
ANGLE
24°
18°
12°
6°
0
6°
12°
18°
24°
30°
144°
108°
72°
36°

FIG. XVI

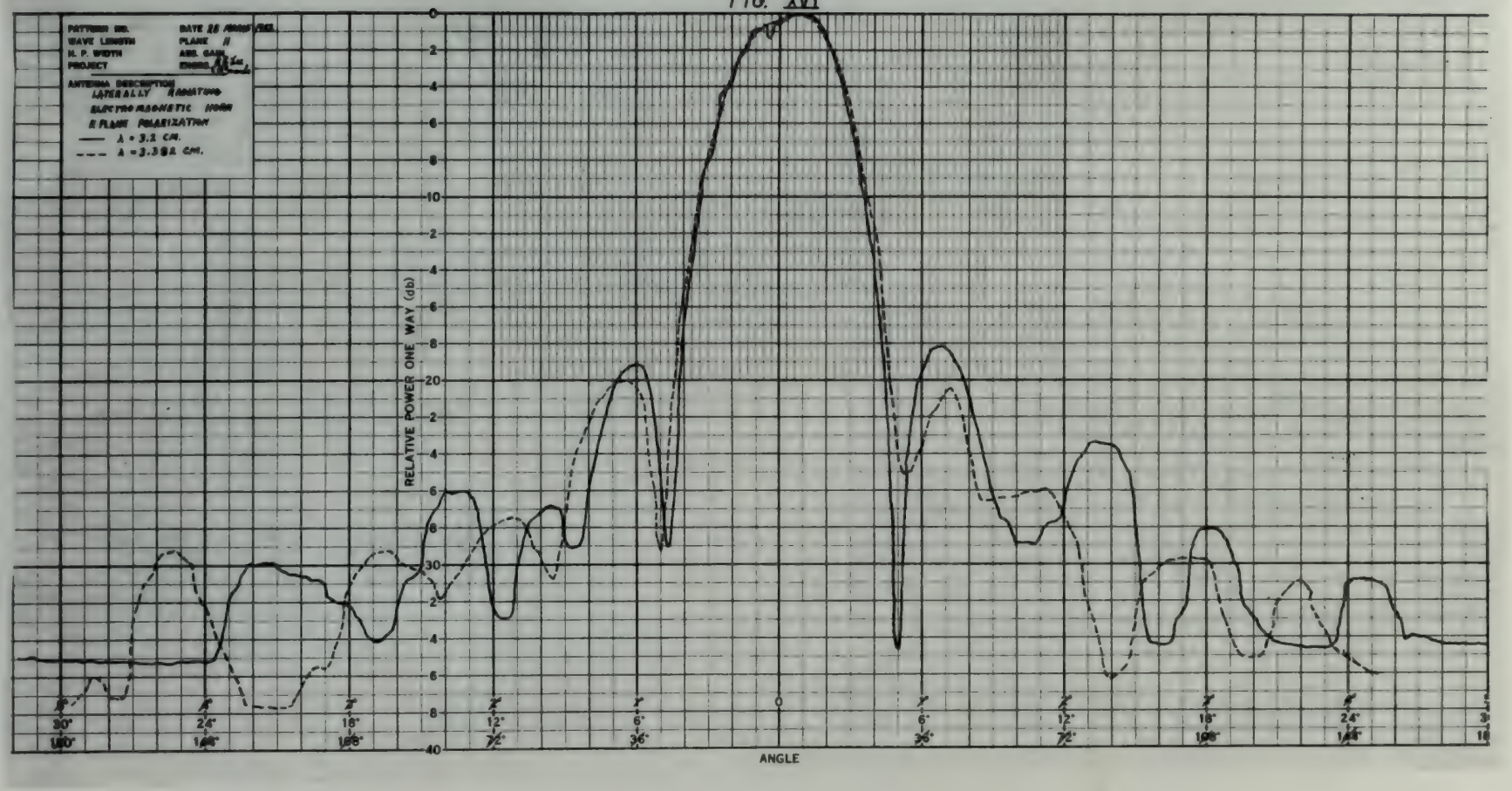
PATTERN NO.
WAVE LENGTH
H. P. WIDTH
PROJECT
DATE 25 /1950
PLANE H
ANTENNA DESCRIPTION
LATERALLY RADIATING
ELECTROMAGNETIC HORN
E PLANE POLARIZATION
λ = 3.2 CM.
λ = 3.38 CM.
RELATIVE POWER ONE WAY (db)
0
2
4
6
8
10
20
30
40
30°
180°
24°
18°
12°
6°
0
6°
12°
18°
24°
ANGLE

FIG. XVII

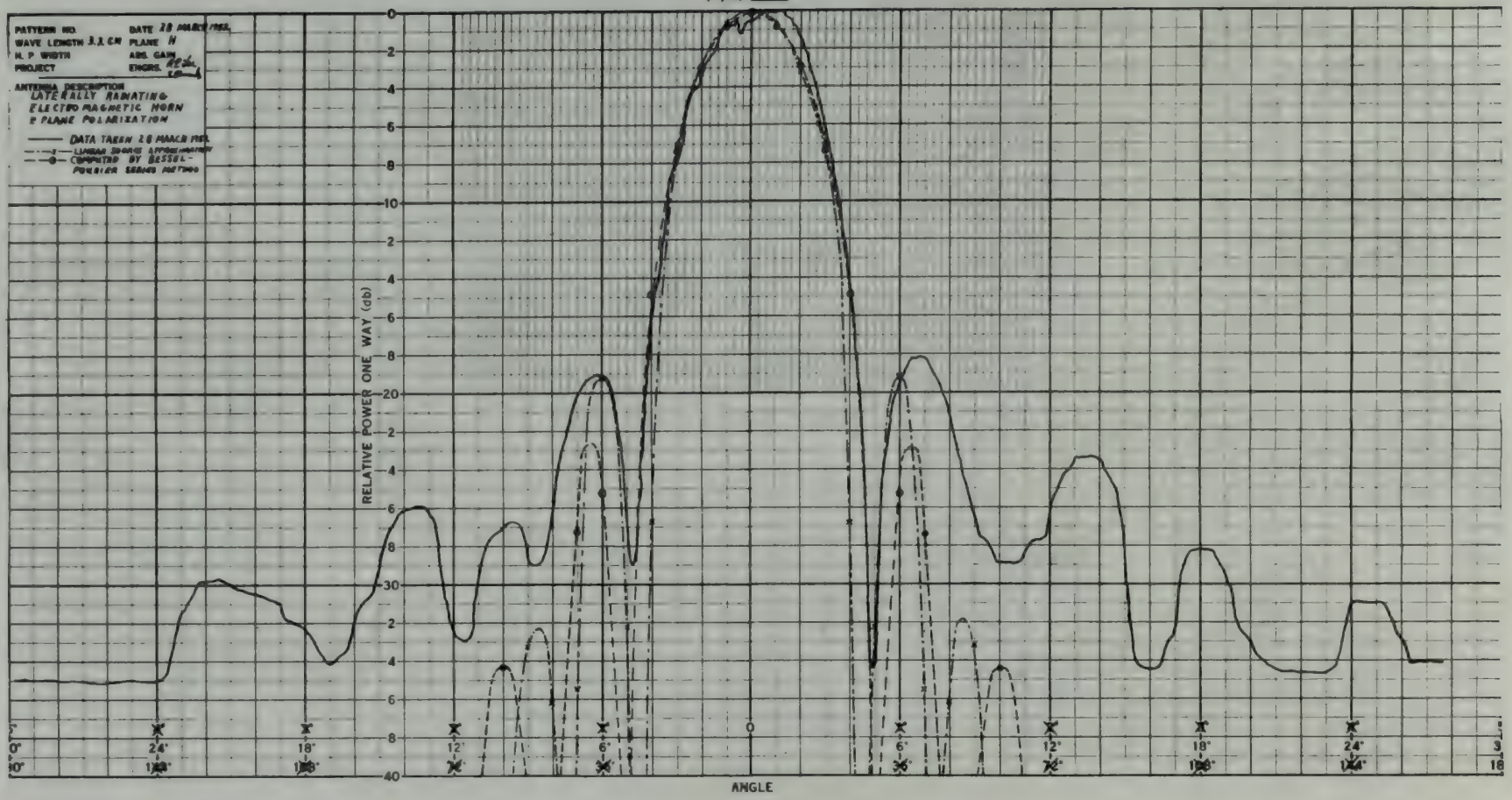
PATTERN NO.
DATE 28 MARCH 1951
WAVE LENGTH 3.2 CM
PLANE H
H. P WIDTH
ABS. GAIN
PROJECT
ENGRS.
ANTENNA DESCRIPTION
LATERALLY RADIATING
ELECTRO MAGNETIC HORN
E PLANE POLARIZATION
DATA TAKEN 28 MARCH 1951
RELATIVE POWER ONE WAY (db)
0
2
4
6
8
10
20
30
40
24°
18°
12°
6°
0
ANGLE

FIG. XVIII

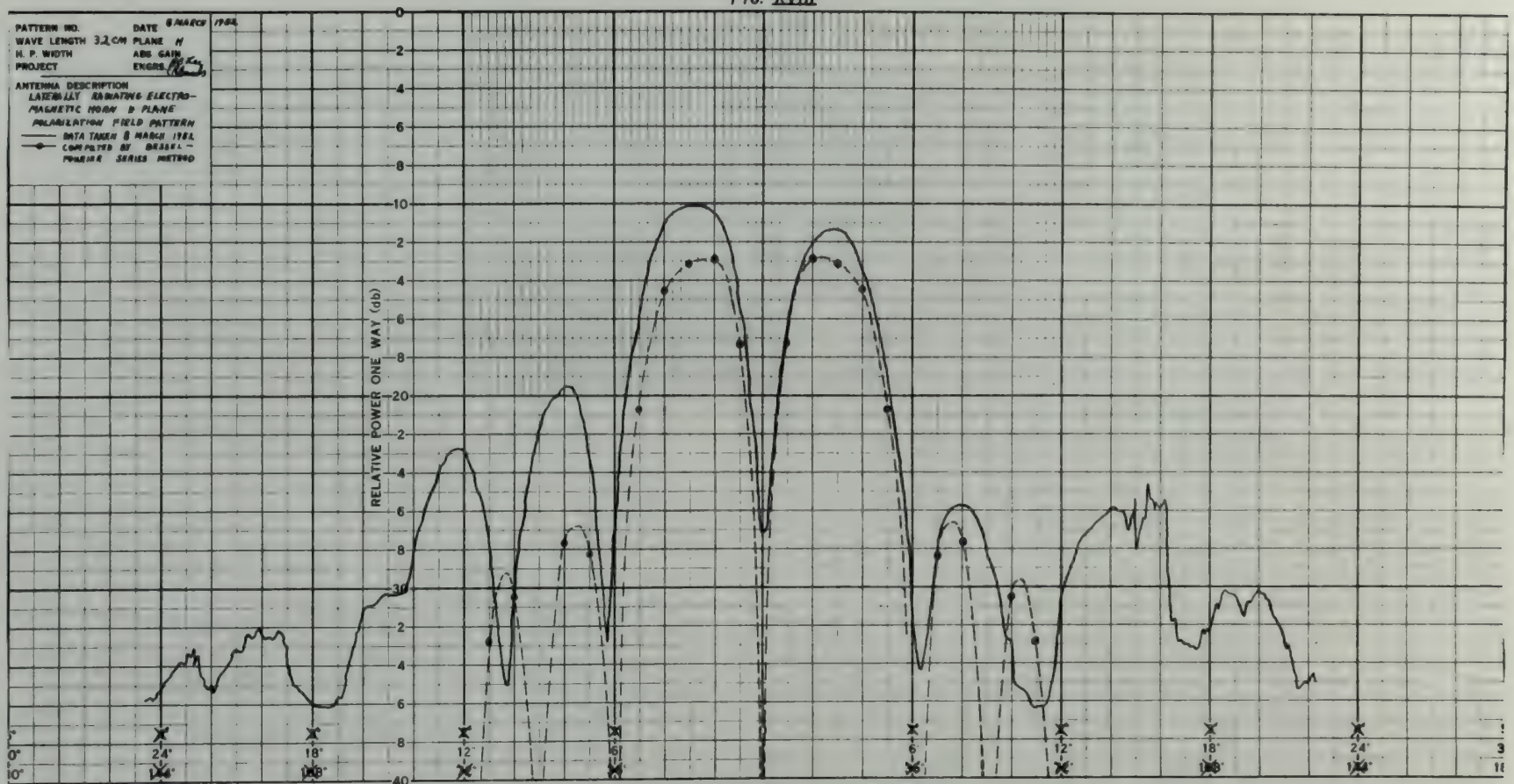
PATTERN NO.
DATE 8 MARCH 1951
WAVE LENGTH 3.2 CM
PLANE H
H. P. WIDTH
ABS GAIN
PROJECT
ENGRS.
ANTENNA DESCRIPTION
LATERALLY RADIATING ELECTRO-MAGNETIC HORN D PLANE
POLARIZATION FIELD PATTERN
DATA TAKEN 8 MARCH 1951
COMPUTED BY BESSEL-FOURIER SERIES METHOD
RELATIVE POWER ONE WAY (db)
0
2
4
6
8
10
20
30
40
24°
18°
12°
6°
6°
12°
18°
24°
ANGLE

FIG. XIX

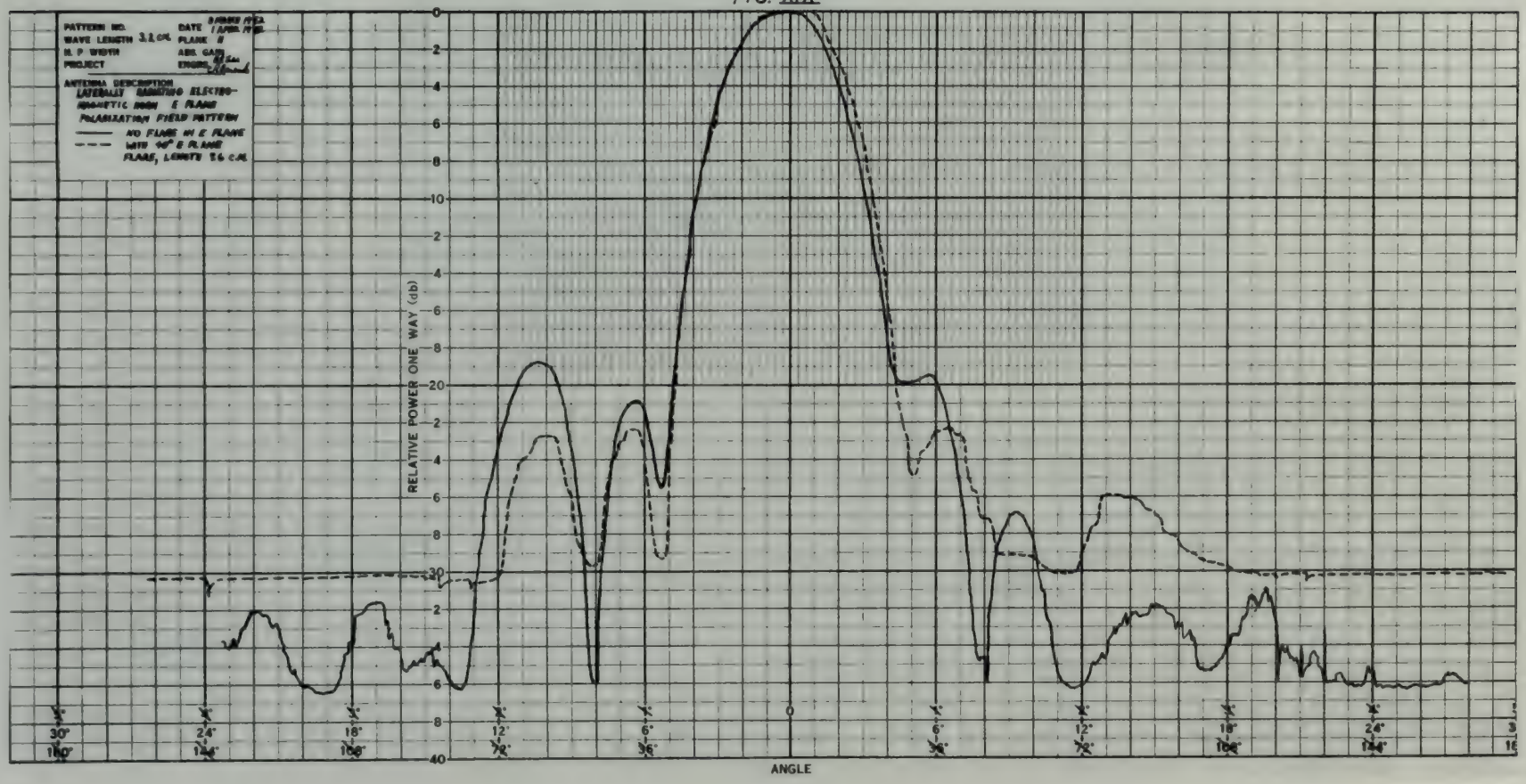
PATTERN NO.
DATE
WAVE LENGTH 3.2 CM.
PLANE H
H. P. WIDTH
ABS. GAIN
PROJECT
ANTENNA DESCRIPTION
LATERALLY RADIATING ELECTRO-MAGNETIC HORN E PLANE POLARIZATION FIELD PATTERN
NO FLARE IN E PLANE
WITH 14° E PLANE FLARE, LENGTH 2.6 C.M.
RELATIVE POWER ONE WAY (db)
0
2
4
6
8
10
20
30
40
30°
24°
18°
12°
6°
0
6°
12°
18°
24°
ANGLE

FIG. XX

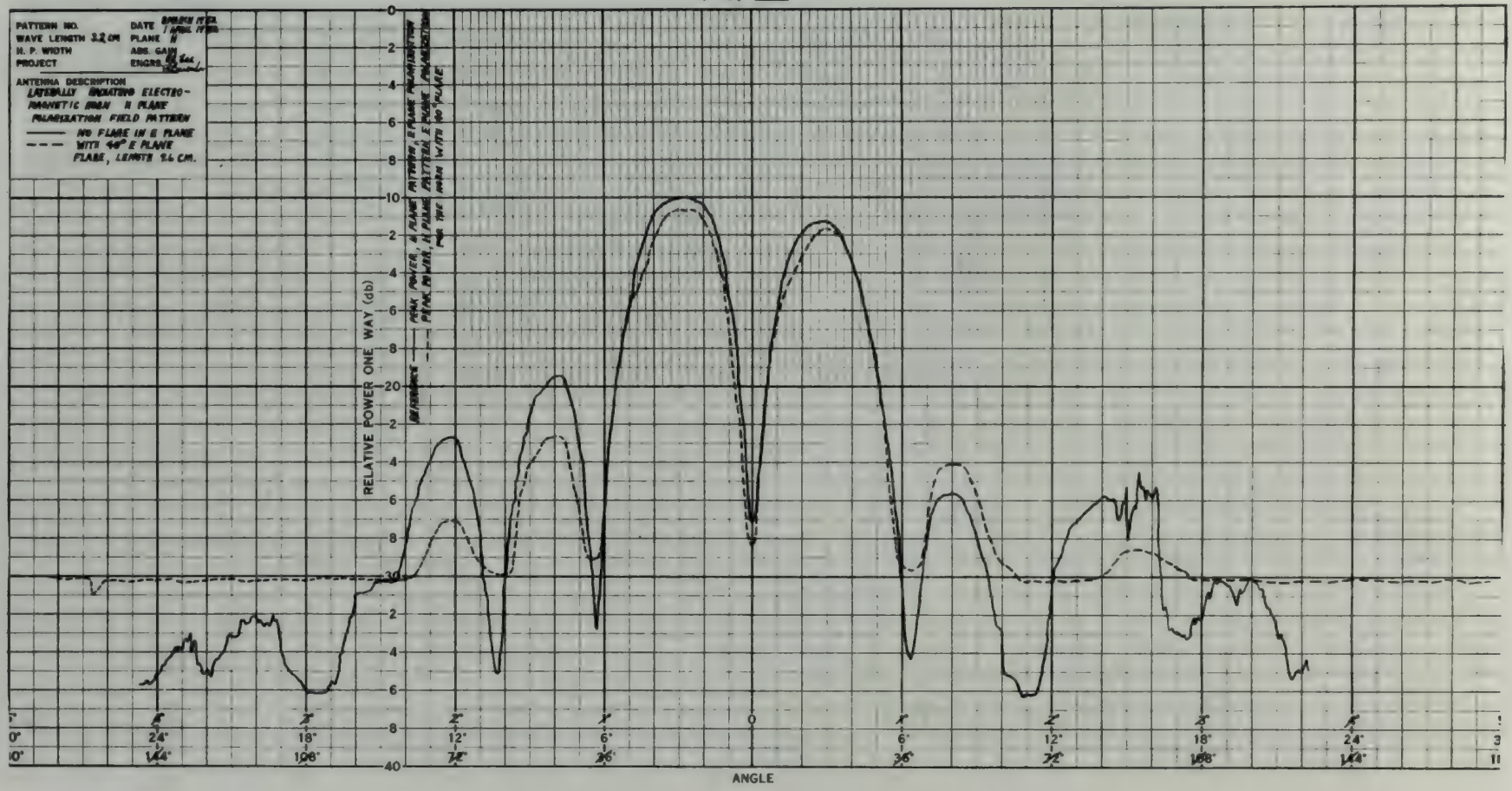
PATTERN NO.
DATE
WAVE LENGTH 3.2 CM
PLANE H
H. P. WIDTH
ABS. GAIN
PROJECT
ENGR.
ANTENNA DESCRIPTION
LATERALLY ROTATING ELECTRO-MAGNETIC BEAM H PLANE POLARIZATION FIELD PATTERN
——— NO FLARE IN E PLANE
– – – WITH 40° E PLANE FLARE, LENGTH 9.6 CM.
REMARKS
RELATIVE POWER ONE WAY (db)
ANGLE
0
2
4
6
8
10
20
30
40
24°
144°
18°
108°
12°
72°
6°
36°
0

FIG XXI

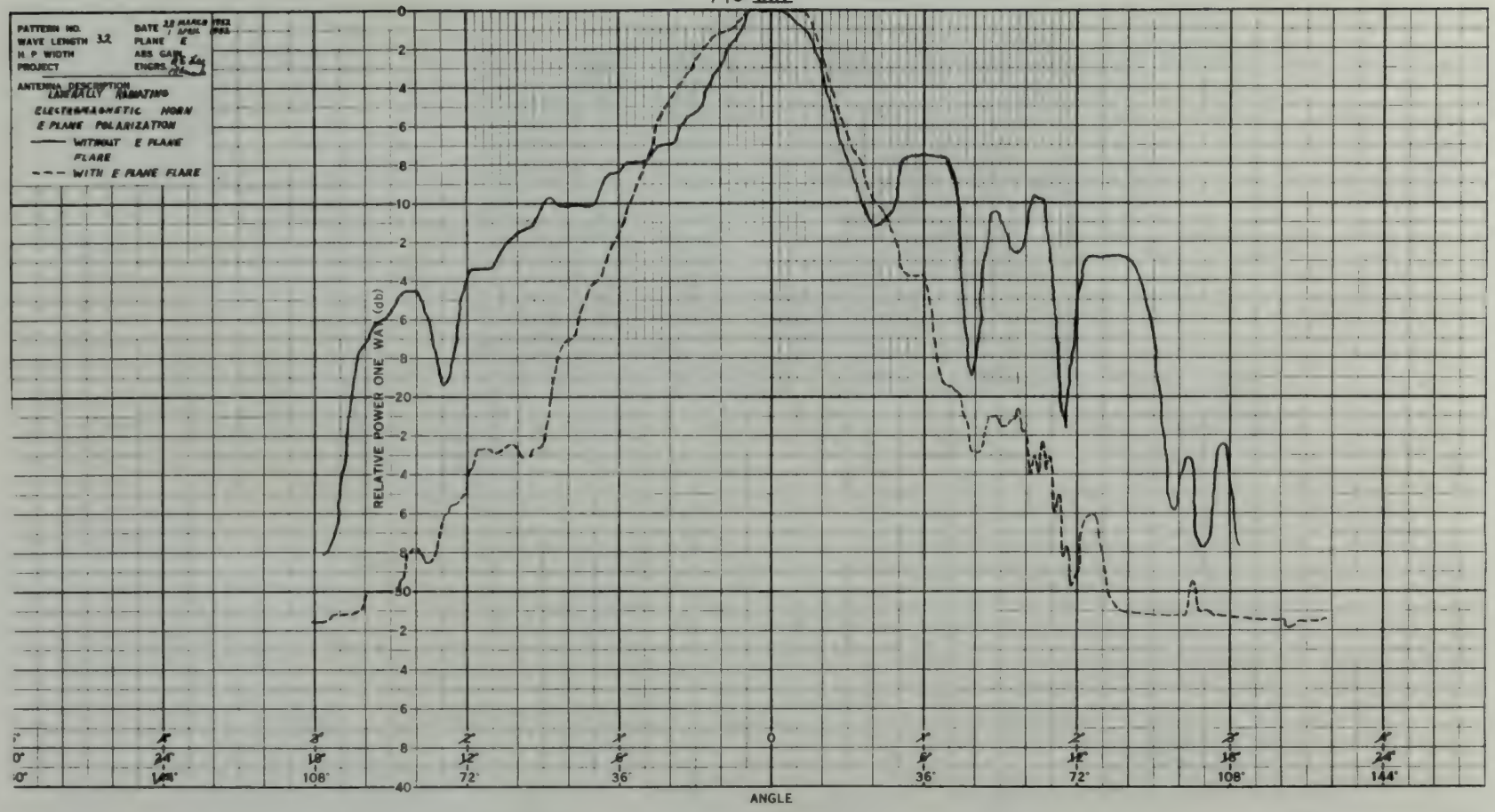
PATTERN NO.
WAVE LENGTH 3.2
H P WIDTH
PROJECT
DATE 23 MARCH 1951
PLANE E
ABS GAIN
ENGRS
ANTENNA DESCRIPTION
LONGITUDINALLY RADIATING
ELECTROMAGNETIC HORN
E PLANE POLARIZATION
WITHOUT E PLANE FLARE
WITH E PLANE FLARE
RELATIVE POWER ONE WAY (db)
0
2
4
6
8
10
20
30
40
ANGLE
144°
108°
72°
36°
0
36°
72°
108°
144°

FIG. XXII

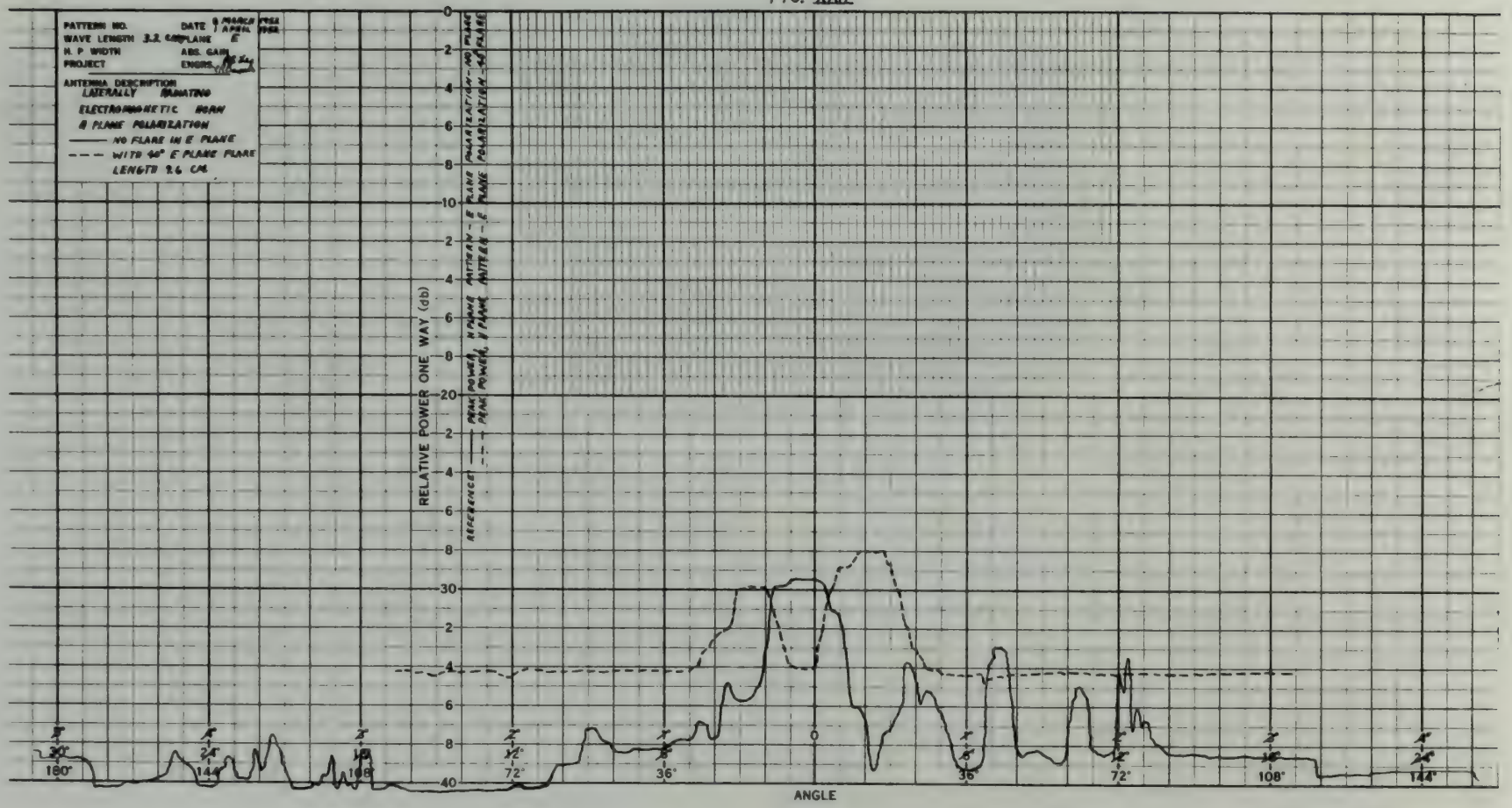
PATTERN NO.
DATE
WAVE LENGTH 3.2 cm
PLANE E
H. P. WIDTH
ABS. GAIN
PROJECT
ENGRS.
ANTENNA DESCRIPTION
LATERALLY RADIATING
ELECTROMAGNETIC HORN
E PLANE POLARIZATION
—— NO FLARE IN E PLANE
– – – WITH 40° E PLANE FLARE
LENGTH 2.6 CMS.
RELATIVE POWER ONE WAY (db)
RECEIVED
PEAK POWER, H PLANE ANTENNA – E PLANE POLARIZATION
PEAK POWER, H PLANE ANTENNA – E PLANE POLARIZATION
0
2
4
6
8
10
20
30
40
30°
24°
18°
12°
6°
0
6°
12°
18°
24°
30°
180°
144°
108°
72°
36°
36°
72°
108°
144°
ANGLE

FIG. XXIII

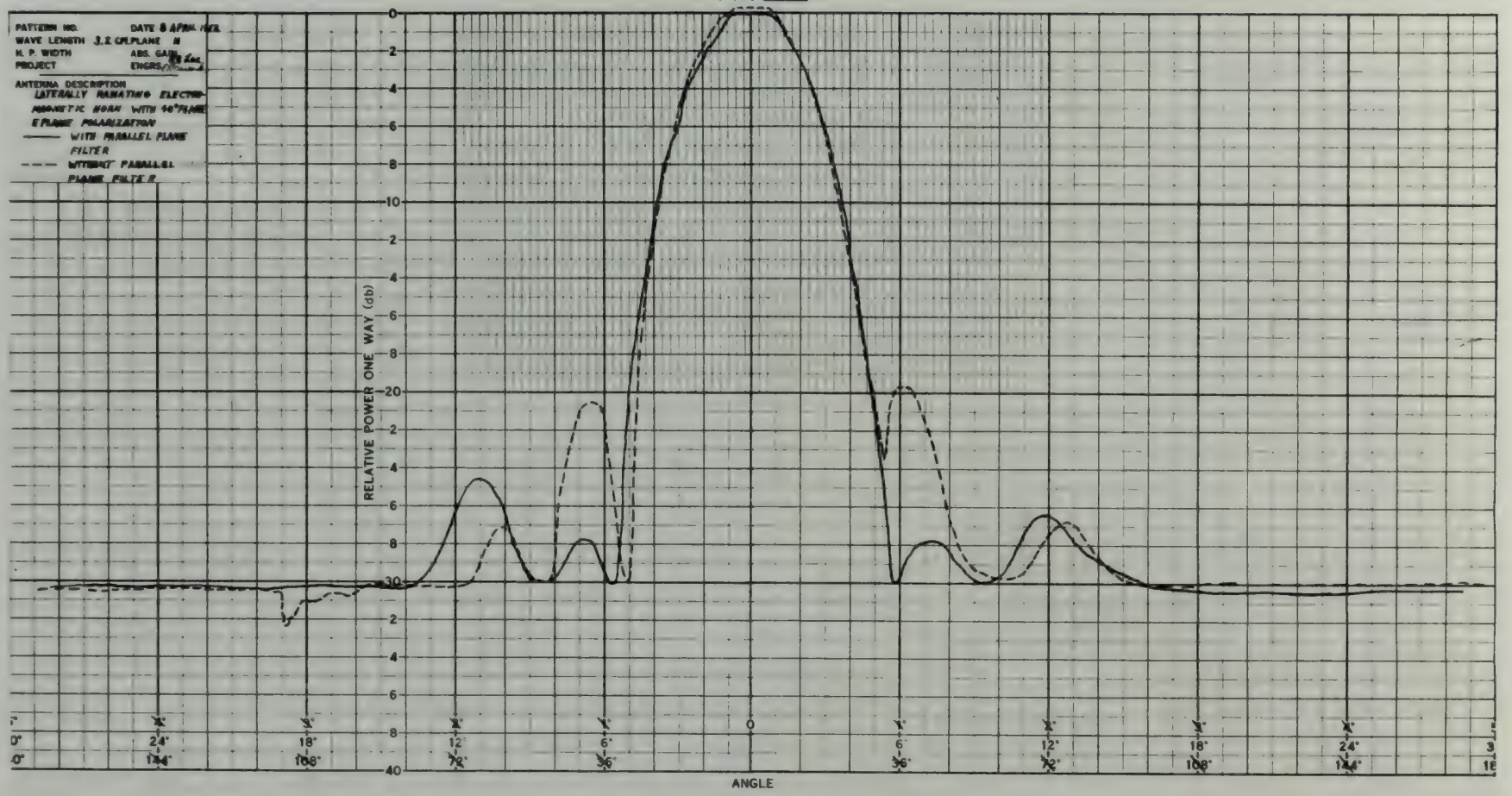
PATTERN NO.
DATE 8 APRIL 1943
WAVE LENGTH 3.2 CM PLANE H
H. P. WIDTH
ABS. GAIN
PROJECT
ENGRS.
ANTENNA DESCRIPTION
LATERALLY RADIATING ELECTROMAGNETIC HORN WITH 40° FLARE E PLANE POLARIZATION
WITH PARALLEL PLANE FILTER
WITHOUT PARALLEL PLANE FILTER
RELATIVE POWER ONE WAY (db)
0
2
4
6
8
10
20
30
40
24°
18°
12°
6°
0
6°
12°
18°
24°
ANGLE

FIG. XXIV

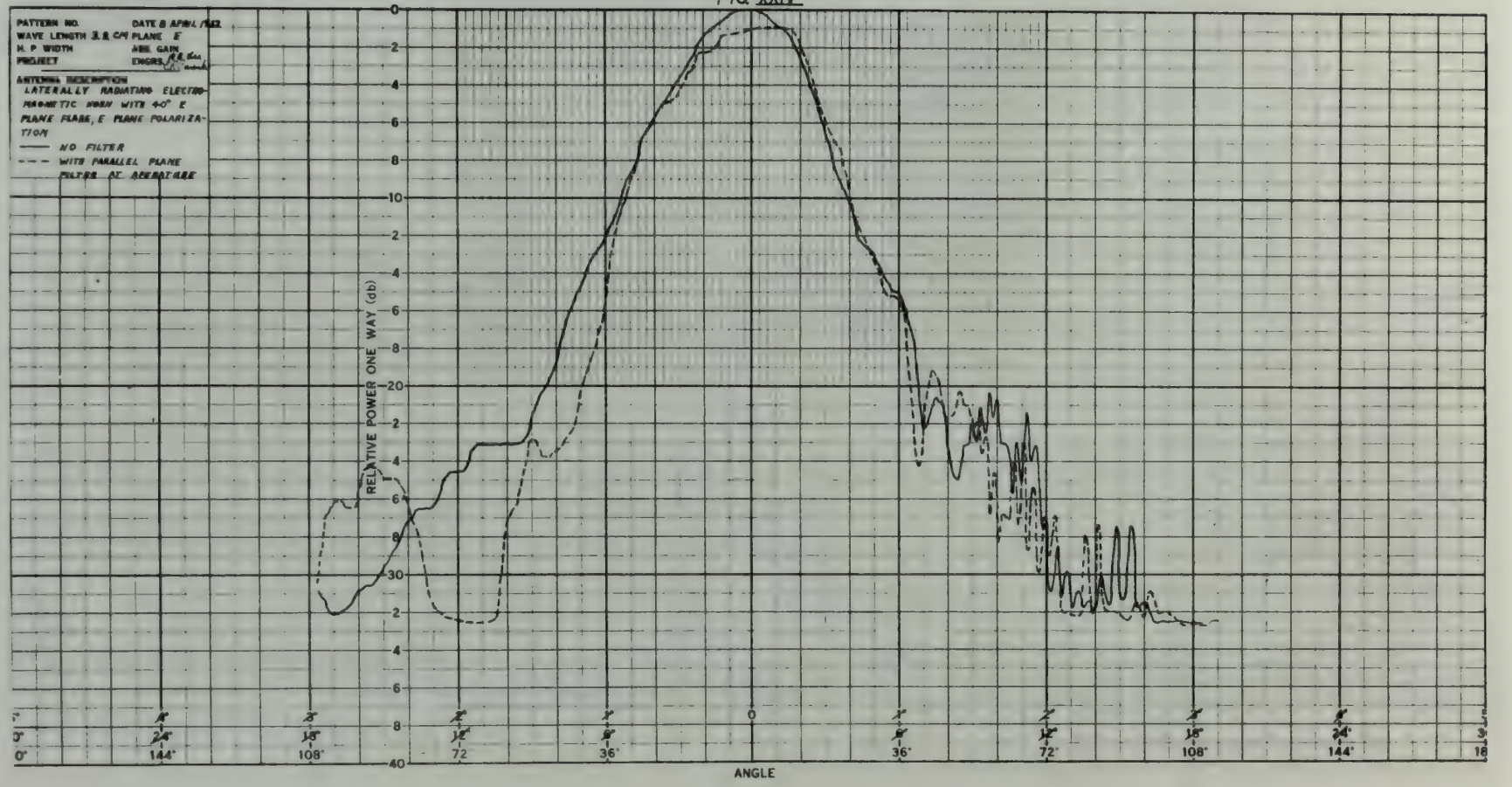
PATTERN NO.
DATE 8 APRIL 1942
WAVE LENGTH 3.2 CM
PLANE E
H. P. WIDTH
ANT. GAIN
PROJECT
ENGRS.
ANTENNA DESCRIPTION
LATERALLY RADIATING ELECTROMAGNETIC HORN WITH 40° E PLANE FLARE, E PLANE POLARIZATION
NO FILTER
WITH PARALLEL PLANE FILTER AT APERATURE
RELATIVE POWER ONE WAY (db)
0
2
4
6
8
10
20
30
40
ANGLE
144°
108°
72
36°
0
36°
72°
108°
144°

FIG. XXV

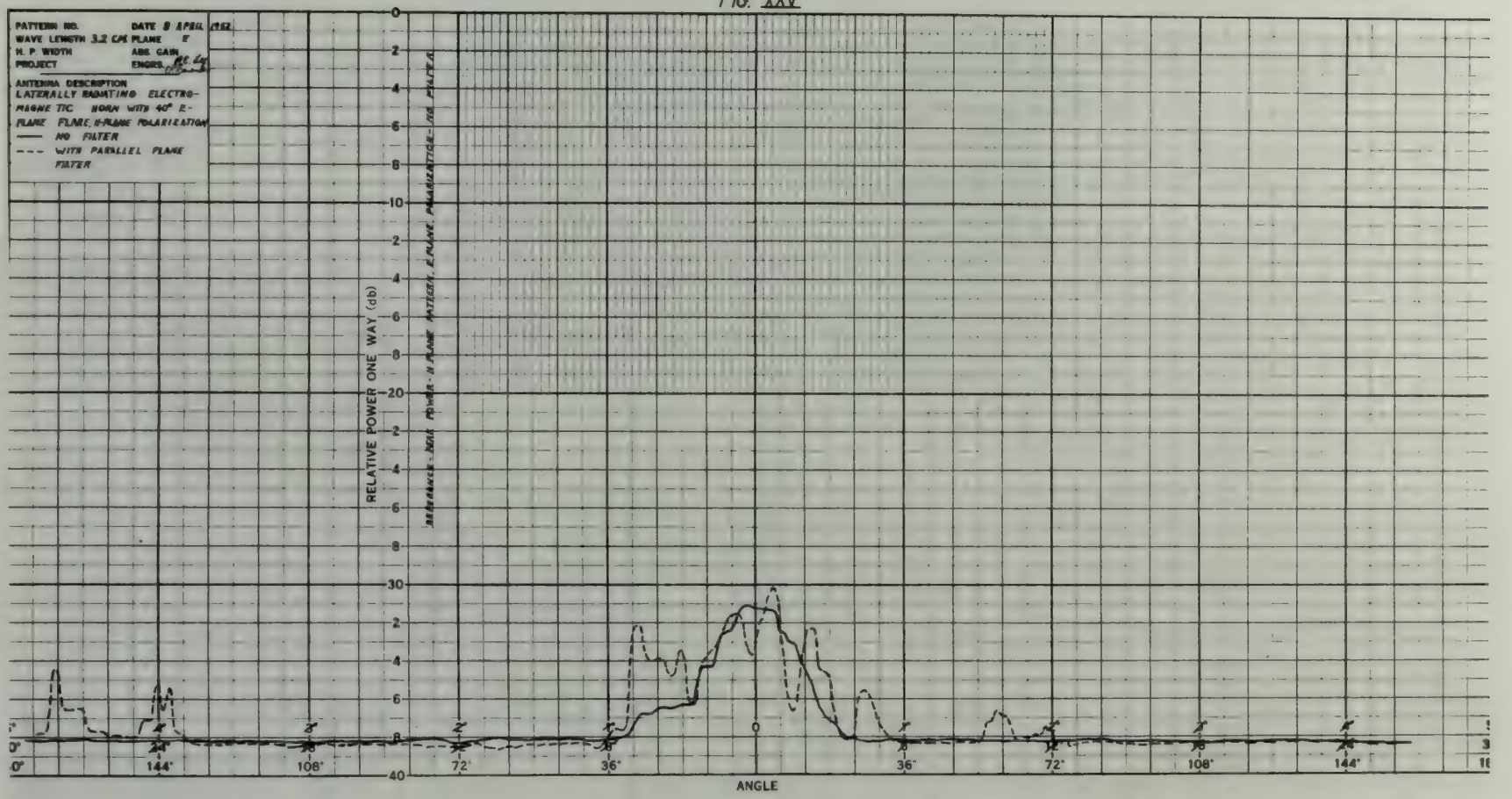
PATTERN NO. DATE 8 APRIL 1942
WAVE LENGTH 3.2 CM PLANE E
H. P. WIDTH ABS. GAIN
PROJECT ENGRS.
ANTENNA DESCRIPTION
LATERALLY RADIATING ELECTRO-MAGNETIC HORN WITH 40° E-PLANE FLARE, H-PLANE POLARIZATION
—— NO FILTER
--- WITH PARALLEL PLANE FILTER
RELATIVE POWER ONE WAY (db)
0
2
4
6
8
10
20
30
40
144°
108°
72°
36°
0
ANGLE

FIG. XXVI

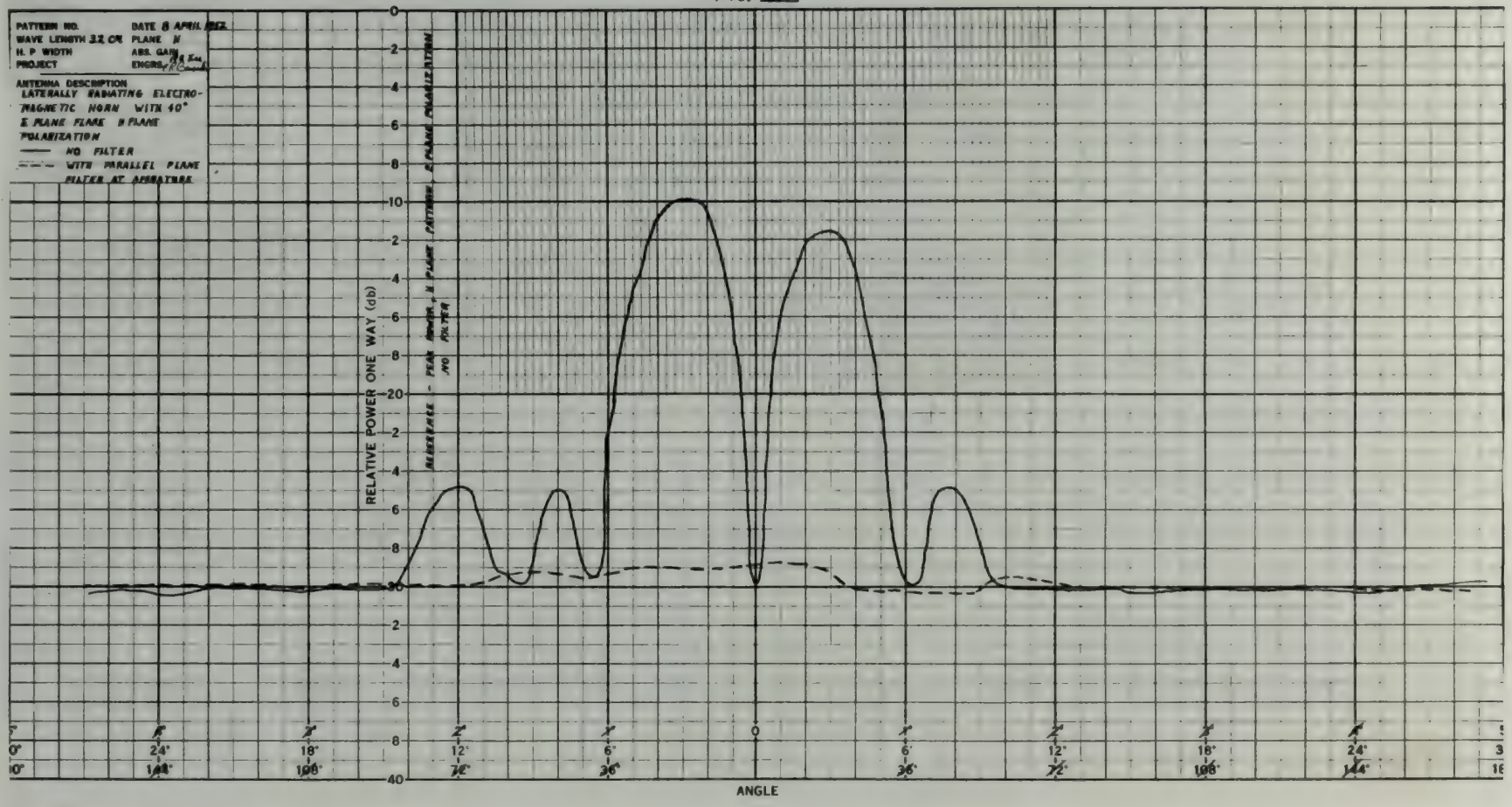
PATTERN NO.
DATE 8 APRIL 1942
WAVE LENGTH 3.2 CM
PLANE H
H. P WIDTH
ABS. GAIN
PROJECT
ENGRS.
ANTENNA DESCRIPTION
LATERALLY RADIATING ELECTRO-MAGNETIC HORN WITH 40° E PLANE FLARE H PLANE POLARIZATION
NO FILTER
WITH PARALLEL PLANE FILTER AT APERATURE
RELATIVE POWER ONE WAY (db)
0
2
4
6
8
10
20
30
40
24°
18°
12°
6°
0
6°
12°
18°
24°
ANGLE

FIG. XXVII

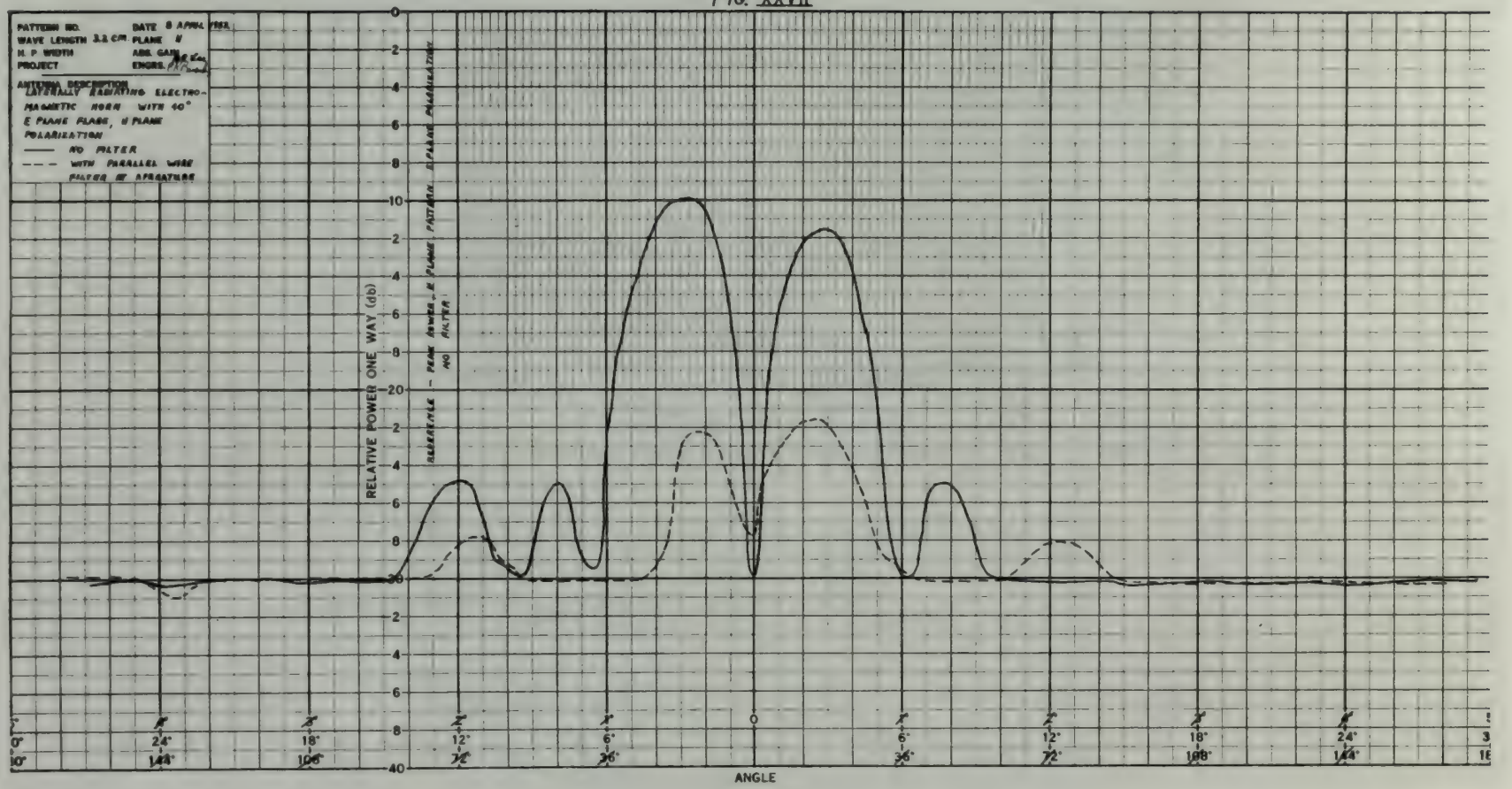
PATTERN NO.
DATE 8 APRIL 1952
WAVE LENGTH 3.2 CM.
PLANE H
H. P. WIDTH
ABS. GAIN
PROJECT
ENGRS.
ANTENNA DESCRIPTION
LATERALLY RADIATING ELECTRO-MAGNETIC HORN WITH 40° E PLANE FLARE, H PLANE POLARIZATION
NO FILTER
WITH PARALLEL WIRE FILTER IN APERATURE
REFERENCE - PEAK POWER, E PLANE PATTERN, E PLANE POLARIZATION, NO FILTER
RELATIVE POWER ONE WAY (db)
0
2
4
6
8
10
20
30
40
24°
18°
12°
6°
0
6°
12°
18°
24°
144°
108°
72°
36°
36°
72°
108°
144°
ANGLE

FIG. XXVIII

PLOT OF ELLIPTICITY OF THE LATERALLY RADIATING ELECTROMAGNETIC HORN FOR POSITIVE θ AND RIGHT ELLIPTICAL POLARIZATION

P.d.R. Saunders A.E. Lu

16 April 1952

Relative Power is in Brackets

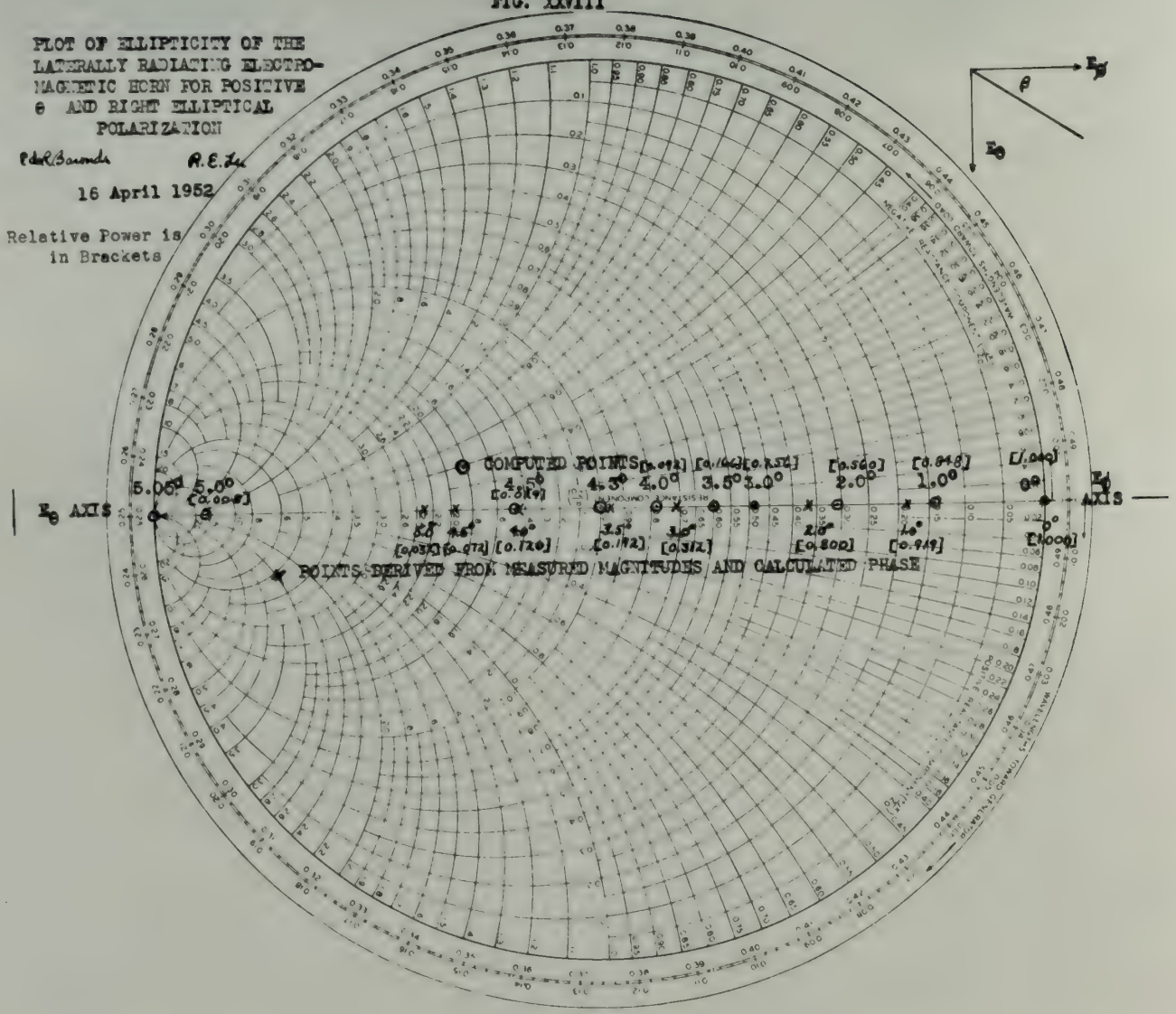

FIG. XXIX

PLOT OF ELLIPTICITY OF THE LATERALLY RADIATING ELECTRO-MAGNETIC HORN FOR NEGATIVE θ AND LEFT ELLIPTICAL POLARIZATION

E.A.R. Bernales R.E. Lee
16 April 1952

Relative Power is in Brackets.

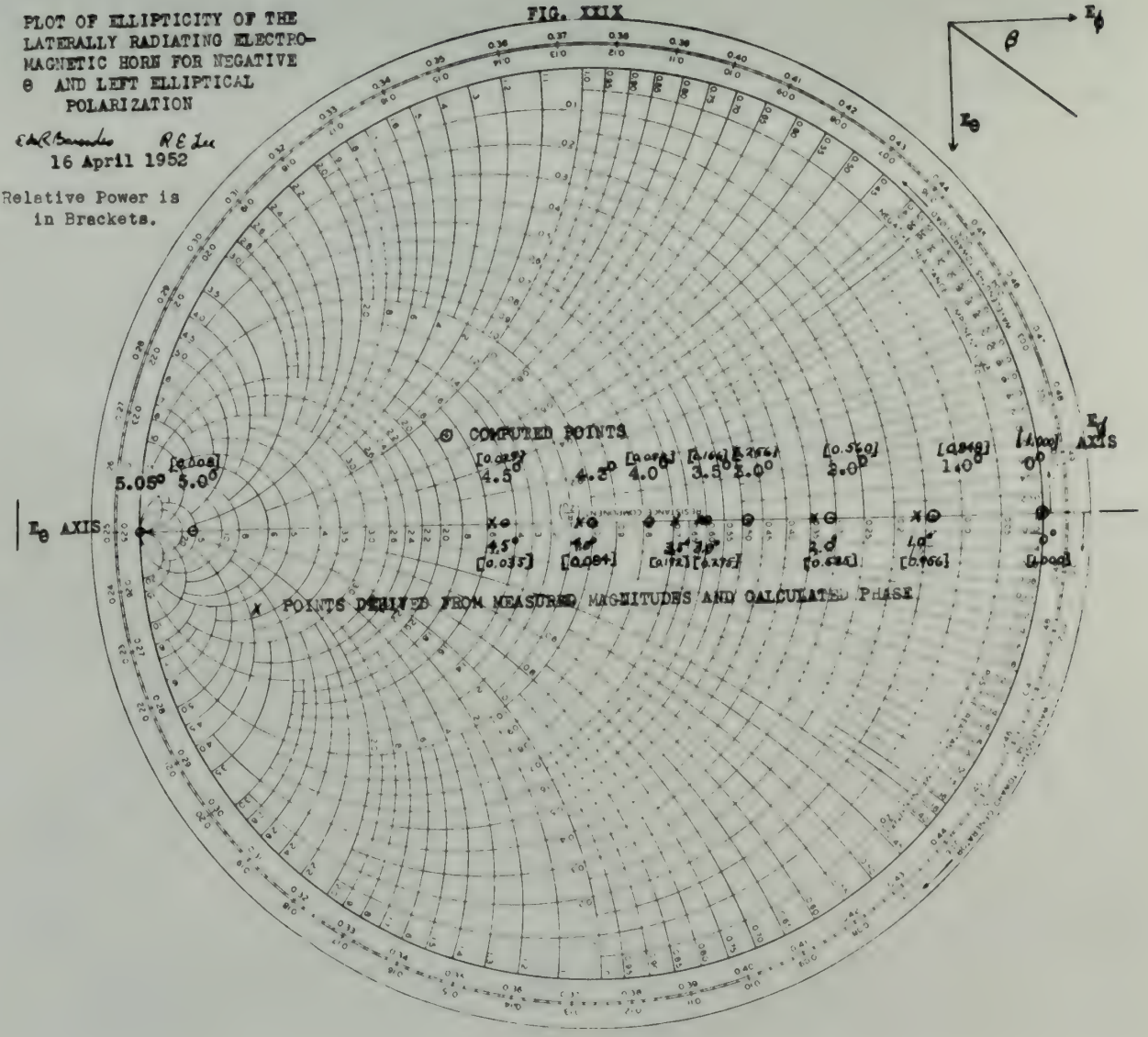

FIG. XXX

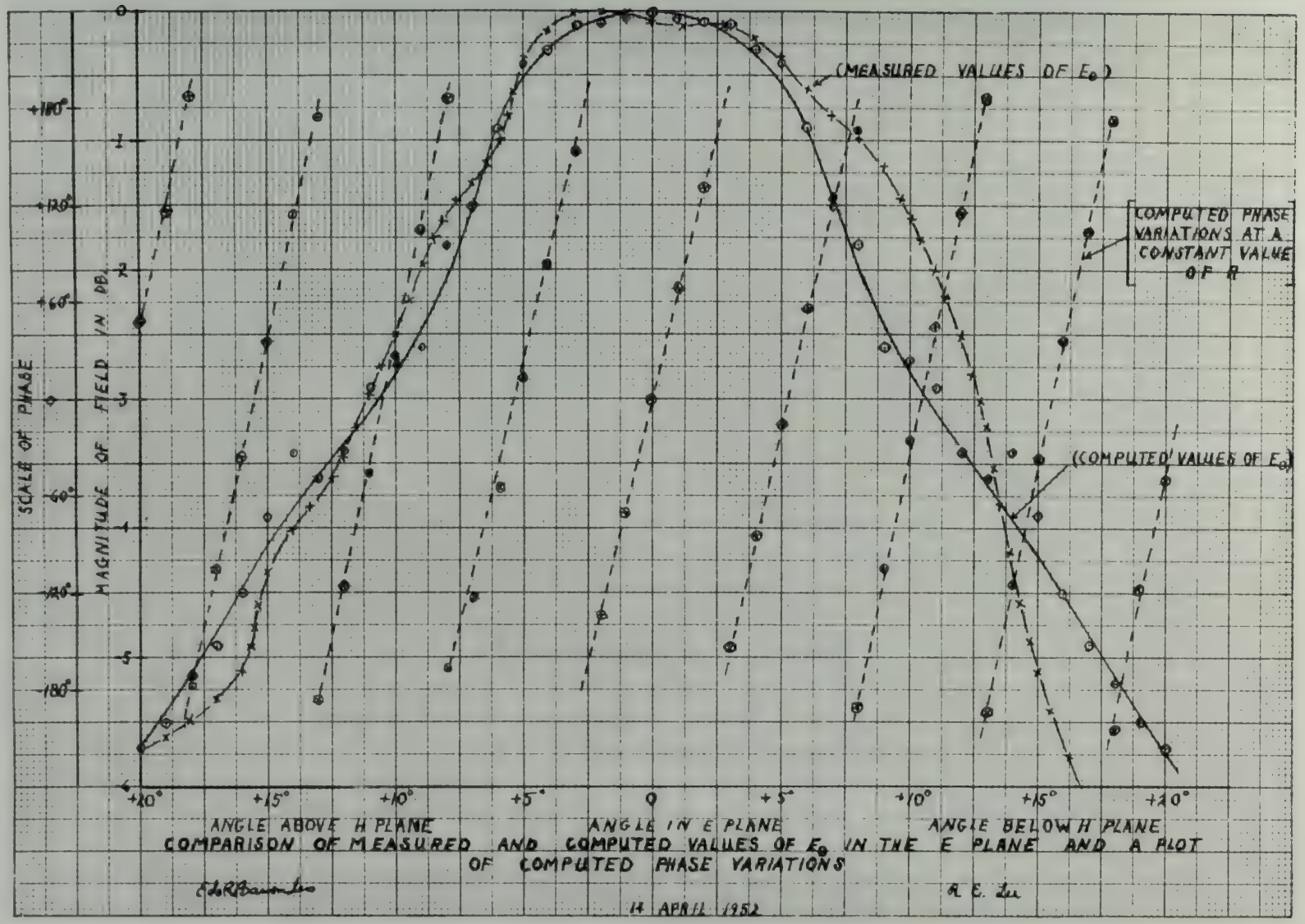

COMPARISON OF MEASURED AND COMPUTED VALUES OF E_θ IN THE E PLANE AND A PLOT OF COMPUTED PHASE VARIATIONS

E. L. Bauman

14 APRIL 1952

R. E. Lee

FIG. XXXI

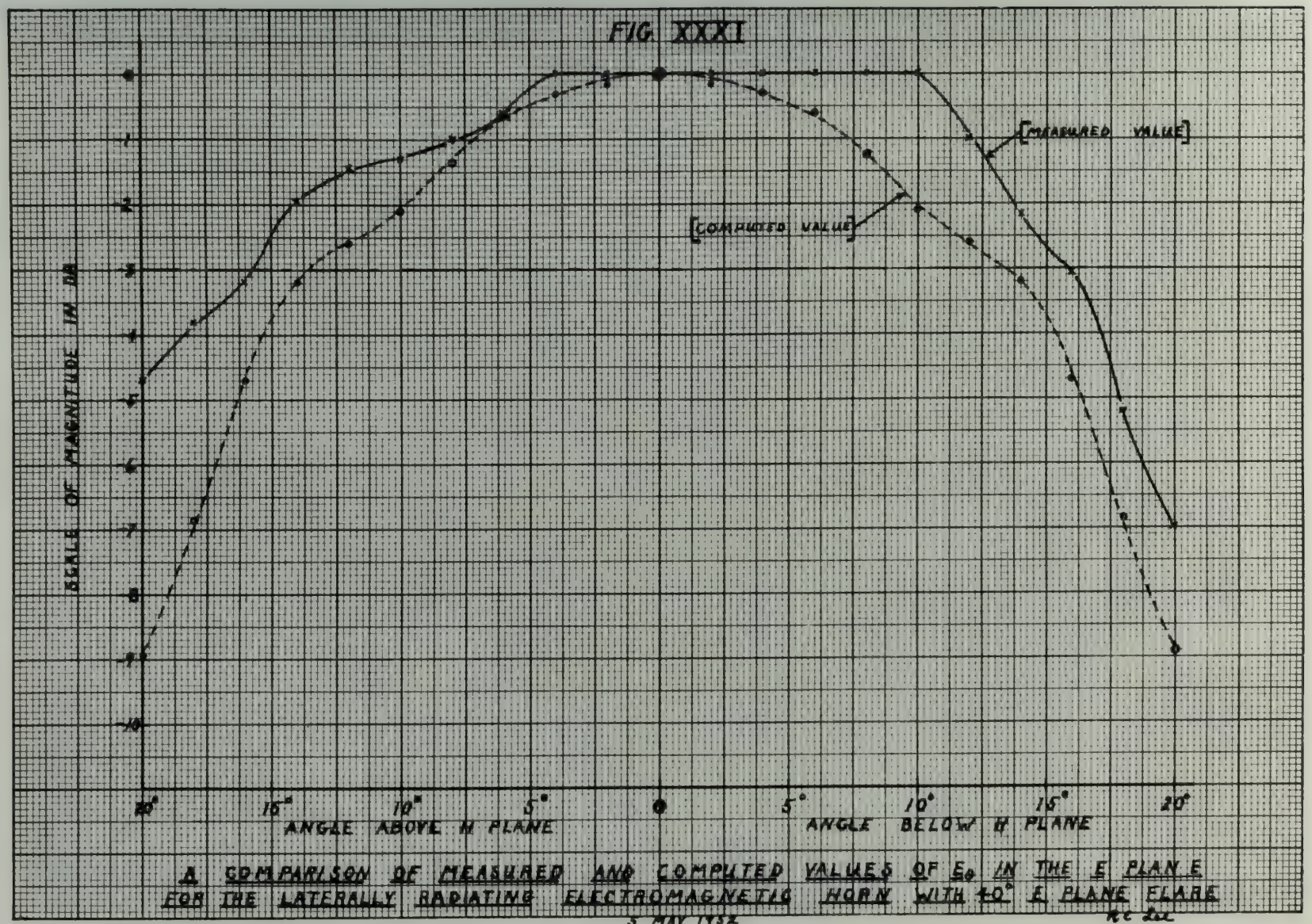

A COMPARISON OF MEASURED AND COMPUTED VALUES OF E_θ IN THE E PLANE FOR THE LATERALLY RADIATING ELECTROMAGNETIC HORN WITH 40° E PLANE FLARE

5 MAY 1952

Rc 2xc

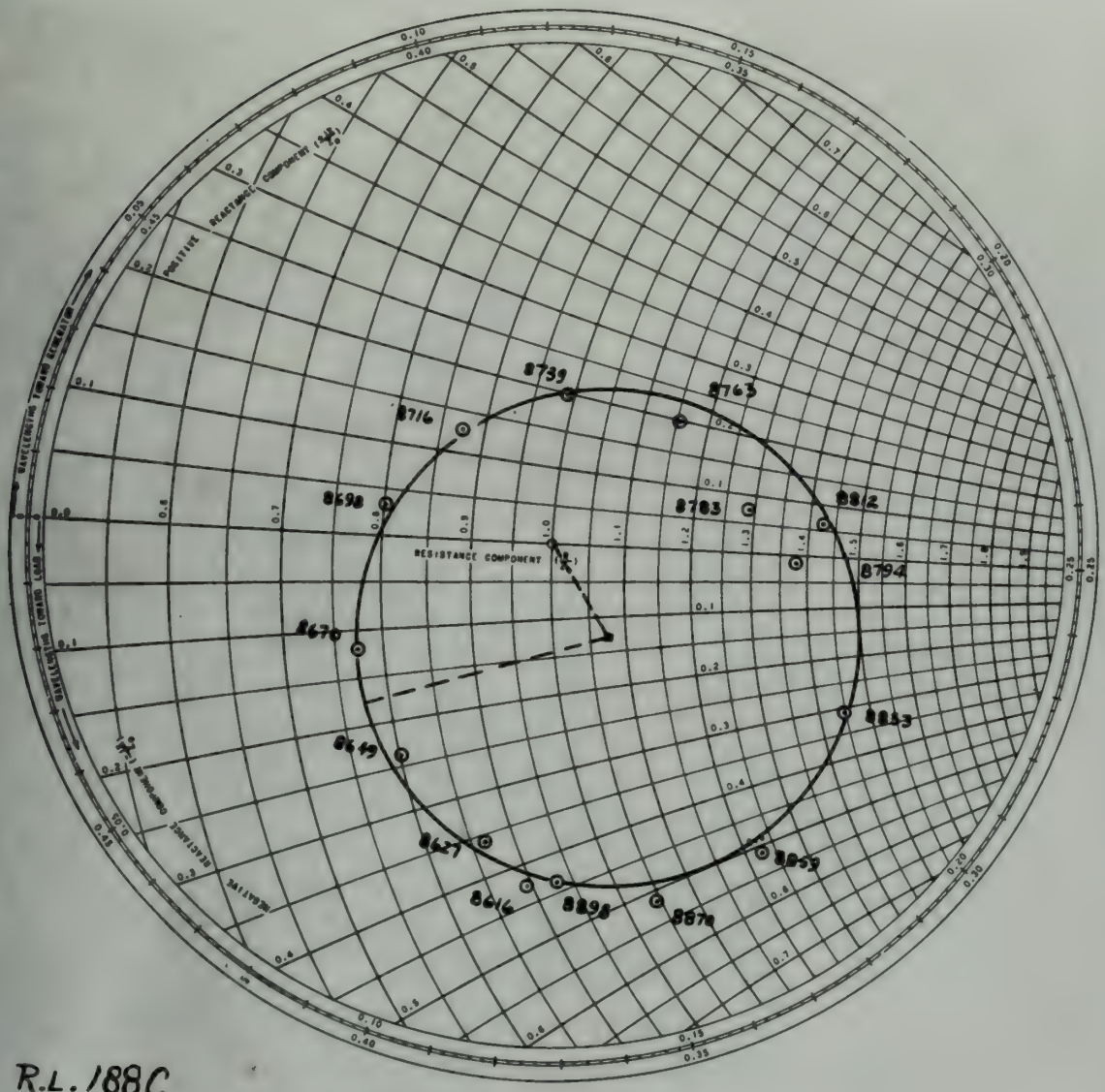

R.L. 188C

ADMITTANCES OF THE UNCOMPENSATED HORN,
(CONDITION 1), FOR DIFFERENT FREQUENCY,
TRANSFERRED TO THE THROAT.

R.E. Lee
E.R. Baxendale
1 May 1952

XXXIII

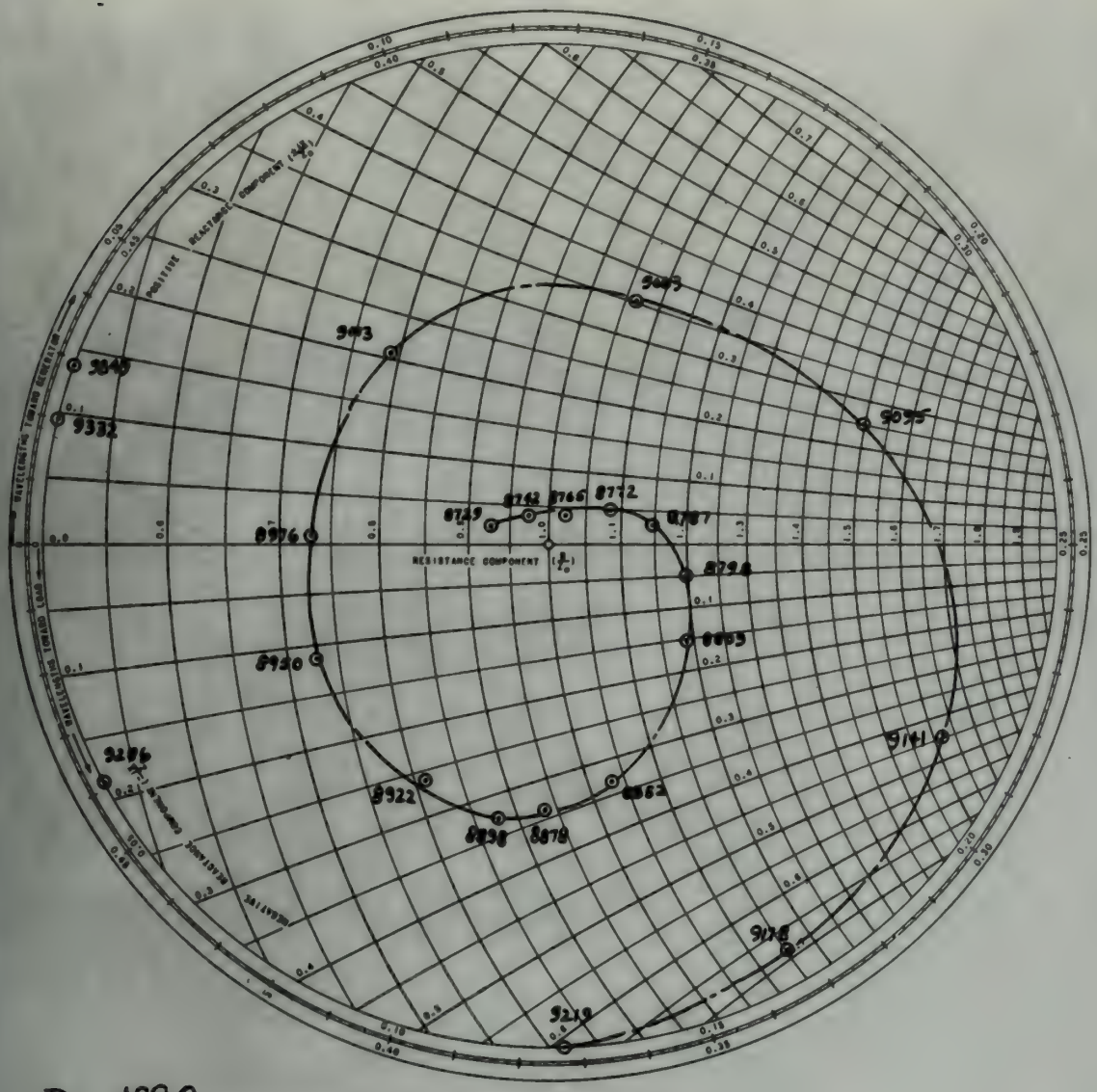

R.L. 188C

ADMITTANCES OF THE HORN WITH PLANE PARALLEL PLATE FILTER, NO E PLANE FLARE, (CONDITION 2), FOR DIFFERENT FREQUENCY, TRANSFERRED TO THE THROAT.

R E Lee
E R Barnes
1 May 1952

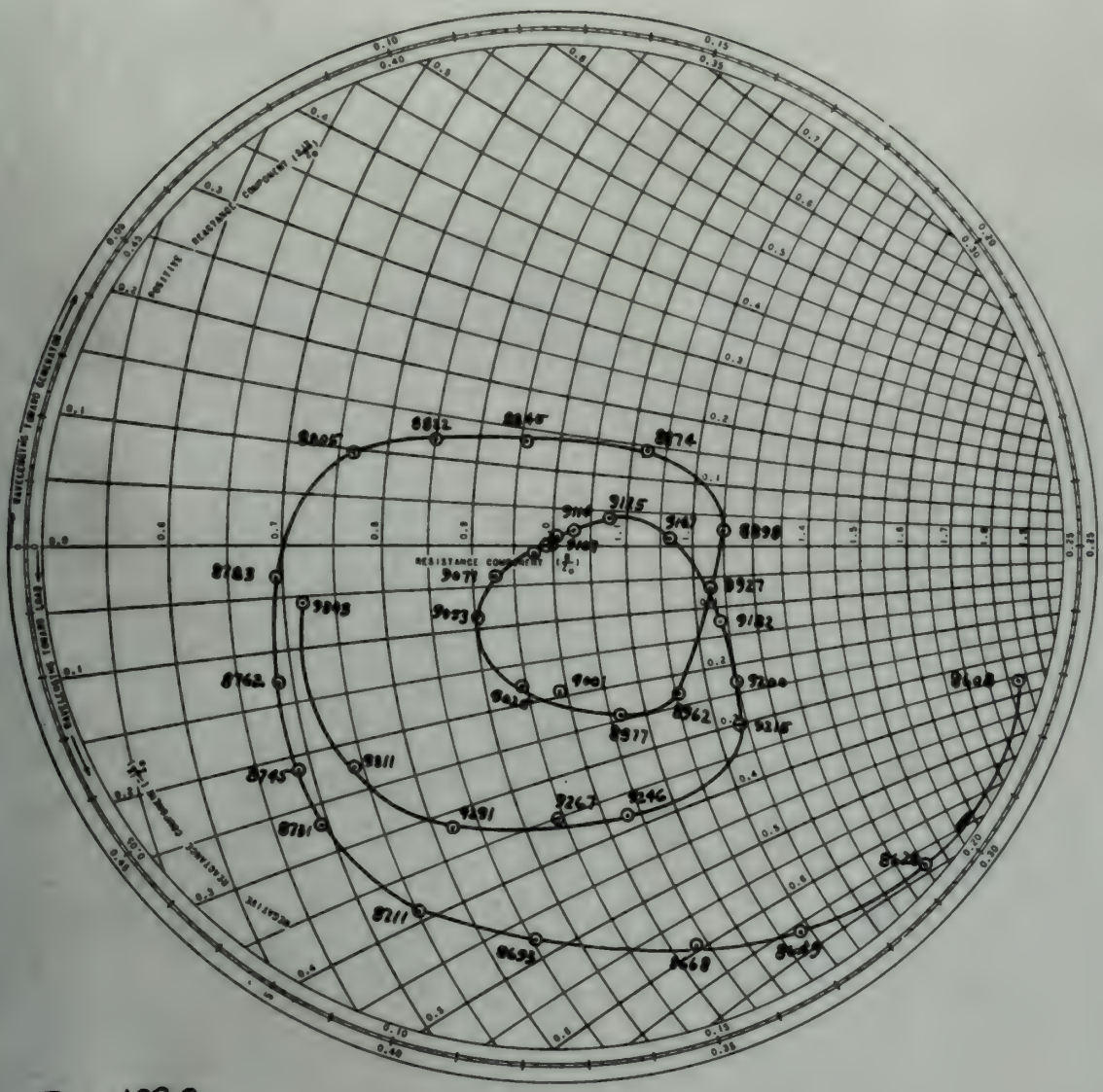

R.L. 188C

ADMITTANCES OF THE HORN WITH E PLANE FLARE, NO FILTER, (CONDITION 4), FOR DIFFERENT FREQUENCY, TRANSFERRED TO THE THROAT.

R E Lee
E R Barnes
1 May 1952

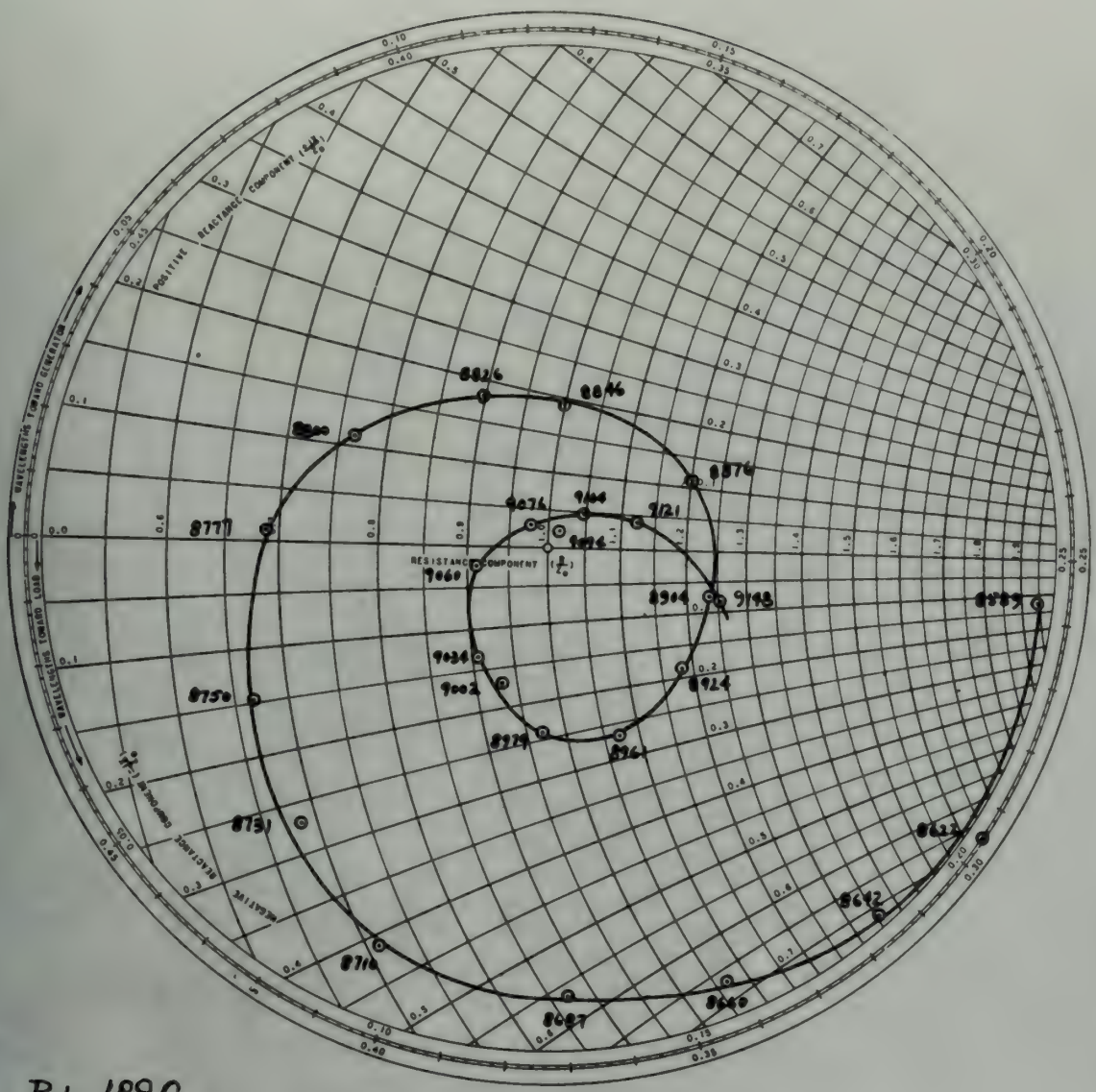

R.L. 188C

ADMITTANCES OF THE HORN WITH E PLANE FLARE, PLANE PARALLEL FILTER, (CONDITION 4), FOR DIFFERENT FREQUENCY, TRANSFERRED TO THE THROAT.

R E Lee
E R Barcodes
1 May 1952

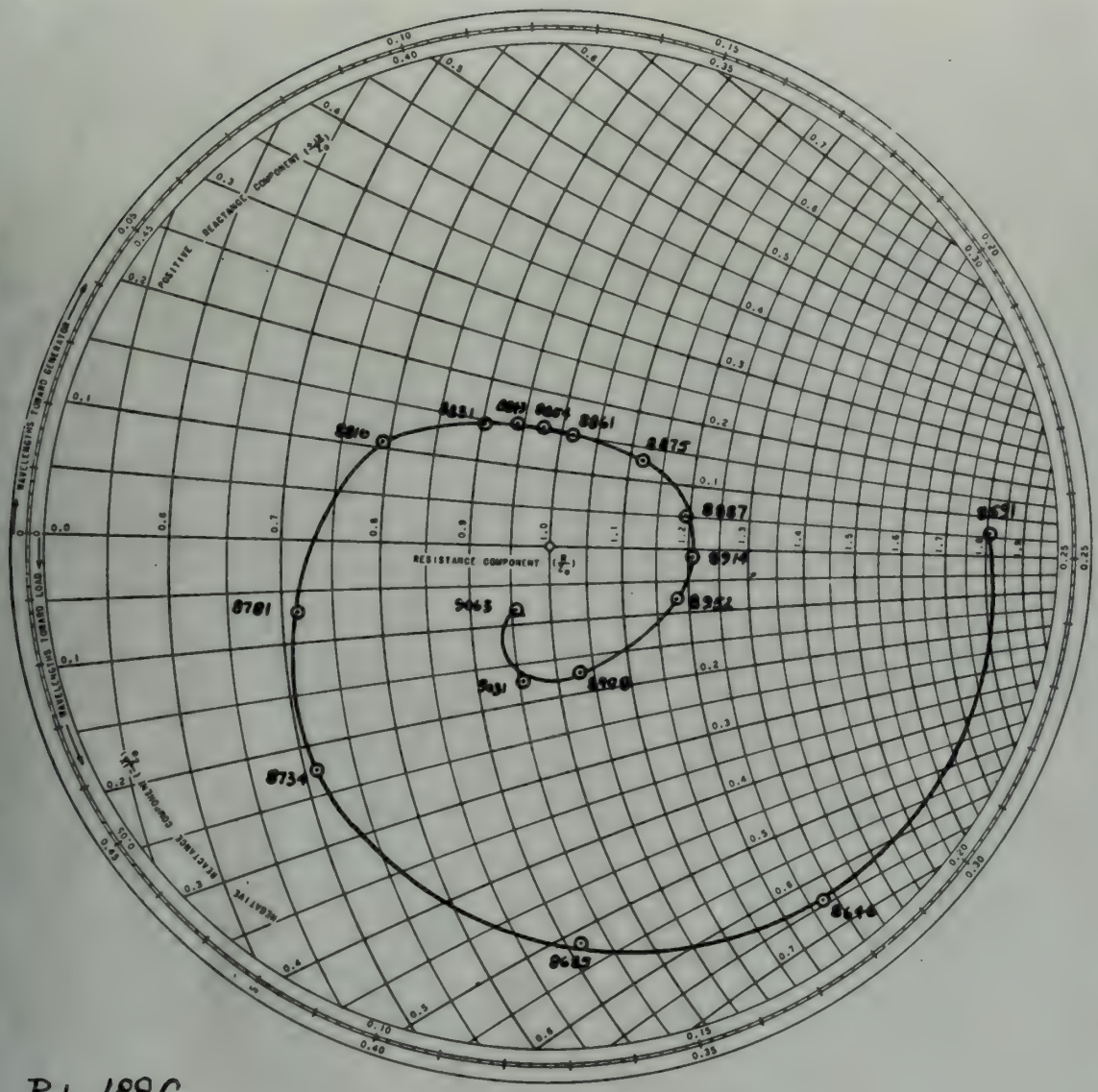

R.L. 188C

ADMITTANCES OF THE HORN WITH E PLANE FLARE, PARALLEL WIRE FILTER, (CONDITION 5), FOR DIFFERENT FREQUENCY, TRANSFERRED TO THE THROAT.

R E Lee
E R Barnes
1 May 1952

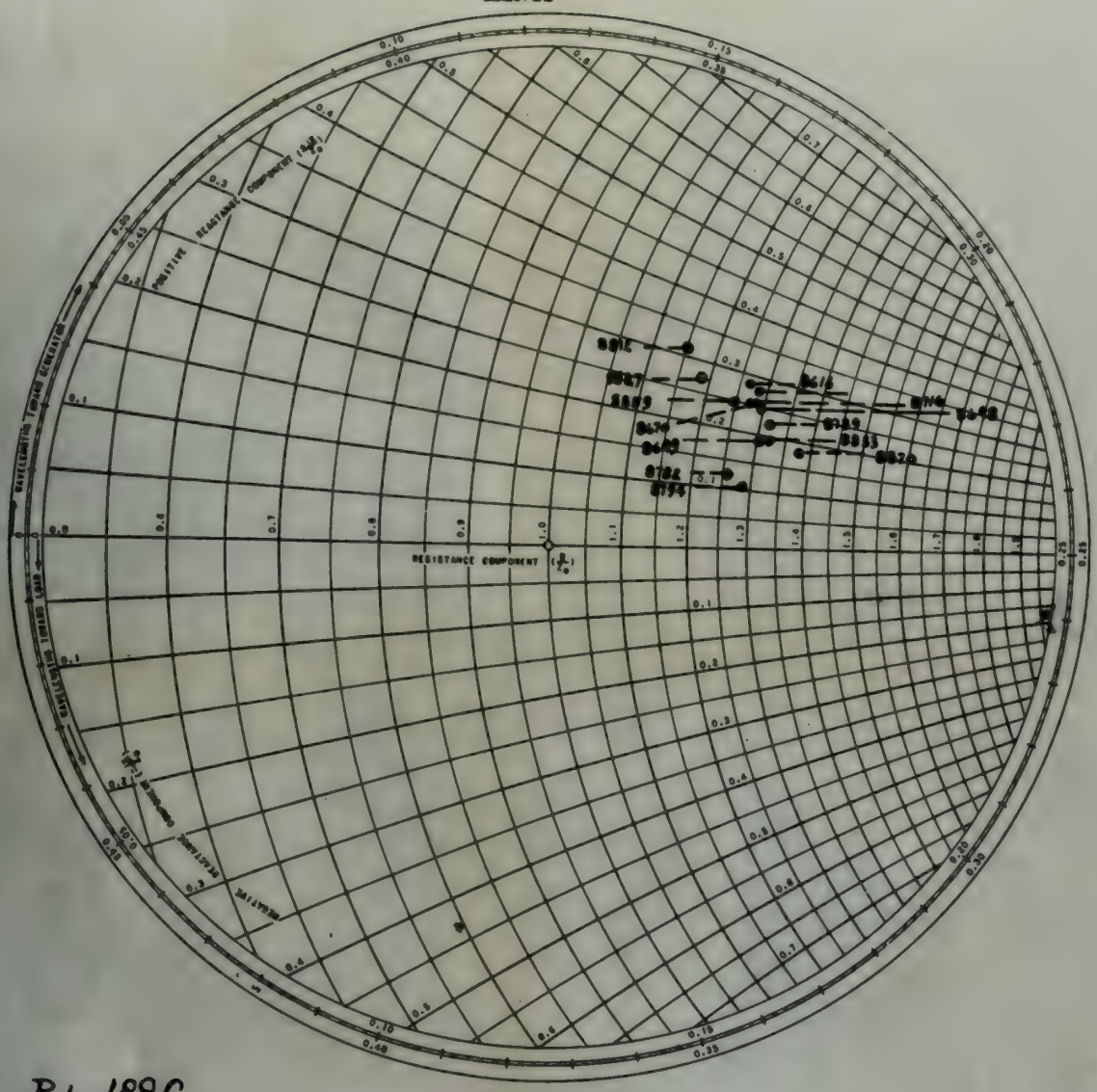

R.L. 188C

ADMITTANCE COMPONENTS AT THE HORN APERATURE FOR THE UNCOMPENSATED HORN, (CONDITION 1), FOR DIFFERENT FREQUENCY, TRANSFERRED TO THE APERATURE FROM THE THROAT.

R C Lee
E R Barnes
1 May 1952

Fig. XXXVIII
The Laterally Radiating
Horn on the Turntable.

Fig. XXXIX
The Laterally Radiating
Horn with 40° Plane Flare)
on the Turntable.

APPENDIX, SECTION B

DETAILS OF PROCEDURE

The Fraunhofer Diffraction Theory Applied to the Laterally Radiating Electromagnetic Horn

In order to determine analytically the performance of the horn, the first step is to develop the integral field equations applicable to the Fraunhofer region of space. These equations have been developed[30] and will be integrated to obtain the radiation pattern of the horn. The coordinate system is given in Figure II.

$$E_{p\theta} = \frac{jk\,\varepsilon^{-jkR}}{4\pi R}\left(1+a\sqrt{\frac{\mu}{\varepsilon_o}}\,\mathrm{Cos}\,\theta\right)\left[N_x\,\mathrm{Cos}\,\phi + N_y\,\mathrm{Sin}\,\phi\right] \qquad (A\text{-}1)$$

$$E_{p\phi} = \frac{-jk\,\varepsilon^{-jkR}}{4\pi R}\left(\mathrm{Cos}\,\theta + a\sqrt{\frac{\mu}{\varepsilon_o}}\right)\left[N_x\,\mathrm{Sin}\,\phi - N_y\,\mathrm{Cos}\,\phi\right] \qquad (A\text{-}2)$$

Where a is defined by the relationship,

$$H = a(S \times E) \qquad (A\text{-}3)$$

and

$$N_x = \int_s E_{sx}\,\varepsilon^{jk(x\,\mathrm{Sin}\,\theta\,\mathrm{Cos}\,\phi + y\,\mathrm{Sin}\,\theta\,\mathrm{Sin}\,\phi)}\,\delta s \qquad (A\text{-}4)$$

$$N_y = \int_s E_{sy}\,\varepsilon^{jk(x\,\mathrm{Sin}\,\theta\,\mathrm{Cos}\,\phi + y\,\mathrm{Sin}\,\theta\,\mathrm{Sin}\,\phi)}\,\delta s \qquad (A\text{-}5)$$

In order to integrate the field expressions it is necessary to make a valid assumption of the fields existing at the aperture of the horn. Consider the laterally radiating electromagnetic horn as an H plane flared sectoral horn with a gradual E plane bend of low curvature as illustrated in Figure I. The fields in the sectoral horn[31] for the geometry in Figure III are given by:

CHAPTER II SECTION 2

[illegible]

The Dyadic Green's Function Applied to the Radiation Problem

Introductory Remarks

In order to determine analytically the performance of the horn, the Close and Jy is to derive the dyadic field equations applicable to the Cartesian region of space. These equations have been derived[10] and will be integrated to obtain the radiation pattern of the horn. The coordinate system is given in Figure II.

$$E^x_{pq} = \frac{-jk\,e^{-jkr}}{4\pi r}\left(1+\sqrt{\frac{\epsilon}{\mu}}\cos\theta\right)\left[\beta^x\cos\phi+\beta^y\sin\phi\right] \tag{2-3}$$

$$E^y_{pq} = \frac{-jk\,e^{-jkr}}{4\pi r}\left(\cos\phi+\sqrt{\frac{\epsilon}{\mu}}\right)\left[\beta^x\sin\phi-\beta^y\cos\phi\right] \tag{2-4}$$

Where α is defined by the relationship,

$$k = \omega(\mu\epsilon)^{\frac{1}{2}} \tag{2-5}$$

and

$$\beta^x = \int_z^x e^{jk(x\sin\alpha\cos\beta+y\sin\alpha\sin\beta)}\,dx \tag{2-6}$$

$$\beta^y = \int_z^y e^{jk(x\sin\alpha\cos\beta+y\sin\alpha\sin\beta)}\,dy \tag{2-7}$$

In order to integrate the first expression it is necessary to make a valid assumption of the field existing at the aperture of the horn. Consider the ideally radiating electromagnetic horn as an H plane flared sectoral horn with a finite H plane flare angle as pictured in Figure I. The E-field in the aperture may[10] for the geometry in Figure III are given by:

$$E_y = A_1 \left[\cos \frac{\pi\theta}{2\theta_o} \right] \left[H^{(2)}_{\left(\frac{\pi}{2\theta}\right)_o}(kr) + C_1 H^{(1)}_{\left(\frac{\pi}{2\theta}\right)_o}(kr) \right] \tag{A-6}$$

$$H_r = \frac{\pi A_1}{2r\theta_o\, j\omega\mu} \left[\sin \frac{\pi\theta}{2\theta_o} \right] \left[H^{(2)}_{\left(\frac{\pi}{2\theta}\right)_o}(kr) + C_1 H^{(1)}_{\left(\frac{\pi}{2\theta}\right)_o}(kr) \right] \tag{A-7}$$

$$H_\theta = \frac{kA_1}{j\omega\mu} \left[\cos \frac{\pi\theta}{2\theta_o} \right] \left[H^{(2)'}_{\frac{\pi}{2\theta_o}}(kr) + C_1 H^{(1)'}_{\frac{\pi}{2\theta_o}}(kr) \right] \tag{A-8}$$

$H^{(1)}(kr)$ and $H^{(2)}(kr)$ are Hankel functions of the first and second kinds respectively. Because only large flare angles and large radii will be employed in this investigation the asymptotic expressions for the Hankel functions may be employed.

$$H^{(1)}_n(kr) \cong \left[\frac{2}{\pi kr}\right]^{\frac{1}{2}} \varepsilon^{j\left(kr - \frac{(2n+1)\pi}{4}\right)} \tag{A-9}$$

$$H^{(2)}_n(kr) \cong \left[\frac{2}{\pi kr}\right]^{\frac{1}{2}} \varepsilon^{-j\left(kr - \frac{(2n+1)\pi}{4}\right)} \tag{A-10}$$

Equations (A-9) and (A-10) indicate that the equiphase surfaces are separated by free space wavelength near the aperture. Considering only the solution of the wave traveling in the positive r direction, the fields at a fixed radius, r_o, from the origin in Figure III become:

$$E_y = A_1 \cos\left(\frac{\pi\theta}{2\theta_o}\right) H^{(2)}_{\left(\frac{\pi}{2\theta_o}\right)}(kr_o) \tag{A-11}$$

$$H_r = \frac{\pi A_1}{2r_o\theta_o\, j\omega\mu} \sin\left(\frac{\pi\theta}{2\theta_o}\right) H^{(2)}_{\left(\frac{\pi}{2\theta_o}\right)}(kr_o) \tag{A-12}$$

$$\left[\begin{array}{c} \\ \end{array}\right] \left[\begin{array}{c} \\ \end{array}\right] \left[\begin{array}{c} \\ \end{array}\right] \tag{A-4}$$

$$\left[\begin{array}{c} \\ \end{array}\right] \left[\begin{array}{c} \\ \end{array}\right] \left[\begin{array}{c} \\ \end{array}\right] \tag{A-5}$$

$$\left[\begin{array}{c} \\ \end{array}\right] \left[\begin{array}{c} \\ \end{array}\right] \left[\begin{array}{c} \\ \end{array}\right] \tag{A-6}$$

$J_{\nu}^{(1)}(kr)$ and $H_{\nu}^{(2)}(kr)$ are chosen functions of the first and second kinds respectively. Because only large Hankel angles and large radii will be employed in this investigation the asymptotic expressions for the Hankel functions can be employed.

$$H_{\nu}^{(1)}(kr) \approx \left[\frac{2}{\pi kr}\right]^{\frac{1}{2}} e^{j\left(kr - \frac{\nu\pi}{2} - \frac{\pi}{4}\right)} \tag{A-7}$$

$$H_{\nu}^{(2)}(kr) \approx \left[\frac{2}{\pi kr}\right]^{\frac{1}{2}} e^{-j\left(kr - \frac{\nu\pi}{2} - \frac{\pi}{4}\right)} \tag{A-8}$$

Equations (A-5) and (A-8) indicate that the outgoing cylindrical waves are separated by $\frac{\pi}{2}$ from the corresponding incoming waves. Considering only the solution of the wave traveling in the positive r direction, the fields at a fixed radius, r_0, from the origin in Figure III become

$$E_z^0 = E_z^0 \cos\left(\frac{n\pi}{\phi_0}\theta\right) J_{\frac{n\pi}{\phi_0}}(kr_0) \tag{A-9}$$

$$H_r^0 = \frac{-E_z^0}{j\eta_0} \left(\frac{n\pi}{\phi_0}\right) J'_{\frac{n\pi}{\phi_0}}(kr_0) \tag{A-10}$$

$$H_\theta = \frac{KA_1}{j\omega\mu} \cos\left[\frac{\pi\theta}{2\theta_o}\right] \frac{H^{(2)'}(kr_o)}{\left(\frac{\pi}{2\theta}\right)_o} \tag{A-13}$$

Because the laterally radiating electromagnetic horn design in Figure I has a constant mean path length between the origin and any point on the aperture, the aperture can be considered to be a surface of constant phase with a distance between constant phase surfaces in the traveling wave of free space wavelength. These constant phase surfaces lie in a plane, but the surface is fixed by geometry as an arc of a circle. Consider the aperture arc in the coordinate system in Figure II. E_y in Figure III becomes E_r in Figure II; H_r in Figure III becomes H_z in Figure II; and H_θ in Figure III becomes H_ϕ in Figure II. The field expressions near the aperture become:

$$E_r = A_1 \cos\left(\frac{\pi\phi}{\phi_o}\right) \frac{H^{(2)}(kr_o)}{\left(\frac{\pi}{\phi}\right)_o} \tag{A-14}$$

$$H_z = \frac{A_1 \pi}{\phi_o j\omega\mu r_o} \sin\left(\frac{\pi\phi}{\phi_o}\right) \frac{H^{(2)}(kr_o)}{\left(\frac{\pi}{\phi}\right)_o} \tag{A-15}$$

$$H_\phi = -j\, A_1 \sqrt{\frac{\varepsilon_o}{\mu}} \cos\left(\frac{\pi\phi}{\phi_o}\right) \frac{H^{(2)}(kr_o)}{\left(\frac{\pi}{\phi}\right)_o} \tag{A-16}$$

At moderately large values of r_o

$$-j\, H_n^{(2)'} = H_n^{(2)} \tag{A-17}$$

and approximately free space wave impedance exists at the aperture. The field components which lie in the aperture plane can now be written as:

$$E_r = B_1 \cos\frac{\pi\phi}{\phi_o} \tag{A-18}$$

$$H_\phi = B_1 \sqrt{\frac{\varepsilon_o}{\mu}} \cos\frac{\pi\phi}{\phi_o} \tag{A-19}$$

$$A^{\beta} = \frac{1}{|\rho|} \cos\left[\omega t - \beta_0 \left(\frac{\rho}{\rho_0}\right)^{\alpha+1}\right] \qquad (4\text{-}13)$$

Because the internally radiating electromagnetic wave leaves an aperture I have a constant wave path length between the origin and any point on the aperture, the aperture can be considered to be a surface of constant phase with a flatness between constant phase surfaces in the traveling wave of free space wavelength. Each constant phase surface lie in a plane, but the surface is fixed by geometry as an arc of a circle. Consider the aperture are in the coordinate system in Figure II. E^{β} in Figure III becomes F^{β} in Figure II; A^{β} in Figure III becomes f^{β} in Figure II and H^{β} in Figure III becomes G^{β} in Figure II. The field expressions over the aperture become:

$$E^{\beta} = C^{\beta} \cos\left(\frac{kr}{\rho_0}\right) \frac{(1)}{\left(\frac{kr}{\rho_0}\right)} \qquad (4\text{-}14)$$

$$H^{\beta} = \frac{k^{\beta} \cos\theta}{\gamma^{\beta} a} \sin\left(\frac{kr}{\rho_0}\right) \frac{(1)}{\left(\frac{kr}{\rho_0}\right)} \qquad (4\text{-}15)$$

$$H^{\beta} = -j\, Y^{\beta} \sqrt{\frac{\rho}{\rho_0}} \cos\left(\frac{kr}{\rho_0}\right) \frac{(1)}{\left(\frac{kr}{\rho_0}\right)} \qquad (4\text{-}16)$$

At moderately large values of ρ_0

$$-j\, E^{\beta}(r) = E^{\beta}(r) \qquad (4\text{-}17)$$

and approximately free space wave impedance exists at the aperture. The field approximates what it is for the aperture plane can now be written by:

$$E^{\beta} = E^{\beta} \cos\frac{kr}{\rho_0} \qquad (4\text{-}18)$$

$$H^{\beta} = E^{\beta} \sqrt{\frac{\rho}{\rho_0}} \cos\frac{kr}{\rho_0} \qquad (4\text{-}19)$$

Where:

$$B_1 = A_1 \left(\frac{H^{(2)}}{\frac{\pi}{\phi}}\right)_o (kr_o) \qquad \text{(A-20)}$$

From Equation (A-18) the values of the x and y components of the electric field intensities can be written.

$$E_{sx} = B_1 \left(\frac{\cos\frac{\pi\phi}{\phi_o}}{\cos\phi}\right) \qquad \text{(A-21)}$$

$$E_{sy} = B_1 \left(\frac{\cos\frac{\pi\phi}{\phi_o}}{\sin\phi}\right) \qquad \text{(A-22)}$$

Higher order H modes may exist at the aperture, but these will be considered later.

The Linear Equivalent Source Method of Determining the E Plane Polarized, H Plane Field Pattern

Because this pattern is of primary interest and because this method of approach yields simple expressions for the field patterns, the linear equivalent source method will be presented first. The geometry of this linear equivalent source is given in Figure IV. The assumed fields in this linear equivalent source are the fields projected from the arc to the line.

$$y_o = r_{av} \sin\left(\frac{\phi_o}{2}\right) \qquad \text{(A-23)}$$

$$E_{sx} = B_1 \cos\left(\frac{\pi y}{2y_o}\right) \cos\left(\frac{\phi_o y}{2y_o}\right) \qquad \text{(A-24)}$$

$$E_{sy} = B_1 \cos\left(\frac{\pi y}{2y_o}\right) \sin\left(\frac{\phi y}{2y_o}\right) \qquad \text{(A-25)}$$

N_x may now be computed by first substituting Equation (A-24) into Equation (A-4)

$$N_x = B_1 \int_{-y_o}^{+y_o} \int_{-\Delta x_o}^{+\Delta x_o} \cos\frac{\pi y}{2y_o} \cos\frac{\phi_o y}{2y_o} \, \varepsilon^{jkx \sin\theta \cos\phi} \, \varepsilon^{jk\, y \sin\theta \sin\phi} \, \delta x \, \delta y$$

(A-26)

$$\vec{E}^{x} = \hat{x}\, E_0^{x} \sin\left(\frac{\pi z}{a}\right) \tag{4-20}$$

From Equation (4-19) the values of the x and y components of the electric field intensities can be written.

$$E_{0x} = E_0^{x} \cos\left(\frac{\pi z}{a}\right) e^{-j\beta z} \tag{4-21}$$

$$E_{0y} = E_0^{y} \cos\left(\frac{\pi z}{a}\right) e^{-j\beta z} \tag{4-22}$$

Either order I modes may exist in the waveguide, but these will be considered later.

The Linear Equivalent Source Method of Determining the E Plane Fields

The Linear Equivalent source method of determining the E plane fields, is of primary interest and because this method of expressing fields explicitly requires the field patterns, the linear equivalent source method will be presented first. The geometry of this linear equivalent source is given in Figure 17. The assumed fields in this linear equivalent source are the fields produced from the wall to the line.

$$E_0^{x} = x_{ax} \sin\left(\frac{\pi z}{a}\right) \tag{4-23}$$

$$E_{0x} = E_0^{x} \sin\left(\frac{\pi z}{a}\right) \cos\left(\frac{\pi z}{a}\right) \tag{4-24}$$

$$E_{0z} = E_0^{z} \cos\left(\frac{\pi z}{a}\right) \sin\left(\frac{\pi z}{a}\right) \tag{4-25}$$

E^{x} may now be computed by first considering Equation (4-23) into Equation (4-1)

$$E^{x} = E_0^{x} \int_0^{a} \sin\frac{\pi z}{a} \cos\frac{\pi z}{a} e^{-j\beta z} \, dz$$

(4-26)

After integrating Equation (A-26) becomes:

$$N_x = \frac{B_1\, 2j\, \Delta x_o}{\Delta x_o\, jk \sin\theta \cos\phi}\left[\frac{\varepsilon^{+jk\Delta x_o \sin\theta\cos\phi/2} - \varepsilon^{-jk\Delta x_o \sin\theta\cos\phi/2}}{2j}\right]$$

$$\frac{y_o}{2}\left[\frac{\sin\left\{\frac{(\pi+\phi_o)}{2y_o} - k\sin\phi\sin\theta\right\}y_o}{\left\{\frac{(\pi+\phi_o)}{2y_o} - k\sin\phi\sin\theta\right\}y_o} + \frac{\sin\left\{\frac{(\pi+\phi_o)}{2y_o} + k\sin\phi\sin\theta\right\}y_o}{\left\{\frac{(\pi+\phi_o)}{2y_o} + k\sin\phi\sin\theta\right\}y_o}\right.$$

$$\left. + \frac{\sin\left\{\frac{(\pi-\phi_o)}{2y_o} - k\sin\phi\sin\theta\right\}y_o}{\left\{\frac{(\pi-\phi_o)}{2y_o} - k\sin\phi\sin\theta\right\}y_o} + \frac{\sin\left\{\frac{(\pi-\phi_o)}{2y_o} + k\sin\phi\sin\theta\right\}y_o}{\left\{\frac{(\pi-\phi_o)}{2y_o} + k\sin\phi\sin\theta\right\}y_o}\right] \qquad \text{(A-27)}$$

In the H plane $\phi = \frac{\pi}{2}$

$$N_x = \frac{B_1\, \Delta x_o\, y_o}{2}\left[\frac{\sin\left\{\frac{(\pi+\phi_o)}{2y_o} - k\sin\theta\right\}y_o}{\left\{\frac{(\pi+\phi_o)}{2y_o} - k\sin\theta\right\}y_o} + \frac{\sin\left\{\frac{(\pi+\phi_o)}{2y_o} + k\sin\theta\right\}y_o}{\left\{\frac{(\pi+\phi_o)}{2y_o} + k\sin\theta\right\}y_o}\right.$$

$$\left. + \frac{\sin\left\{\frac{(\pi-\phi_o)}{2y_o} - k\sin\theta\right\}y_o}{\left\{\frac{(\pi-\phi_o)}{2y_o} - k\sin\theta\right\}y_o} + \frac{\sin\left\{\frac{(\pi-\phi_o)}{2y_o} + k\sin\theta\right\}y_o}{\left\{\frac{(\pi-\phi_o)}{2y_o} + k\sin\theta\right\}y_o}\right] \qquad \text{(A-28)}$$

Equation (A-28) will give highly accurate values for the half power beam widths, and moderately accurate results for the peak power densities of the first side lobes and the angles at which the side lobes occur.

After integrating (Y-29) becomes

$$\left[\frac{\qquad\qquad}{\qquad\qquad}\right]$$

$$\frac{\left\{\frac{\qquad}{\qquad}\right\}}{\left\{\frac{\qquad}{\qquad}\right\}} + \frac{\left\{\frac{\qquad}{\qquad}\right\}}{\left\{\frac{\qquad}{\qquad}\right\}}$$

$$+ \frac{\left\{\frac{\qquad}{\qquad}\right\}}{\left\{\frac{\qquad}{\qquad}\right\}} + \frac{\left\{\frac{\qquad}{\qquad}\right\}}{\left\{\frac{\qquad}{\qquad}\right\}}$$

In the Z plane $z = \frac{1}{2}$

$$\left[\frac{\qquad\qquad}{\qquad\qquad}\right]$$

$$\frac{\left\{\frac{\qquad}{\qquad}\right\}}{\left\{\frac{\qquad}{\qquad}\right\}} + \frac{\left\{\frac{\qquad}{\qquad}\right\}}{\left\{\frac{\qquad}{\qquad}\right\}}$$

$$+ \frac{\left\{\frac{\qquad}{\qquad}\right\}}{\left\{\frac{\qquad}{\qquad}\right\}} + \frac{\left\{\frac{\qquad}{\qquad}\right\}}{\left\{\frac{\qquad}{\qquad}\right\}}$$

(Y-30)

Equation (Y-29) with five velocity increments gives the velocity

impulses of the first nine burns for Delta IV-A. Only the first burn

has been plotted, and numerically accurate results for the rest of the

Linear equivalent source methods used in computing the other three principal patterns in the H and E planes are highly inaccurate. If the fields are assumed to be projected directly without any factors which take into account the curvature of the physical source and the effect of equivalent area variations with curvature, then the integrals will result in functions which have the same symmetry, but erroneous relative magnitudes.

The Array Factor Applied to the Antenna, Type B

$$F = \int_{-\phi_o}^{+\phi_o} \text{Cos}\, \frac{\pi\phi'}{\phi_o}\, \text{Cos}\, \phi'\, \varepsilon^{+jkr_{av}\, \text{Sin}\, \theta\, \text{Sin}\, \phi'}\, \delta\phi' \qquad \text{(A-29)}$$

When $\phi_o = \frac{\pi}{2}$, $r_{av}\, \text{Sin}\, \phi' = y$ (A-30)

is substituted in Equation (A-29), it becomes:

$$F = \int_{-y_o}^{+y_o} 1 - 2\frac{y^2}{r_{av}^2}\, \varepsilon^{ay}\, \delta y \qquad \text{(A-31)}$$

Where

$$a = jk\, \text{Sin}\, \theta \qquad \text{(A-32)}$$

This changes the variable of integration to an integration with respect to y. (Straight line equivalent).

$$F = \frac{\varepsilon^{ay_o} - \varepsilon^{-ay_o}}{a} - \frac{2}{r^2 a^3}\left[(\varepsilon^{ay_o} - \varepsilon^{-ay_o})(a^2 y_o^2 + 2) - 2ay_o(\varepsilon^{ay_o} + \varepsilon^{-ay_o})\right] \qquad \text{(A-33)}$$

Which reduces to:

$$F = 2\left\{\frac{\text{Sin}\, ay_o}{j}\left(\frac{1}{k\, \text{Sin}\, \theta} - \frac{2y_o^2}{r_{av}^2\, k\, \text{Sin}\, \theta} + \frac{4}{r_{av}^2\, k^3\, \text{Sin}^3\theta}\right) + \right.$$

$$\left. + \frac{\text{Cos}\, ay_o}{j}\left[\frac{4y_o}{-r_{av}^2\, k^2\, \text{Sin}^2\theta}\right]\right\} \qquad \text{(A-34)}$$

linear equivalent source methods used in computing the other three principal patterns in the E and H planes are highly inaccurate. If the fields are assumed to be polarized directly without any factors which take into account the curvature of the physical source and the effect of equivalent area variations with curvature, then the integrals will result in functions which have the same dependence, but erroneous relative magnitudes.

The Array Factor Applied to the Antenna, Case 2

$$f = \int_{-\theta_0}^{\theta_0} (\cos\tfrac{\pi}{2}\tfrac{\theta}{\theta_0})^{q_2} e^{+j2\pi\rho \sin\theta \sin\phi_1} d\phi_1 \qquad (4\text{-}29)$$

When $\psi_1^0 = \frac{\pi}{2}, \rho_{2\lambda} \sin\phi_1 = x$ (4-30)

it becomes:

$$f = \int_{-\theta_0}^{\theta_0} 1 - \tfrac{1}{2}\left(\tfrac{x}{\rho_{2\lambda}}\right)^2 e^{jx} dx \qquad (4\text{-}31)$$

Where

$$x = j\rho \sin\theta \qquad (4\text{-}32)$$

This changes the variable of integration to an integration with respect to x. (Straight line equivalent).

$$f = \frac{e^{j\theta_0} - e^{-j\theta_0}}{x} - \frac{2}{x^2}\left[(e^{j\theta_0} + e^{-j\theta_0})(x^2\psi_0^2 + 2) - 2x\psi_0(e^{j\theta_0} + e^{-j\theta_0})\right] \qquad (4\text{-}33)$$

Which reduces to:

$$f = \int \left[\frac{\sin\theta_0}{\psi_0^2}\left(\frac{\pi^2}{4} - \frac{\rho_{2\lambda}^2 \sin^2\theta}{\psi_0^2}\right) + \frac{\rho_{2\lambda}^2 \sin^2\theta}{\psi_0^2}\left(\frac{\rho_{2\lambda}^2 \sin^2\theta}{4} - \right.\right.$$

$$\left.\left. - \frac{\cos\theta_0}{2}\left[\frac{\rho_{2\lambda}^2 \sin^2\theta}{\psi_0^2} - 1\right]\right)\right] \qquad (4\text{-}34)$$

For the dimensions of the horn this reduces to:

$$F = +0.000728 \frac{\text{Sin}\,(ky_o \text{ Sin } \theta)}{\text{Sin}^3\theta} - 0.038 \frac{\text{Cos}\,(ky_o \text{ Sin } \theta)}{\text{Sin}^2\theta} \qquad \text{(A-35)}$$

The Fourier-Bessel Series Method of Field Pattern Evaluation

Converting Equations (A-4) and A-5) into an integration in the xy plane in plane polar coordinates by means of the relationships:

$$x = r' \text{ Cos } \phi' \qquad \text{(A-36)}$$

$$y = r' \text{ Sin } \phi' \qquad \text{(A-37)}$$

the diffraction integrals become

$$N_{\substack{x \\ y}} = \int_s E_{\substack{x \\ y}} \varepsilon^{jk \text{ Sin } \theta \, r' \text{ Cos } (\phi - \phi')} \, r' \, \delta r' \, \delta\phi' \qquad \text{(A-38)}$$

Solving first for N_x we must substitute Equation (A-21) into Equation (A-38).

$$N_x = E_1 \int_{\frac{-\phi_o}{2}}^{\frac{+\phi_o}{2}} \int_{r_1}^{r_2} \text{Cos } \frac{n\phi'}{\phi_o} \text{ Cos } \phi' \, \varepsilon^{jkr' \text{ Sin } \theta \text{ Cos } (\phi - \phi')} \, r' \, \delta r' \, \delta\phi' \qquad \text{(A-39)}$$

Integrating first with respect to ϕ' can be accomplished employing the expansion:

$$\varepsilon^{jur \text{ Cos } (\phi - \phi')} = \sum_{n=-\infty}^{+\infty} j^n J_n(ur) \, \varepsilon^{jn(\phi - \phi')} \qquad \text{(A-40)}$$

or by the approximation

$$\text{Cos } (\phi - \phi') = 1 - \frac{(\phi - \phi')^2}{2!} \qquad \text{(A-41)}$$

Either method yields extremely complicated formulas that cannot be integrated with respect to r' readily.

However, Equation (A-39) may be integrated first with respect to r'.

to k_1.

However Equation (4-28) may be homogeneous first with respect

be integrated with respect to k_1 now.[37]

Since medium yields extremely complicated integrals that cannot

$$\sin(\theta - \theta_1) = \gamma \frac{\sin\theta}{(k - k_1)^2} \tag{4-31}$$

or by the expansion

$$e^{ikr\cos(\theta-\theta_1)} = \sum_{m=-\infty}^{+\infty} j_m^B(kr)\, e^{im(\theta-\theta_1)} \tag{4-32}$$

Integrating first with respect to θ_1 and a succeeding multiplying the expression

$$N^0 = \gamma^2 \int_{\frac{\pi}{2}-\frac{\alpha}{2}}^{\frac{\pi}{2}+\frac{\alpha}{2}} \int_{r_1}^{r_2} \sum_{m=-\infty}^{+\infty} j_m^B(kr) \sin\theta \sin(\theta - \theta_1) \, d\theta \, dr \tag{4-33}$$

Deriving first for N^0 we have substituting expression (4-32) into expression (4-28).

$$\frac{\partial N^0}{\partial \theta} = \int_{r_1}^{r_2} \int_{\frac{\pi}{2}-\frac{\alpha}{2}}^{\frac{\pi}{2}+\frac{\alpha}{2}} \sin\theta \sin(\theta - \theta_1) \, d\theta \, dr \tag{4-34}$$

the differentiation integrals become

$$\gamma = r_1 \sin\theta_1 \tag{4-35}$$

$$z = r_1 \cos\theta_1 \tag{4-36}$$

if there is plane polar coordinate. As sense of the relationships

Conversely Equations (4-35) and (4-36) into an integration in the

The Fourier-Bessel Series Method of Field Pattern Evaluation

$$\frac{\sin(\alpha\sin\theta)}{\alpha^2} - \frac{\cos(\alpha\sin\theta)}{\alpha} \qquad \frac{\sin(\alpha^2\sin\theta)}{\alpha^2} \tag{4-37}$$

For the dimensions of the horn this reduces to

Let

$$M = k \cos(\phi - \phi') \sin\theta \tag{A-42}$$

Integrate and evaluate limits.

$$N_x = B_1 \int_{-\frac{\phi_o}{2}}^{+\frac{\phi_o}{2}} \frac{\cos \frac{\pi\phi'}{\phi_o} \cos\phi'}{-M^2} \left[\varepsilon^{jMr_2}(jMr_2 - 1) - \varepsilon^{jMr_1}(jMr_1 - 1) \right] \delta\phi' \tag{A-43}$$

Let

$$r_2 = r_1 + \delta r \tag{A-44}$$

$$N_x = B_1 \int_{-\frac{\phi_o}{2}}^{+\frac{\phi_o}{2}} \frac{\cos \frac{\pi\phi'}{\phi_o} \cos\phi'}{-M^2} \left[\varepsilon^{jMr_1 + jM\delta r}(jMr_1 + jM\delta r - 1) - \varepsilon^{jMr_1}(jMr_1 - 1) \right] \delta\phi \tag{A-45}$$

As a second order approximation, let

$$\varepsilon^{jM\delta r} = 1 + jM\delta r + \frac{(jM\delta r)^2}{2} \tag{A-46}$$

Substitute Equation (A-46) into Equation (A-45). After an elimination of terms of higher order than the third power of δr, the equation becomes:

$$N_x = B_1 \int_{-\frac{\phi_o}{2}}^{+\frac{\phi_o}{2}} \cos \frac{\pi\phi'}{\phi_o} \quad \varepsilon^{jMr_1}\left(r_1\delta r + \frac{(\delta r)^2}{2} + \frac{jM(\delta r)^2 r_1}{2}\right) \cos\phi' \, \delta\phi' \tag{A-47}$$

Because M appears in the terms which are also a function of r, it is necessary to resort to only a first order approximation to the field pattern. Substituting Equation (A-42) into (A-47)

Let

$$\phi = x \cos(\psi - \psi_1) \sin\theta \qquad (4-24)$$

Integrate and evaluate limits.

$$M^x = \beta^2 \int_{-\frac{\pi}{2}}^{+\frac{\pi}{2}} \int_{\frac{\pi}{2}}^{\frac{\pi}{2}} \left[+ e^{\beta x \cos(\psi - \psi_1) \sin\theta} (\beta x \cos(\psi - \psi_1) \sin\theta - 1) - e^{-\beta x \cos(\psi - \psi_1) \sin\theta} (\beta x \cos(\psi - \psi_1) \sin\theta + 1) \right] \cos^2\theta \, d\theta \, d\psi \qquad (4-25)$$

Let

$$\beta x = \lambda^2 + i\mu \qquad (4-26)$$

$$M^x = \beta^2 \int_{-\frac{\pi}{2}}^{+\frac{\pi}{2}} \int_{\frac{\pi}{2}}^{\frac{\pi}{2}} \left[+ e^{\lambda^2 x} (\cos\mu x + i \sin\mu x) - e^{-\lambda^2 x} (\cos\mu x - i \sin\mu x) \right] \cos^2\theta \, d\theta \, d\psi \qquad (4-27)$$

In a manner quite analogously, let

$$\beta x = \lambda^2 + i\mu \qquad (4-28)$$

Substitute Equation (4-28) into Equation (4-27). After an elimination of terms of higher order than the third power of $\lambda\mu$, the equation becomes

$$M^x = \beta^2 \int_{-\frac{\pi}{2}}^{+\frac{\pi}{2}} \int_{\frac{\pi}{2}}^{\frac{\pi}{2}} \cos\frac{\mu x}{R} \cdot e^{\lambda^2 x} \left(\cos\frac{\mu x}{R} + \frac{(\lambda^2 x)}{1} \frac{\sin\frac{\mu x}{R}}{\frac{\mu x}{R}} \right) \cos^2\theta \, d\theta \, d\psi \qquad (4-29)$$

Because λ appears in the term which are also a function of η it is necessary to remove it only a first order approximation is the result pro-

vided. Substituting Equation (4-28) into Equation (4-29)

$$N_x = B_1 r_1 \delta r \int_{-\frac{\phi_o}{2}}^{+\frac{\phi_o}{2}} \text{Cos}\frac{\pi\phi'}{\phi_o} \text{Cos}\,\phi' \; \varepsilon^{jkr_1 \text{ Sin } \theta \text{ Cos } (\phi - \phi')} \; \delta\phi' \tag{A-48}$$

Employing the identity[26]

$$\varepsilon^{jkr_1 \text{ Sin } \theta \text{ Cos } (\phi - \phi')} = \sum_{n=-\infty}^{+\infty} j^n J_n(kr_1 \text{ Sin } \theta) \; \varepsilon^{jn(\phi - \phi')} \tag{A-49}$$

and the obvious trigonometric identity, we obtain

$$N_x = \frac{B_1 r_1 \delta r}{2} \sum_{n=-\infty}^{+\infty} j^n J_n(kr_1 \text{ Sin } \theta) \; \varepsilon^{jn\theta} \int_{-\frac{\phi_o}{2}}^{+\frac{\phi_o}{2}} \left[\text{Cos}\left(\frac{\pi}{\phi_o}+1\right)\phi' + \text{Cos}\left(\frac{\pi}{\phi_o}-1\right)\phi'\right]$$

$$\left[\text{Cos } n\phi' - j \text{ Sin } n\phi'\right] \delta\phi' \tag{A-50}$$

Because the limits on the integrals are symmetrical, the integrals having odd functions integrands will be zero. After integrating and evaluating limits, Equation (A-50) becomes:

$$N_x = \frac{B_1 r_1 \delta r}{2} \sum_{n=-\infty}^{+\infty} j^n J_n(kr_1 \text{ Sin } \theta) \; \varepsilon^{jn\theta} \left(\frac{\phi_o}{2}\right) A(n, \phi_o) \tag{A-51}$$

Where

$$A(n,\phi_o) = \frac{\text{Sin}\left(\frac{\pi}{\phi_o}+1+n\right)\frac{\phi_o}{2}}{\left(\frac{\pi}{\phi_o}+1+n\right)\frac{\phi_o}{2}} + \frac{\text{Sin}\left(\frac{\pi}{\phi_o}+1-n\right)\frac{\phi_o}{2}}{\left(\frac{\pi}{\phi_o}+1-n\right)\frac{\phi_o}{2}} +$$

$$+ \frac{\text{Sin}\left(\frac{\pi}{\phi_o}-1+n\right)\frac{\phi_o}{2}}{\left(\frac{\pi}{\phi_o}-1+n\right)\frac{\phi_o}{2}} + \frac{\text{Sin}\left(\frac{\pi}{\phi_o}-1-n\right)\frac{\phi_o}{2}}{\left(\frac{\pi}{\phi_o}-1-n\right)\frac{\phi_o}{2}} \tag{A-52}$$

Employing the identity

$$J_{-n}(kr_1 \text{ Sin } \theta) = (-)^n J_n(kr_1 \text{ Sin } \theta) \tag{A-53}$$

Equation (A-51) becomes

$$N_x = \frac{B_1 r_1 \delta r \, \phi_o}{4}\left[A(0,\phi_o)\, J_o(kr_1 \text{ Sin } \theta) + \right.$$

$$\left. + \sum_{n=1}^{\infty} J_n(kr_1 \text{ Sin } \theta)\, A(n,\phi_o)\, B(n,\phi)\right] \tag{A-54}$$

where

$$B(n,\phi) = j^n \varepsilon^{jn\phi} + (-)^n j(-n)\, \varepsilon^{-jn\phi} \tag{A-55}$$

The computation of N_y by direct integration may also be accomplished by substituting Equation (A-22) into Equation (A-38) and repeating the steps from Equation (A-39) to Equation (A-50).

$$N_y = \frac{B_1 r_1 \delta r}{2} \sum_{n=-\infty}^{+\infty} j^n J_n(kr_1 \text{ Sin } \theta)\, \varepsilon^{jn\phi} \int_{-\frac{\phi_o}{2}}^{+\frac{\phi_o}{2}}$$

$$\left[\text{Sin}(1-\tfrac{\pi}{\phi_o})\phi' + \text{Sin}\,(1+\tfrac{\pi}{\phi_o})\phi'\right]\left[\text{Cos } n\phi' - j \text{ Sin } n\phi'\right]\delta\phi' \tag{A-56}$$

Because the limits on the integrals are symmetrical, the integrals having odd function integrands will be zero. After integrating and evaluating limits and employing the identity given in Equation (A-53), Equation (A-56) becomes

$$N_y = \frac{B_1 r_1 \, \delta r \, \phi_o}{4}\left[C(0,\phi_o)\, J_o(kr_1 \text{ Sin } \theta) + \right.$$

$$\left. + \sum_{n=1}^{\infty} J_n(kr_1 \text{Sin } \theta)\, C(n,\phi_o)\, D(n,\phi)\right] \tag{A-57}$$

employing the identity

$$J_{-n}(kr' \sin\theta) = (-)_n J_n(kr' \sin\theta) \tag{A-32}$$

Equation (A-31) becomes

$$H_n^s = \frac{4}{\pi^2 kr \sin\theta} \left[i(\cos\theta_0^s) J_0^s(kr' \sin\theta) + \right.$$

$$\left. + \sum_{m=1}^{\infty} J_m^s(kr' \sin\theta) i(\cos\theta_0^s) \cos(m\phi) \right] \tag{A-33}$$

where

$$\cos(\phi_0^s) = \frac{1}{2} e^{jm\phi} + (-)^n \frac{1}{2} e^{-jm\phi} \tag{A-34}$$

The computation of H_n^s is direct (integration may also be accomplished by substituting Equation (A-28) into Equation (A-38) and replacing the steps from Equation (A-39) to Equation (A-32).

$$H_n^s = \frac{2}{\pi^2 kr} \sum_{m=-\infty}^{+\infty} J_m J_n^s(kr' \sin\theta) \, e^{jm\phi} \Bigg|_{-\frac{\pi}{2}+\theta_0}^{\frac{\pi}{2}+\theta_0}$$

$$\left[\sin(\tfrac{\pi}{2} - \tfrac{\pi}{2} + \theta_0) + m \sin(\tfrac{\pi}{2} + \tfrac{\pi}{2} + \theta_0) \right] \left[\cos m\phi \, J \sin m\phi \right] d\phi \tag{A-35}$$

Because the limits on the integrals are symmetrical, the integrals involving odd function integrands will be zero. After integrating and evaluating limits and employing the identity given in Equation (A-32), Equation (A-36) becomes

$$H_n^s = \frac{4}{\pi^2 kr \sin\theta} \left[i(\cos\theta_0^s) J_0^s(kr' \sin\theta) + \right.$$

$$\left. + \sum_{m=1}^{\infty} J_m^s(kr' \sin\theta) \, i(\cos\theta_0^s) \cos(m\phi) \right] \tag{A-37}$$

where

$$C(n,\phi_o) = \frac{\text{Sin}\,(1-\frac{\pi}{\phi_o}-n)\,\frac{\phi_o}{2}}{(1-\frac{\pi}{\phi_o}-n)\,\frac{\phi_o}{2}} + \frac{\text{Sin}\,(1+\frac{\pi}{\phi_o}-n)\,\frac{\phi_o}{2}}{(1+\frac{\pi}{\phi_o}-n)\,\frac{\phi_o}{2}} - \frac{\text{Sin}\,(1-\frac{\pi}{\phi_o}+n)\,\frac{\phi_o}{2}}{(1-\frac{\pi}{\phi_o}+n)\,\frac{\phi_o}{2}} - \frac{\text{Sin}\,(1-\frac{\pi}{\phi_o}-n)\,\frac{\phi_o}{2}}{(1+\frac{\pi}{\phi_o}+n)\,\frac{\phi_o}{2}} \qquad \text{(A-58)}$$

and

$$D(n,\phi) = j^n\,\varepsilon^{jn\phi} - (-)^n j^{(-n)}\,\varepsilon^{-jn\phi} \qquad \text{(A-59)}$$

N_x and N_y substituted in Equations (A-1) and (A-2) adequately express the fields for any point in Fraunhofer space. As a result of the approximation employed, these formulas are limited to the case when the aperture distance in the radial direction is small in comparison to the average radius of the aperture. However, we may apply the continuous array factor concept to the aperture to obtain a better approximation to the E plane fields that will result when the E plane flare is added to the laterally radiating horn.

Employing the Array Factor to Obtain the E Plane Fields of a Large Aperture Horn

By symmetry and the Fourier-Bessel series field equations E_ϕ is zero in the E plane. Consider the field from the differential radiating element in the aperture in Figure IX to be given by the Fourier-Bessel field pattern equations. Let δr become $\delta x'$ and integrate in the x' direction.

$$E_{\theta,1} = \int_{\frac{-\Delta x'_o}{2}}^{\frac{+\Delta x'_o}{2}} \frac{E_\theta}{\delta r}\,\varepsilon^{jk\,\text{Sin}\,\theta\,\text{Cos}\,\phi\,x'}\,\delta r' \qquad \text{(A-60)}$$

After integrating, evaluating, and letting

$$\frac{\sin\left(1-\frac{k_0}{k}-n\right)\frac{k}{2}}{\left(1-\frac{k_0}{k}-n\right)\frac{k}{2}} + \frac{\sin\left(1+\frac{k_0}{k}-n\right)\frac{k}{2}}{\left(1+\frac{k_0}{k}-n\right)\frac{k}{2}} -$$

$$\frac{\sin\left(1-\frac{k_0}{k}+n\right)\frac{k}{2}}{\left(1-\frac{k_0}{k}+n\right)\frac{k}{2}} - \frac{\sin\left(1+\frac{k_0}{k}+n\right)\frac{k}{2}}{\left(1+\frac{k_0}{k}+n\right)\frac{k}{2}} \qquad (4-39)$$

and

$$\Gamma(n,k) = \frac{1}{2} e^{jnq} - (-1)^n e^{-jnq} \qquad (4-40)$$

$\mathcal{E}^0$ and $\mathcal{E}^1$ constituent in Equations (4-1) and (4-4) respectively express the field for any point in Fraunhofer space. As a result of the approximation employed, these formulae are limited to the case when the aperture dimension is much greater than a wavelength of the energy radius of the aperture. However, we may apply the continuous array factor concept to the equation to obtain a better approximation to the E plane field but will result when the x plane flare is added to the laboratory radiating horn.

Radiation Line Source Pattern in Middle Ide E Plane Plane of a Horn Aperture Horn

By symmetry and the Fourier-Bessel series field equations $\mathcal{E}^0$ is zero in the E plane. Consider the field from the differential radiating element in the aperture in Figure 12 to be given by the Fourier-Bessel field pattern equations. Let $\mathcal{E}^0$ become $\mathcal{E}^0_x$ and integrate in the x' direction.

$$\mathcal{E}^0_x = \int_{\frac{-dx'}{2}}^{\frac{dx'}{2}} \frac{k}{2\pi} e^{-jk\,\sin\theta\,\cos\zeta\,x'}\,dx' \qquad (4-41)$$

After integrating, evaluating, and letting

$$\delta x' = \delta r \tag{A-61}$$

the field expression becomes for $\phi = 0^{\circ}$

$$E_{\theta,1} = E_{\theta} \frac{\operatorname{Sin}\left(\frac{\pi \Delta x'_{o}}{\lambda} \operatorname{Sin} \theta\right)}{\left(\frac{\pi \Delta x'_{o}}{\lambda} \operatorname{Sin} \theta\right)} \tag{A-62}$$

In this integration the area M was excluded and the area N was included although it was not physically in the aperture. However, in the majority of antennas of this type errors due to this approximation are negligible because the fields in the ends of the aperture are very small in magnitude.

The Fraunhofer Field Expressions for $H_{i,0}$ Modes at the Aperture

The radiation fields for modes of higher order than H_{10} may be developed by employing an identical procedure as that employed in the development of the Fourier-Bessel series method. Because of the narrow aperture dimensions, the E modes are attenuated before they reach the aperture from the bend. By symmetry the even ordered $H_{i,0}$ modes cannot exist at the aperture. The odd order $H_{i,0}$ modes may exist by symmetry. Through a similar analysis to that preceeding this discussion, for the fields given by

$$E_{xi} = B_i \operatorname{Cos} \frac{i\pi\phi'}{\phi_o} \operatorname{Cos} \phi' \tag{A-63}$$

$$E_{yi} = B_i \operatorname{Cos} \frac{i\pi\phi'}{\phi_o} \operatorname{Sin} \phi' \tag{A-64}$$

the diffraction integrals are given by

$$N_x = \sum_{i=1}^{\infty} \frac{E_i r_1 \delta r \phi_o}{4} \left[A_i(0,\phi_o)\, J_o(kr_1 \operatorname{Sin} \theta) + \right.$$

$$\left. + \sum_{n=1}^{\infty} J_n(kr_1 \operatorname{Sin} \theta)\, A_i(n,\phi_o)\, B(n\phi) \right] \tag{A-65}$$

$$\rho x_1 = \rho x \qquad (9-21)$$

the field expansion becomes for $k = 0$,

$$E^{0y} = E^0 \frac{\int_0^{\pi} \sin\theta \, d\theta}{\left(\frac{\rho}{2} \sin\theta\right)} \qquad (9-4)$$

In this integration the area π was neglected and the area λ was included although it was not physically in the aperture. However, in the majority of common of this type errors due to this approximation are negligible because the fields in the ends of the aperture are very small in magnitude.

The Fraunhofer Field Expansion for $H^{1,0}$ Modes at the Aperture

The radiation fields for modes of higher order than E^{10} may be developed by employing an identical procedure as that employed in the development of the Fourier-Bessel series method. Because of the narrow aperture dimensions, the k modes are attenuated before they reach the aperture from the mouth. By symmetry the even ordered $H^{1,0}$ modes cannot exist at the aperture. The odd order $H^{1,0}$ modes may exist if symmetry through a similar analysis to that preceding this discussion, for the fields given by

$$E^{0x} = Y^0 \cos\frac{\pi\rho_1}{\rho_0} \cos\theta_1 \qquad (9-22)$$

$$E^{0y} = Y^0 \cos\frac{\pi\rho_1}{\rho_0} \sin\theta_1 \qquad (9-23)$$

the diffraction integrals are given by

$$E^x = \sum_{j=1}^{\infty} \frac{j^2\pi^2\rho_0}{\rho^2} \left[Y^j(\rho,\theta_0^0) \int_0^{\rho} (\rho x^T \sin\theta) \right.$$

$$\left. \sum_{p=1}^{\infty} \int_0^{\pi} (\rho x^T \sin\theta) \, Y^T(x,\theta_0^0) \, d(x\theta) \right] \qquad (9-24)$$

$$N_y = \sum_{i=1}^{\infty} \frac{B_i r_1 b r \phi_o}{4} \left[C_i(0,\phi_o)\ J_o(kr_1 \sin\theta) + \right.$$

$$\left. + \sum_{n=1}^{\infty} J_n(kr_1 \sin\theta)\ C_i(n,\phi_o)\ D(n,\phi) \right] \qquad \text{(A-66)}$$

where

$$A_i(n,\phi_o) = \frac{\sin\left(\frac{i\pi}{\phi_o}+1+n\right)\frac{\phi_o}{2}}{\left(\frac{i\pi}{\phi_o}+1+n\right)\frac{\phi_o}{2}} + \frac{\sin\left(\frac{i\pi}{\phi_o}+1-n\right)\frac{\phi_o}{2}}{\left(\frac{i\pi}{\phi_o}+1-n\right)\frac{\phi_o}{2}} +$$

$$+ \frac{\sin\left(\frac{i\pi}{\phi_o}-1+n\right)\frac{\phi_o}{2}}{\left(\frac{i\pi}{\phi_o}-1+n\right)\frac{\phi_o}{2}} + \frac{\sin\left(\frac{i\pi}{\phi_o}-1-n\right)\frac{\phi_o}{2}}{\left(\frac{i\pi}{\phi_o}-1-n\right)\frac{\phi_o}{2}} \qquad \text{(A-67)}$$

$$C_i(n,\phi_o) = \frac{\sin\left(1-n-\frac{i\pi}{\phi_o}\right)\frac{\phi_o}{2}}{\left(1-n-\frac{i\pi}{\phi_o}\right)\frac{\phi_o}{2}} + \frac{\sin\left(1+\frac{i\pi}{\phi_o}-n\right)\frac{\phi_o}{2}}{\left(1+\frac{i\pi}{\phi_o}-n\right)\frac{\phi_o}{2}} -$$

$$- \frac{\sin\left(1-\frac{i\pi}{\phi_o}+n\right)\frac{\phi_o}{2}}{\left(1-\frac{i\pi}{\phi_o}+n\right)\frac{\phi_o}{2}} - \frac{\sin\left(1+\frac{i\pi}{\phi_o}+n\right)\frac{\phi_o}{2}}{\left(1+\frac{i\pi}{\phi_o}+n\right)\frac{\phi_o}{2}} \qquad \text{(A-68)}$$

Employment of the Smith Chart to Plot Ellipticity in the H Plane

In order to make use of the ellipticity of the uncompensated laterally radiating electromagnetic horn the H plane field pattern ellipticity from $\theta = -5^\circ$ to $\theta = +5^\circ$ is plotted on the Smith chart in Figures XXVIII and XXIX. The computed values were obtained from Equations (6) and (7) and the measured values were obtained from the values on Figures XIX and XX and by assuming the phase relationships given by Equations (6) and (7) hold. The following conventions are employed:

1. All points having the same direction of rotation are plotted on one Smith Chart.
2. Circles of constant standing wave ratio are circles of constant $\frac{E_\theta}{E_\phi}$ ratio.
3. The angle at which the major axis of the ellipse is oriented with respect to the E_ϕ axis is half the physical angle on the Smith chart.

The Method of Computing E_θ in the E Plane for the Horn with 40° E Plane Flare

Equation (8) was employed. $G(\theta)$ was obtained from Figure 10.11 of Reference (36) which gave the values for a 40° E plane sectoral horn with a length of 3λ. $E_{p\theta}(G,0)$ was taken from the values of the computed E plane field pattern given in Figure XXXI.

3. All points having the same direction of rotation are plotted on the Delta Chart.

4. Circles of constant standing wave ratio are plotted on constant $\frac{R}{Z_0}$ ratio.

5. The angle at which the outer axis of the ellipse is oriented with respect to the E_y axis is half the physical angle on the Smith Chart.

The method of Construction E_y in the X Plane for the same pair of E_{inc} X Plane Plots

Equation (X) was acquired. $G(x)$ was obtained from Figure IV.11 of reference (30) which gave the values for $\alpha\lambda_0$. X plane scanned data with a length of 3λ. $E_{yo}(0,x)$ was taken from the values of the computed X plane Plank potens given in Figure XXII.

APPENDIX, SECTION C

ADMITTANCE DATA

ADMITTANCE DATA

Condition 1 - Uncompensated Horn

freq.	VSWR	λ	λ_g	minima	to space	short circ.	minima	rotation
9266	2.30	3.2376	4.56	10.55	12.86	10.22	12.50	0.065
9190	2.20	3.2649	4.66	9.82	12.18	9.99	12.32	0.166
9153	2.00	3.2776	4.69	9.49	11.87	9.90	12.21	0.213
8898	1.57	3.3715	5.00	8.99	11.42	9.02	11.52	0.180
8870	1.65	3.3822	5.00	8.89	11.39	9.12	11.58	0.151
8859	1.65	3.3864	5.02	8.70	11.24	9.06	11.56	0.176
8833	1.57	3.3963	5.06	8.48	10.97	9.00	11.53	0.212
8812	1.43	3.4045	5.10	8.12	10.62	8.90	11.45	0.260
8794	1.375	3.4114	5.12	7.86	10.45	8.64	11.17	0.298
8783	1.30	3.4157	5.15	7.70	10.30	8.60	11.15	0.268
8763	1.26	3.4235	5.16	7.36	9.98	8.49	11.09	0.315
8739	1.225	3.4329	5.18	7.03	9.58	8.43	11.02	0.371
8716	1.21	3.4419	5.20	9.15	11.35	10.90	13.50	0.432
8698	1.25	3.4491	5.22	8.84	11.45	10.90	13.47	0.486
8670	1.335	3.4602	5.25	8.39	11.03	8.15	10.71	0.044
8649	1.41	3.4686	5.27	8.07	10.76	8.03	10.68	0.080
8627	1.50	3.4775	5.28	7.83	10.48	7.95	10.59	0.112
8616	1.58	3.4818	5.34	7.70	10.40	7.90	10.58	0.123

"a" = 3.3 cm.

Condition 2 - Horn with Plane Parallel Filter, No Flare

9349	2.00	3.2089	4.98	9.04	11.36	10.47	0.471
9332	2.00	3.2148	4.52	8.94	11.16	10.40	0.480
9286	2.00	3.2306	4.56	8.49	10.73	10.25	0.039
9219	2.00	3.2542	4.64	7.77	10.09	10.04	0.127
9178	1.90	3.2687	4.70	7.37	9.75	9.91	0.167
9141	1.80	3.2819	4.74	9.40	11.73	9.80	0.214
9095	1.57	3.2986	4.80	8.91	11.25	9.65	0.279
9063	1.41	3.3102	4.82	8.47	10.87	9.54	0.347
9013	1.38	3.3285	4.86	7.89	10.30	9.37	0.429
8976	1.37	3.3422	4.94	9.82	12.23	9.24	0.497
8950	1.40	3.3520	4.94	9.54	12.00	9.15	0.036
8922	1.42	3.3625	4.96	9.18	11.65	9.05	0.086
8898	1.45	3.3715	5.00	8.95	11.40	8.95	0.110
8878	1.42	3.3791	5.01	8.72	11.22	8.89	0.123
8852	1.38	3.3891	5.04	8.59	10.91	8.78	0.145
8809	1.25	3.4056	5.12	8.10	10.58	8.61	0.201
8787	1.15	3.4142	5.14	10.28	12.82	11.09	0.264
8772	1.10	3.4199	5.18	7.52	10.05	8.96	0.291
8765	1.05	3.4227	5.18	9.97	12.40	11.02	0.331
8742	1.05	3.4317	5.22	9.41	11.85	10.94	0.421
8729	1.08	3.4376	5.22	8.98	11.53	10.90	0.474

"a" = 3.3 cm.

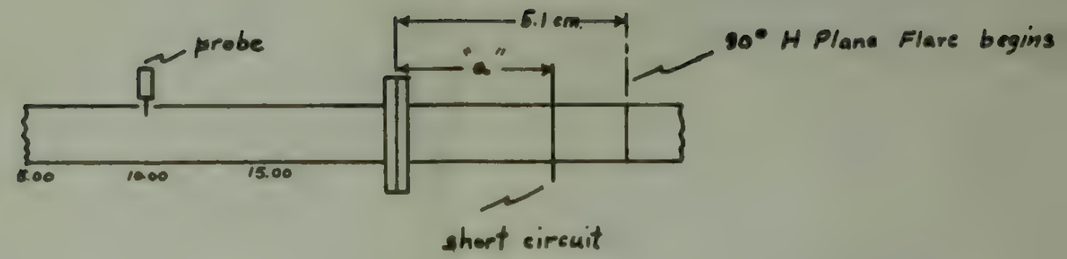

Schematic of Measuring Equipment

Note:

1. All frequencies are megacycles, all distances centimeters.
2. "a" is the distance from the short circuit to the flange.
3. "Rotation" signifies the Smith Chart rotation toward the load to be used for plotting admittances.

Condition 3 - Horn with E Plane Flare, No Filter

freq.	VSWR	λ	λg	minima to space		short circ. minima		rotation
9343	1.40	3.2109	4.98	10.97	13.38	10.74	12.98	0.018
9311	1.98	3.2221	4.54	10.70	12.96	10.63	12.90	0.067
9291	1.99	3.2291	4.60	10.97	12.74	10.57	12.84	0.098
9267	1.44	3.2373	4.60	10.25	12.56	10.49	12.79	0.126
9246	1.95	3.2447	4.62	10.14	12.40	10.42	12.73	0.196
9215	1.905	3.2555	4.65	9.82	12.11	10.32	12.65	0.189
9200	1.36	3.2608	4.66	9.65	12.02	10.28	12.61	0.199
9182	1.27	3.2672	4.70	9.54	11.88	10.22	12.57	0.216
9147	1.165	3.2798	4.72	9.30	11.59	10.11	12.48	0.256
9125	1.08	3.2877	4.74	8.98	11.37	10.04	12.42	0.288
9114	1.03	3.2916	4.76	8.86	11.25	10.00	12.39	0.305
9107	1.01	3.2942	4.76	8.67	11.02	9.98	12.37	0.347
9102.5	1.005	3.2958	4.78	8.32	10.35	9.97	12.36	0.484
9102	1.01	3.2959	4.78	10.26	12.67	9.97	12.36	0.499
9093	1.025	3.2992	4.78	10.19	12.96	9.94	12.33	0.036
9071	1.08	3.3022	4.82	10.00	12.37	9.87	12.27	0.041
9053	1.15	3.3138	4.83	9.80	12.21	9.80	12.22	0.062
9025	1.21	3.3241	4.84	9.50	1190	9.71	12.13	0.108
9001	1.21	3.3329	4.88	9.32	11.72	9.62	12.07	0.129
8977	1.27	3.3418	4.90	9.10	11.54	9.54	12.00	0.155
8962	1.29	3.3475	4.94	8.96	11.32	9.48	11.95	0.181
8927	1.24	3.3605	4.96	8.50	10.96	9.36	11.84	0.229
8898	1.245	3.3678	5.00	8.25	10.72	9.26	11.76	0.258
8874	1.19	3.3806	5.01	10.32	12.86	9.17	11.68	0.314
8845	1.15	3.3917	5.04	9.86	1235	9.06	11.58	0.395
8822	1.23	3.4005	5.08	9.97	12.04	8.96	11.51	0.441
8805.5	1.33	3.4072	5.12	9.27	11.85	8.90	11.45	0.465
8783	1.44	3.4157	5.17	8.96	11.55	8.80	11.39	0.009
8762	1.50	3.4239	5.18	8.72	11.32	8.72	11.31	0.037
8745.5	1.57	3.4305	5.20	8.60	11.16	8.65	11.26	0.058
8731	1.62	3.4361	5.22	8.40	11.06	8.59	11.21	0.070
8711	1.69	3.4439	5.25	8.17	10.82	8.50	11.14	0.097
8693	1.70	3.4511	5.28	8.00	10.62	8.43	11.08	0.121
8668	1.77	3.4610	5.32	10.39	13.02	8.32	10.98	0.162
8649	1.86	3.4686	5.34	10.16	12.80	8.23	10.90	0.170
8628	1.94	3.4771	5.35	9.95	12.59	8.15	10.82	0.193
8608	1.92	3.4852	5.39	9.68	12.38	8.06	10.75	0.227

"a" = 3.6 cm.

Condition 4 - Horn with E Plane Flare, Plane Parallel Plate Filter

freq.	VSWR	λ	λg	minima to space		short circ. minima		rotation
9148	1.25		4.74	11.73	14.06	12.18		0.229
9121	1.135		4.76	11.40	13.78	12.10		0.275
9104	1.07		4.78	11.15	13.60	9.68		0.313
9094	1.025		4.80	10.98	13.50	9.64		0.333
9076	1.03		4.80	10.62	12.94	9.62		0.425
9060	1.10		4.82		12.45	9.55		0.022
9034	1.18		4.86	12.06	14.52	9.46		0.083
9002	1.205		4.90	11.86	14.30	9.33		0.102
8979	1.275		4.92	11.67	14.10	9.24		0.125
8961	1.305		4.96	11.44	13.91	9.17		0.156
8924	1.27		5.00	11.13	13.59	9.03		0.194
8904	1.27		5.02	10.82	13.41	8.95		0.228
8876	1.23		5.08	10.95	12.99	8.84		0.287
8846	1.21		5.10	9.96	12.47	8.72		0.368
8826	1.24		5.10	9.64	12.19	8.65		0.409
8800	1.34		5.14	9.26	11.85	8.55		0.460
8777	1.45		5.18	8.98	11.58	8.46		0.497
8750	1.55		5.22	8.64	11.24	8.35		0.040
8731	1.64		5.24	8.40	11.04	8.28		0.069
8710	1.79		5.26	8.18	10.82	8.20		0.095
8687	1.84		5.28	7.90	10.53	8.10		0.130
8660	1.89		5.30	7.62	10.30	8.00		0.158
8642	1.96		5.34	7.42	10.08	7.94		0.185
8622	2.05		5.36	7.20	9.84	7.82		0.205
8589	1.96		5.41	6.80	9.51	7.67		0.243

"a" = 3.3 cm.

Condition 5 - Horn with E Plane Flare, Parallel Wire Filter

9063	1.10	4.82	9.80	12.11	11.98	0.097
9081	1.20	4.88	9.58	11.91	11.87	0.111
8998	1.18	4.92	9.14	11.63	11.77	0.144
8952	1.20	4.98	8.65	11.08	11.62	0.220
8914	1.205	5.02	8.26	10.73	11.49	0.246
8887	1.20	5.05	8.10	10.64	11.40	0.259
8875	1.175	5.08	7.79	10.32	11.37	0.311
8861	1.16	5.08	7.52	10.02	11.32	0.361
8860	1.11	5.08	7.51	10.17	11.32	0.
8854	1.17	5.08	7.39	9.89	11.30	0.381
8843	1.18	5.10	7.23	9.67	11.27	0.393
8831	1.20	5.12	7.01	9.63	11.22	0.415
8810	1.30	5.14	6.70	9.32	11.15	0.457
8781	1.41	5.18	8.95	11.45	11.06	0.022
8734	1.53	5.24	8.40	11.04	10.90	0.063
8685	1.71	5.30	7.86	10.52	10.15	0.133
8646	1.83	5.32	7.49	10.15	10.63	0.179
8591	1.81	5.40	6.86	9.53	10.45	0.254

"a" = 3.3 cm.

APPENDIX, SECTION D

SAMPLE CALCULATIONS

Sample Calculations of the Linear Equivalent Source Method of Computing the E Plane Polarized, H Plane Field Pattern

Formula (2) is applicable.

$$E_x = \frac{jk\, e^{-jkR}(1+\cos\theta)\, B\, x_o y_o}{4\pi R} \left[\frac{\sin\left[\frac{(\pi+\phi_o)}{2} - ky_o \sin\theta\right]}{\left[\frac{(\pi+\phi_o)}{2} - ky_o \sin\theta\right]} + \frac{\sin\left[\frac{(\pi+\phi_o)}{2} + ky_o \sin\theta\right]}{\left[\frac{(\pi+\phi_o)}{2} + ky_o \sin\theta\right]} + \frac{\sin\left[\frac{(\pi-\phi_o)}{2} - ky_o \sin\theta\right]}{\left[\frac{(\pi-\phi_o)}{2} - ky_o \sin\theta\right]} + \frac{\sin\left[\frac{(\pi-\phi_o)}{2} + ky_o \sin\theta\right]}{\left[\frac{(\pi-\phi_o)}{2} + ky_o \sin\theta\right]} \right]$$

Let $\phi_o = \frac{\pi}{2}$; $r_{av} = 37.7$ cm.; $\lambda = 3.2$ cm.; $ky_o = \frac{2\pi}{\lambda}\, r_{av} \sin\frac{\phi}{2}o$

Table I

Linear Equivalent Source Sample Calculation

θ Degrees	A $ky_o \sin\theta$	B $\frac{(\pi+\phi_o)}{2} - A$	C $\frac{(\pi+\phi_o)}{2} + A$	D $\frac{\sin B}{B}$	E $\frac{\sin C}{C}$	F $\frac{(\pi-\phi_o)}{2} - A$
0	0	2.3562	2.3562	0.3000	0.3000	0.7854
1	1.087	1.2692	3.4432	0.7520	-0.0854	-0.3016
2	2.175	0.1812	4.5312	0.9946	-0.2171	-1.3896
3	3.260	-0.9038	5.6162	0.8695	-0.1111	-2.4746
4	4.340	-1.984	6.6960	0.4610	0.0604	-3.5550
5	5.420	-3.064	7.7760	0.0245	0.1281	-4.5350

LINEAR RELATIONS

Formula Relationships of the Planar Bipolarity Vortex Method of Computing the X Plane Potential, Z Plane Field Pattern

Formula (2) is expressible.

$$f^x = \frac{i\pi\, e^{-2i\alpha_0}(1+\cos\theta)\; z\, e^{i\alpha_0}}{\pi a} \left[\frac{\sin\left[\frac{\pi}{(\pi+\beta_0^c)} - i\alpha^0\right]\sin\theta}{\left[\frac{\pi}{(\pi+\beta_0^c)} - i\alpha^0\sin\theta\right]}\right]$$

$$+ \frac{\sin\left[\frac{\pi}{(\pi-\beta_0^c)} + i\alpha^0\sin\theta\right]}{\left[\frac{\pi}{(\pi+\beta_0^c)} + i\alpha^0\sin\theta\right]} \frac{\sin\left[\frac{\pi}{(\pi-\beta_0^c)} - i\alpha^0\sin\theta\right]}{\left[\frac{\pi}{(\pi-\beta_0^c)} - i\alpha^0\sin\theta\right]}$$

$$+ \left[\frac{\sin\left[\frac{\pi}{(\pi-\beta_0^c)} + i\alpha^0\sin\theta\right]}{\left[\frac{\pi}{(\pi-\beta_0^c)} + i\alpha^0\sin\theta\right]}\right]$$

Let $\beta_0^c = \frac{\pi}{8}$; $r_{av} = 71{,}7$ cm.; $\gamma = 3.1$ cm.; $\alpha_0^c = \frac{\gamma}{2r}\, e_{av}\, \sin\frac{\pi}{\beta_0^c}$

Table I

Linear Equivalent Source Sample Calculation

Degrees	$\alpha_0^c \sin\theta$	$\frac{\pi}{(\pi+\beta_0^c)} - i$	$\frac{\pi}{(\pi+\beta_0^c)} + i$	$\frac{\pi}{\sin\beta}$	$\frac{\pi}{\sin\alpha}$	$\frac{\pi}{(\pi-\beta_0^c)} - i$
	A	B	C	D	E	F
0	0	4.1502	3.7168	3.3800	3.3000	0.7954
1	1.0000	1.2898	3.6432	0.7300	-0.0894	-0.3114
2	4.1715	0.1818	4.5312	0.9940	-0.1174	-1.3864
3	3.1500	-0.8030	3.8194	0.8695	-0.1111	-2.1749
4	4.3400	-1.7864	6.6900	0.1490	0.0184	-3.5550
5	5.4300	-3.0864	7.7780	0.0249	3.1683	-4.1350

Θ	G	H	I	J	K
Degrees	$\frac{(\pi - \phi_o)}{2} + A$	$\frac{\text{Sin } F}{F}$	$\frac{\text{Sin } G}{G}$	D+E+H+G	E_x in db.
0	0.7854	0.9000	0.9000	2.400	0.00
1	1.8724	0.9650	0.5110	2.163	- 0.90
2	2.9604	0.7077	0.0610	1.646	- 3.26
3	4.0454	0.4900	-0.1936	1.0548	- 7.12
4	5.1250	-0.1125	-0.1785	0.1096	-26.84
5	6.2050	-0.2170	-0.0125	0.057	-32.48

Variations in the term $(1 + \text{Cos } \Theta)$ are considered to be negligible in this range. A plot of E_x is given on Figure XVII.*

The Fourier-Bessel Series Method of Computing the E Plane Polarized, H Plane Field Pattern

In order to determine the H plane field pattern, let $\phi = \frac{\pi}{2}$ in Formula (6), and the resultant equation becomes:

$$E_x = -E_\phi = \frac{jk\, \varepsilon^{-jkR}\, B\, r\, \delta r}{32\, R} (1 + \text{Cos } \Theta) \left[A(0, \tfrac{\pi}{2})\, J_o(kr_1 \text{ Sin } \Theta) + \right.$$

$$\left. + \sum_{n=1}^{\infty} J_n(kr_1 \text{ Sin } \Theta)\, A(n, \tfrac{\pi}{2})\, B(n, \tfrac{\pi}{2}) \right]$$

The argument of the Bessel function can be computed. For this antenna

$$kr_1 = \frac{2\pi}{\lambda} r_1 = \frac{2\pi\ 37.7}{3.2} = 73.$$

The first step is to make a table of $A(n, \phi_o)$ and $B(n, \phi)$.

---

* In order to simplify the calculations of $\frac{\text{Sin } x}{x}$ terms Reference (10) may be employed.

Degrees	$\frac{(r-R_0')}{\lambda}+A$	$\frac{\sin\theta}{\lambda}$	$\frac{\sin\theta}{a}$	$k+2+n+a$	E^x in erg
0	0.7834	0.7000	0.7000	5.000	0.80
1	1.8774	0.9898	0.9713	4.183	- 8.40
2	2.9044	0.7017	0.6843	4.849	- 3.44
3	4.0834	0.4400	-0.1436	4.0243	- 7.12
4	5.1830	-0.1145	-0.1121	3.8944	-46.82
5	6.2830	-0.4170	-0.3125	3.777	-32.42

Variations in the term $(1+\cos\theta)$ are considered to be negligible in this range. A plot of E^x is given on Figure XXIII.*

The Fourier-Bessel series method of describing the H plane intensity.

H Plane Field Pattern

In order to determine the H plane field pattern, let $\beta = \frac{\pi}{2}$ in formula $(6)_3$ and the resultant equation becomes:

$$E^x = -E_\beta^x = \frac{je^{-jkr}}{2r}\frac{a}{\lambda}\pi\alpha\,(1+\cos\theta)\left[J_0(\alpha\tfrac{a}{\lambda})\,J_0(\alpha\tfrac{a}{\lambda}\sin\theta) + \right.$$

$$\left. + \sum_{n=1}^{\infty} 2J_n(\alpha\tfrac{a}{\lambda}\sin\theta)\,J_n(\alpha\tfrac{a}{\lambda})\,\cos(n\tfrac{\pi}{2})\right]$$

The argument of the Bessel function can be computed. For this reference

$$R\alpha_1' = \frac{\alpha a}{\lambda}\,r_1' = \frac{2\alpha\,(r_1-r)}{\lambda} = 2\pi.$$

The first zero is to make a table of $J(\alpha\frac{a}{\lambda})$ and $J(\alpha\frac{a}{\lambda}\sin\theta)$.

---

* In order to simplify the mathematics of $\frac{\sin\theta}{\lambda}$ terms reference (19) may be employed.

Table II

Values of $A(n,\phi_o)$ for $\phi_o = \frac{\pi}{2}$ and n = 0, $\pm$ 1, $\pm$ 2, ...

N	$\frac{\sin[\frac{\pi}{\phi_o}+N+1]\frac{\phi_o}{2}}{[\frac{\pi}{\phi_o}+N+1]\frac{\phi_o}{2}}$	$\frac{\sin[\frac{\pi}{\phi_o}-N+1]\frac{\phi_o}{2}}{[\frac{\pi}{\phi_o}-N+1]\frac{\phi_o}{2}}$	$\frac{\sin[\frac{\pi}{\phi_o}+N+1]\frac{\phi_o}{2}}{[\frac{\pi}{\phi_o}+N-1]\frac{\phi_o}{2}}$	$\frac{\sin[\frac{\pi}{\phi_o}-N-1]\frac{\phi_o}{2}}{[\frac{\pi}{\phi_o}-N-1]\frac{\phi_o}{2}}$	$A(N,\frac{\pi}{2})$
0	0.2984	0.2984	0.9000	0.9000	2.3968
$\pm$1	0	0.6360	0.6360	1.0000	2.2720
$\pm$2	-0.1800	0.9000	0.2984	0.9000	1.9184
$\pm$3	-0.2118	1.0000	0	0.6360	1.4242
$\pm$4	-0.1283	0.9000	-0.1800	0.2984	0.8900
$\pm$5	0.1000	0.6360	-0.2118	0	0.4240
$\pm$6		0.2984	-0.1283	-0.1800	0.0900

The table of $B(n,\phi)$ may also be constructed. This table will apply to any antenna design.

Table III

Values of $B(n,\phi)$ for $\phi = 0$, $\phi = \pi/2$, and n = $\pm$1, $\pm$2, $\pm$3, ...

n	$B(n,\phi)$	$\phi = 0$	$\phi = \frac{\pi}{2}$	n	$B(n,\phi)$	$\phi = 0$	$\phi = \frac{\pi}{2}$
$\pm$1	2j Cos ϕ	2j	0	$\pm$4	+2j Cos 4ϕ	2	2
$\pm$2	-2 Cos 2ϕ	-2	2	$\pm$5	+2j Cos 5ϕ	2j	0
$\pm$3	-2j Cos 3ϕ	-2j	0	$\pm$6	-2j Cos 6ϕ	-2	2

Table IV

Computation of E_x for the H Plane Field Pattern (Use Equation (7))

θ	$J_0(K\eta_1 \sin\theta)$ $A(1,\frac{\pi}{2})$	$J_2(K\eta_1 \sin\theta)$ $A(2,\frac{\pi}{2})$ $B(2,\frac{\pi}{2})$	$J_4(K\eta_1 \sin\theta)$ $A(4,\frac{\pi}{2})$ $B(4,\frac{\pi}{2})$	$J_6(K\eta_1 \sin\theta)$ $A(6,\frac{\pi}{2})$ $B(6,\frac{\pi}{2})$	E_x	db.
0	+4.7936	0	0	0	+4.7936	0.00
1	+2.9900	+1.3480	+0.0221	0	+4.3601	-0.79
2	-0.3260	+3.4650	+0.2760	+0.0017	+3.4174	-2.93

The E_x H plane pattern field is plotted on Figure XVII.

The Fourier-Bessel Series Method of Computing the H Plane Polarized H Plane Field Pattern

Table II

Values of $J_n(\rho_0 \beta_0^{\nu})$ for $\beta_0^{\nu} = \frac{\pi}{2}$ and $n = \pm\frac{1}{2}, \pm\frac{3}{2}, \pm\frac{5}{2}, \ldots$

n	$\frac{\sin[\beta_0^{\nu}(n+1)]}{\beta_0^{\nu}(n+1)}$	$\frac{\sin[\beta_0^{\nu}(n-1)]}{\beta_0^{\nu}(n-1)}$	$\frac{\sin[\beta_0^{\nu}(n+1)]}{[\beta_0^{\nu}(n+1)]^2}$	$\frac{\sin[\beta_0^{\nu}(n-1)]}{[\beta_0^{\nu}(n-1)]^2}$	$B(n,\beta_0^{\nu})$
$\pm\frac{1}{2}$	0	0.6366	0.9000	1.2732	0.4502
$\pm\frac{3}{2}$	-0.1800	0.9000	-0.2546	1.2732	1.1214
$\pm\frac{5}{2}$	-0.2122	0	-0.8488	0	0.4244
$\pm\frac{7}{2}$	-0.1286	-0.1800	-0.3674	-0.5143	0.4409
$\pm\frac{9}{2}$	-0.0900	-0.2122	-0.2546	-0.6006	0.4276
$\pm\frac{11}{2}$	-0.0661	-0.1286	-0.2122	-0.4127	0.3124

The table of $B(n,\beta_0^{\nu})$ may also be constructed. This table will apply to any antenna design.

Table III

Values of $B(n,\beta_0^{\nu})$ for $\beta_0^{\nu} = \frac{\pi}{2}$, and $n = \pm\frac{1}{2}, \pm\frac{3}{2}, \pm\frac{5}{2}, \ldots$

n	$B(n,\beta_0^{\nu})$	$\beta_0^{\nu} = 0$	$\beta_0^{\nu} = \frac{\pi}{4}$	n	$B(n,\beta_0^{\nu})$	$\beta_0^{\nu} = 0$	$\beta_0^{\nu} = \frac{\pi}{4}$
$\pm\frac{1}{2}$	$\frac{2}{\pi}\cos\beta_0^{\nu}$	$\frac{2}{\pi}$	0	$\pm\frac{4}{2}$	$\frac{2}{\pi}\cos\beta_0^{\nu}$	$\frac{2}{\pi}$	$\frac{2}{\pi}$
$\pm\frac{2}{2}$	$-\frac{2}{\pi}\cos\beta_0^{\nu}$	$-\frac{2}{\pi}$	$\pm\frac{2}{\pi}$	$\pm\frac{5}{2}$	$-\frac{2}{\pi}\cos\beta_0^{\nu}$	$-\frac{2}{\pi}$	0
$\pm\frac{3}{2}$	$-\frac{2}{\pi}\cos\beta_0^{\nu}$	$-\frac{2}{\pi}$	0	$\pm\frac{6}{2}$	$-\frac{2}{\pi}\cos\beta_0^{\nu}$	$-\frac{2}{\pi}$	$-\frac{2}{\pi}$

Table IV

Computation of E_{ϕ}^{x} for the H Plane Field Pattern (Use Equation (7))

ϑ	$H_1(\rho_0\vartheta_0^{\nu})$	$H_2(\rho_0\vartheta_0^{\nu})$	$J_0(\rho_0\sin\vartheta)$	$J_1(\rho_0\sin\vartheta)$	$J_2(\rho_0\sin\vartheta)$	E_{ϕ}^{x}	dB
0	-0.7850	0	0	0	-0.3040	-0.1090	-19.25
1	-0.7850	-0.3488	-0.3488	0	-0.1902	-0.4390	-7.15
2	-0.7850	+1.4140	-0.2760	+0.0717	+3.4174	-0.81	

The E_{ϕ}^{x} H plane pattern field is plotted on Figure XVII.

The Fourier-Bessel Series Method of Computing the H Plane Radiation Pattern

H Plane Field Pattern

Let $\phi = \frac{\pi}{2}$ in Equation (6), $\phi_o = \frac{\pi}{2}$ in the equation for $C(n,\phi_o)$ and construct a table for values of $C(n,\frac{\pi}{2})$

Table V

Values of $C(n,\frac{\pi}{2})$ for n = 0, ± 1, ± 2, ± 3, ...

n	$C(n,\frac{\pi}{2})$	n	$C(n,\frac{\pi}{2})$
0	0	± 4	+0.550
± 1	+0.272	± 5	+0.424
± 2	+0.478	± 6	+0.090
± 3	+0.575		

Next a table of $D(n,\phi)$ is constructed. This table is applicable to all antennas.

Table VI

Table of $D(n,\phi)$ for $\phi = 0$, $\phi = \frac{\pi}{2}$, and n = 1, 2, 3, ...

n	$D(n,\phi)$	$\phi = 0$	$\phi = \frac{\pi}{2}$	n	$D(n,\phi)$	$\phi = 0$	$\phi = \frac{\pi}{2}$
1	$-2 \sin \phi$	0	-2	4	$+2j \sin 4\phi$	0	0
2	$-2j \sin 2\phi$	0	0	5	$-2 \sin 5\phi$	0	-2
3	$+2 \sin 3\phi$	0	-2	6	$-2j \sin 6\phi$	0	0

Evaluating Equation (6) the following table results.

Table VII

Computation of E_θ in the H Plane Field Pattern ($\phi = \frac{\pi}{2}$ in Equation (6))

θ^o	$J_1(K\lambda, \sin\theta)$ $C(1,\frac{\pi}{2})\,D(1,\frac{\pi}{2})$	$J_3(K\lambda, \sin\theta)$ $C(3,\frac{\pi}{2})\,D(3,\frac{\pi}{2})$	$J_5(K\lambda, \sin\theta)$ $C(5,\frac{\pi}{2})\,D(5,\frac{\pi}{2})$	E_θ	db.
0	+0.0000	+0.0000	+0.00000	+0.00000	$-\infty$
1	+0.5610	+0.0888	+0.0014	+0.6512	-17.32
2	+0.5300	+0.5170	+0.0354	+1.0824	-12.93
3	+0.0051	+0.9650	+0.1890	+1.0053	-13.78

Let $\beta = \frac{\pi}{2}$ in equation (4), $R_0^n = \frac{1}{n}$ is the equation for $C(\alpha,\frac{\pi}{2})$

and therefore a table for $C(\alpha,\frac{\pi}{2})$

Table I

Values of $C(\alpha,\frac{\pi}{2})$ for $\alpha = 0, \frac{\pi}{7}, \frac{\pi}{6}, \frac{\pi}{5}, \ldots$

n	$C(\alpha,\frac{\pi}{2})$	α	$C(\alpha,\frac{\pi}{2})$
0	0	$\frac{\pi}{7}$	+0.3[illegible]
$\frac{\pi}{7}$	+0.4[illegible]	$\frac{\pi}{6}$	+0.5[illegible]
$\frac{\pi}{6}$	+0.4[illegible]	$\frac{\pi}{5}$	+1.3[illegible]
$\frac{\pi}{5}$	+0.575		

Next a table of $P(\alpha,\beta)$ is constructed. This table is equivalent to all antecedents.

Table II

Table of $P(\alpha,\beta)$ for $\beta = 0, \frac{\pi}{7}, \frac{\pi}{6}, \frac{\pi}{5}, \ldots$ $\alpha = 1, \frac{\pi}{7}, \frac{\pi}{6}, \ldots$

n	$P(\alpha,\beta)$ $\beta = 0$	$\beta = \frac{\pi}{7}$	n	$P(\alpha,\beta)$ $\beta = 0$	$\beta = \frac{\pi}{7}$
1	$-\alpha \tan \frac{\pi}{7}$	0	1	$+\frac{1}{2} \tan \frac{\pi}{7}$	0
2	$-\frac{\alpha}{2} \tan 2\alpha$	0	2	$-\alpha \tan 2\alpha$	0
3	$-\alpha \tan 3\alpha$	0	3	$-\frac{\alpha}{2} \tan 3\alpha$	0

Substituting Equation (4) the following table results.

Table VII

Computation of R_0^n in the H Plane Plain Problem ($\beta = \frac{\pi}{2}$ in Equation (2))

R_0^n	$C(r,\frac{\pi}{2}) P(r,\frac{\pi}{2})$	$\int_0^r (x, \sin\theta)$	$\int_0^r (x, \sin\theta)$	$\frac{dx}{x}$
0	+0.[illegible]	+0.[illegible]	+0.[illegible]	$-\infty$
1	+0.[illegible]	+0.[illegible]	+0.[illegible]	[illegible]
2	−0.[illegible]	+0.[illegible]	+1.[illegible]	[illegible]
3	[illegible]	+0.[illegible]	+1.[illegible]	[illegible]

The Fourier-Bessel Series Method of Computing the E Plane Polarized E Plane Field Pattern

Substitute $\phi = 0^\circ$ and $\phi_0 = \frac{\pi}{2}$ in Equation (6). The $A(n,\phi_0)$ and the $B(n,0)$ tables have already been computed.

Table VIII

Computation of the Real Part of E_θ in the E plane

θ°	$J_0(K\lambda, \sin\theta)$ $A(0,\pi/2)$	$J_2(K\lambda, \sin\theta)$ $A(2,\pi/2)\,B(2,0)$	$J_4(K\lambda, \sin\theta)$ $A(4,\pi/2)\,B(4,0)$	$J_6(K\lambda, \sin\theta)$ $A(6,\pi/2)\,B(6,0)$	$Re[E_\theta]$
0	+4.7936	0.0000	0.0000	0.0000	+4.7936
1	+2.9900	-1.3491	+0.0220	0.0000	+1.6613
2	+0.3260	-3.4634	+0.2760	-0.0017	-2.8630
3	-1.9280	-3.1071	+0.9030	-0.0141	-4.1762

Table IX

Computation of the Imaginary Part of E_θ in the E Plane

θ°	$J_1(K\lambda, \sin\theta)$ $A(1,\pi/2)\,B(1,0)$	$J_3(K\lambda, \sin\theta)$ $A(3,\pi/2)\,B(3,0)$	$J_5(K\lambda, \sin\theta)$ $A(5,\pi/2)\,B(5,0)$	$Im[E_\theta]$
0	0.0000	0.0000	0.0000	0.0000
1	+4.6830	-0.2195	+0.00136	+4.4649
2	+4.4254	-1.2758	+0.0354	+3.1850
3	+0.0429	-2.3881	+0.1895	-2.1550

Table X

Computation of the Magnitude and Phase of E_θ in the E Plane for Constant R

θ°	$\lvert E_\theta \rvert$	$\angle E_\theta^\circ$	Incremental Source db.	Array Factor	Finite Source db.
0	4.7936	0	0.00	1.00	0.00
1	4.7600	69.6	-0.05	1.00-	-0.05
2	4.6800	132.0	-0.10	1.00-	-0.10
3	4.7000	207.3	-0.10	1.00-	-0.10

These values are plotted on Figure XXX.

3. Finite-Source Contour Method of Computation for 2 Plane Discontinuous H Plane Finite Cylinder

Introduce $\phi = \gamma'$ and $\beta_0 = \frac{\pi}{2}$ in Equations (1). Then $\lambda(\beta_0')$ and the $\chi(\beta_0')$ values have already been computed.

Table VIII

Computation of the Real Part of E_ϕ in the H plane

θ°	$H(\theta, \frac{\pi}{2})$	$R(\theta, \frac{\pi}{2})\, B(\theta)$	$\frac{1}{2}(\mu_1 \sin\theta)$	$\frac{1}{2}(\mu_2 \sin\theta)$	$Re\{E_\theta\}$
0	+1.7958	0.0000	0.4420	0.0000	+2.2378
1	+1.7950	-1.3493	+0.4420	0.0000	+0.8877
2	+0.1940	-3.4543	+0.2768	-0.0017	-3.0852
3	-1.2580	-3.1071	+0.0930	-0.0141	-4.1798

Table IX

Computation of the Imaginary Part of E_θ in the H Plane

θ°	$Re\{R\} B(\theta)$	$\frac{1}{2}(\mu_1 \sin\theta)$	$Im\{E_\theta\}$
0	0.0000	0.1011	0.0000
1	+1.0830	+0.1015	+1.1845
2	+0.4114	+0.0638	+0.4752
3	+0.0429	+0.0213	+0.0642

Table X

Computation of the Normalized Value of E_ϕ in the H Plane Constant E

θ°	$\lvert E_\theta \rvert$	$\frac{E_\theta}{E_\theta^{max}}$	Instrumental Reading $\frac{db}{Maximum}$	Power Reading	Field Strength
0	+2.7134	0	0.00	1.00	0.00
1	+2.7000	+0.6	-0.04	1.00-	-0.03
2	+2.6810	+1.4	-0.11	1.00-	-0.10
3	+2.6520	+2.3	-0.19	1.00-	-0.17

These values are plotted on Figure XXI.

BIBLIOGRAPHY

1. "Calculation of the Radiation Properties of Hollow Pipes and Horns", L. J. Chu, Journal of Applied Physics, Vol. 11, September, 1940, pages 603-610.

2. Microwave Antenna Theory and Design, Samuel Silver, McGraw-Hill Book Company, Inc., 1949, page 357.

3. "The Theory of the Electromagnetic Horn", W. L. Barrow and L. J. Chu, Proceedings of the I. R. E., Vol. 27, pages 51-64, January, 1939.

4. "The Sectoral Electromagnetic Horn", W. L. Barrow and F. D. Lewis, Proceedings of the I. R. E., Vol. 27, pages 41-50, January 1939.

5. "Electromagnetic Horn Design", L. J. Chu and W. L. Barrow, Transactions of the A. I. E. E., Vol. 58, pages 333-337, July, 1939.

6. Antennas, J. D. Kraus, McGraw-Hill Book Company, Inc., 1950, pages 375-377.

7. Microwave Antenna Theory and Design, Samuel Silver, McGraw-Hill Book Company, Inc., 1949, page 401.

8. Microwave Antenna Theory and Design, Samuel Silver, McGraw-Hill Book Company, Inc., 1949, page 408.

9. Antennas, J. D. Kraus, McGraw-Hill Book Company, Inc., 1950, The Diagram on page 377.

10. Tables of the Function $\frac{\sin \phi}{\phi}$ and of its First Eleven Derivitives, Staff of the Computation Laboratory of Harvard University, Harvard University Press, Cambridge, Mass., 1949.

11. Tables of the Bessel Functions of the First Kind of Orders Zero and One; Two and Three; Four, Five, and Six, Staff of the Computation Laboratory of Harvard University, Harvard University Press, Cambridge, Mass., 1947.

12. "Transmission between Elliptically Polarized Antennas", V. H. Rumsey, Proceedings of the I. R. E., Vol. 39, No. 5, May, 1951, page 535.

13. Fields and Waves in Modern Radio, Simon Ramo and J. R. Whinnery, John Wiley and Sons, Inc., 1944, pages 294-299.

14. Introduction to Theoretical Physics, J. C. Slater and N. H. Frank, McGraw-Hill Book Co., Inc., New York, 1933, Chapters 26 and 27.

15. Electromagnetic Theory, J. A. Stratton, McGraw-Hill Book Co., Inc., New York, 1941, Chapter 8.

BIBLIOGRAPHY

1. "Polarization of the Radiation Produced by Moving Pulse and Beams", D. G. Ehm, Journal of Applied Physics, Vol. 12, September, 1941, pages 601-610.

2. Microwave Antenna Theory and Design, Samuel Silver, McGraw-Hill Book Company, Inc., 1949, page 393.

3. "The Theory of the Klystron-Cavity Bunch", W. W. Hansen and L. J. Ohm, Transactions of the I. R. E., Vol. 27, pages 19-24, January 1939.

4. "The Internal Electromagnetic Field", L. J. Barrow and C. C. Lewis, Proceedings of the I.R.E., Vol. 27, pages 41-50, January 1939.

5. "Electromagnetic Horn Design", A. A. Oliner and W. W. Hansen, Transactions of the I. R. E., Vol. 31, pages 179-195, July, 1959.

6. Antennas, J. D. Kraus, McGraw-Hill Book Company, Inc., 1950, pages 175-177.

7. Microwave Antenna Theory and Design, Samuel Silver, McGraw-Hill Book Company, Inc., 1949, page 481.

8. Microwave Antenna Theory and Design, Samuel Silver, McGraw-Hill Book Company, Inc., 1949, page 504.

9. Antennas, J. D. Kraus, McGraw-Hill Book Company, Inc., 1950, The diagram on page 177.

10. Tables of the Function $\frac{\sin x}{x}$ and of the First Eleven Derivatives, Staff of the Computation Laboratory of Harvard University, Harvard University Press, Cambridge, Mass., 1949.

11. Tables of the Bessel Functions of the First Kind of Orders Zero and One, Staff of the Computation Laboratory of Harvard University, Harvard University Press, Cambridge, Mass., 1947.

12. "Translation between Elliptically Polarized Antennas", W. S. Hurley, Transactions of the I. R. E., Vol. PG, No. 3, May, 1952, page 315.

13. Fields and Waves in Modern Radio, Simon Ramo and J. R. Whinnery, John Wiley and Sons, Inc., 1944, pages 492-497.

14. Introduction to Theoretical Physics, L. I. Schiff and C. H. Braun, McGraw-Hill Book Co., Inc., New York, 1949, Chapter 20 and 27.

15. Electromagnetic Theory, J. A. Stratton, McGraw-Hill Book Co., Inc., New York, 1941, Chapter 9.

16. "Some Equivalence Theorems of Electromagnetics and their Applications to Radiation Problems", S. A. Schelkunoff, Bell System Technical Journal, Vol. 15, 1936, pages 92-112.

17. "Diffraction and Radiation of Electromagnetic Waves", S. A. Schelkunoff, Physics Review, Vol. 56, 1939, pages 308-316.

18. Notes on M.I.T. Course No. 6.622, "Antennas", as given by L. J. Chu.

19. "The Diffraction Theory of Electromagnetic Waves", J. A. Stratton and L. J. Chu, Physics Review, Vol. 56, 1939, pages 92-112.

20. Fields and Waves in Modern Radio, S. Ramo and J. R. Whinnery, John Wiley and Sons, New York, 1944, pages 442-457.

21. Electromagnetic Waves, S. A. Schelkunoff, Van Nostrand and Co., 1943, Chapter 8.

22. Principles and Applications of Wave Guide Transmission, George C. Southworth, Van Nostrand and Co., 1950, pages 404-415.

23. "Metal Horns as Directive Receivers of V.H.F. Waves", G. C. Southworth and A. P. King, Proceedings of the I. R. E., Vol. 27, Feb., 1939, pages 95-102.

24. "Radiation Characteristics of Conical Horn Antennas", A. P. King, Proceedings of the I. R. E., March, 1950, pages 249-251.

25. Electromagnetic Waves, S. A. Schelkunoff, Van Nostrand and Co., 1943, pages 360-365.

26. "An Experimental Investigation of the Radiation Patterns of Electromagnetic Horn Antennas", D. R. Rhodes, Proceedings of the I. R. E., Vol. 36, Sept., 1948, pages 1101-1105.

27. "Grating and Screens as Microwave Reflectors", W. D. Hayes, Radiation Laboratory Report No. 54-20, April 1, 1943.

28. A Treatise on the Theory of Bessel Functions, G. N. Watson, Cambridge, London, 1944. Section 2.22.

29. "Characteristics of Horn Feeds on Rectangular Waveguide", J. R. Risser, Radiation Laboratory Report No. 656, December, 1945.

30. Microwave Antenna Theory and Design, S. Silver, McGraw-Hill Book Co., Inc., First Edition, 1949, page 162.

31. Microwave Antenna Theory and Design, S. Silver, McGraw-Hill Book Co., Inc., First Edition, 1949, page 356.

16. "Some Experimental Studies of Electromagnetic and Static Deflection of Cathode Rays", J. A. Anderson, Physical Review, Vol. 28, (1926), pages 691-707.

17. "Electrostatic and Magnetic Deflection of Cathode Rays", J. A. Anderson, Physical Review, Vol. 30, (1927), pages 705-716.

18. [illegible] Vol. [illegible], pages [illegible].

19. "The Effect of Gas Pressure on the Deflection of Cathode Rays by Electrostatic and Magnetic Fields", J. A. Anderson, Physical Review, Vol. 32, (1928), pages 907-922.

20. [illegible] Vol. [illegible], pages [illegible].

21. [illegible] Vol. [illegible], pages [illegible].

22. [illegible] pages [illegible].

23. "Measurements of Electron Velocity by Electron Resonance", J. A. Anderson, Physical Review, Vol. 29, (1927), pages 571-577.

24. "Calculation Characteristics of Coaxial Wire Antennas", J. A. Stratton, Proceedings of the I. R. E., Vol. 23, (1935), pages 425-433.

25. [illegible], J. A. Anderson, Van Nostrand and Co., (1941), pages 90-[illegible].

26. "An Experimental Investigation of the Radiation Pattern of Electromagnetic Horn Antennas", D. E. Beam, Proceedings of the I. R. E., Vol. 35, (1947), pages 1241-1249.

27. "Testing and Forming as Service Methods", W. S. Pope, Radiation Laboratory Report No. 34-M, April 1, 1943.

28. A Treatise on the Theory of Bessel Functions, G. N. Watson, Cambridge, 1941. Section 6.22.

29. "Characteristics of Horn Feeds in Paraboloid Reflectors", S. W. Rhines, Radiation Laboratory Report No. 619, December, 1945.

30. [illegible] Antenna Theory and Design, S. Silver, McGraw-Hill Book Co., Inc., First Edition, 1949, page 326.

31. [illegible] Antenna Theory and Design, S. Silver, McGraw-Hill Book Co., Inc., First Edition, 1949, page 333.

32. Microwave Antenna Theory and Design, S. Silver, McGraw-Hill Book Co., Inc., First Edition, 1949, page 353.

33. "The Design of Reflectionless Corners", N. Elson, ADRDE Research Report No. 129, January, 1942. Graph titled, "Tuning of a Rectangular Waveguide".

34. Microwave Antenna Theory and Design, S. Silver, McGraw-Hill Book Co., Inc., Section 16-5.

35. Antennas Theory and Practice, S. A. Schelkunoff and H. T. Friis, John Wiley and Sons, Inc., 1952, Section 16.7.

36. Microwave Antenna Theory and Design, S. Silver, McGraw-Hill Book Co., Inc. Section 10.10.

37. Characteristics of Horn Feeds on Rectangular Waveguides, J. R. Risser, R. L. Report 656, December, 1945. Figure 5, Appendix.

38. R. L. Report No. 41, Jan. 1945, Section 60 C.

39. Characteristics of Horn Feeds on Rectangular Waveguides, J. R. Risser, R. L. Report 656, December, 1945. Figure 4, Appendix.

40. Ibid., Section D.